CONFIDENTIAL

Copy # 1.

RM SA54I29

NACA

RESEARCH MEMORANDUM

for the

United States Air Force

TESTS OF THE NORTHROP XB-62 MISSILE IN

THE AMES 40- BY 80-FOOT WIND TUNNEL

By David Graham

Ames Aeronautical Laboratory
Moffett Field, Calif.

NATIONAL ADVISORY COMMITTEE
FOR AERONAUTICS

WASHINGTON

Sept. 29, 1954

14

CONFIDENTIAL

NATIONAL ADVISORY COMMITTEE FOR AERONAUTICS

RESEARCH MEMORANDUM

for the

United States Air Force

TESTS OF THE NORTHROP XB-62 MISSILE IN THE AMES 40- BY 80-FOOT WIND TUNNEL

By David Graham

SUMMARY

A series of tests of a full-scale Northrop XB-62 missile was made to determine the cause of a directional out-of-trim condition which was encountered on the initial missile flight tests. The results of the tests indicated that the directional out-of-trim condition was caused by aerodynamic loads induced by engine operation.

Additional data, obtained to determine the basic aerodynamic characteristics of the full-scale missile, are presented but not discussed.

INTRODUCTION

Prior to the subject tests, a series of launchings and flights of the Northrop XB-62, a long-range, surface-to-surface missile, had been attempted at the Air Force Missile Test Center, Patrick Air Force Base. Three of the flights gave indications of a directional out-of-trim condition which was directly responsible for, or contributed to, the early terminations of those flights. Therefore, at the request of the WADC, United States Air Force, an investigation of a full-scale XB-62 missile was made in the Ames 40- by 80-foot wind tunnel. The primary purpose of the tests was to determine the cause of the directional out-of-trim condition. In addition, tests were made to determine the basic aerodynamic characteristics of the full-scale missile at low speed for correlation with Northrop small-scale tests.

NOTATION

The results of the tests are presented as standard NACA coefficients of forces and moments. All force data are referred to the wind axes, and all moment data are referred to the stability axes. The coefficients and symbols are defined below and in figure 1.

b wing span, ft

c wing chord, measured parallel to the plane of symmetry of the missile, ft

$\bar{c}$ mean aerodynamic chord, measured parallel to the plane of symmetry of the missile, $\frac{\int_0^{b/2} c^2 dy}{\int_0^{b/2} c\, dy}$, ft

C_D drag coefficient, $\frac{\text{drag}}{qS}$

C_{D_T} increment of drag due to wind-tunnel-wall interference

$C_{D_{tare}}$ increment of drag coefficient applied for support-strut interference

C_L lift coefficient, $\frac{\text{lift}}{qS}$

C_l rolling-moment coefficient, $\frac{\text{rolling moment}}{qSb}$

C_m pitching-moment coefficient, $\frac{\text{pitching moment}}{qS\bar{c}}$

$C_{m_{tare}}$ increment of pitching-moment coefficient applied for support-strut interference

C_n yawing-moment coefficient, $\frac{\text{yawing moment}}{qSb}$

C_Y side-force coefficient, $\frac{\text{side force}}{qS}$

q free-stream dynamic pressure, $\frac{1}{2}\rho V^2$ (Subscript n indicates nominal q value rounded off to nearest pound per square foot.)

R	Reynolds number, $\frac{V\bar{c}}{\nu}$
S	wing area, sq ft
V	free-stream velocity, ft/sec
y	spanwise distance outboard from wing center line (unless otherwise noted), ft
α	free-stream angle of attack, with reference to the wing-chord plane, deg
α_T	increment of angle of attack due to wind-tunnel-wall interference, deg
β	angle of sideslip, deg
δ_e	symmetric deflection of both elevons, measured perpendicular to the hinge line, positive when trailing edge moves down
δ_a	total antisymmetric deflection of both elevons, measured perpendicular to the hinge line, positive when left elevon has more positive deflection
δ_r	rudder deflection, measured perpendicular to the hinge line, deg
ν	kinematic viscosity, sq ft/sec
ρ	mass density of free-stream air, slugs/cu ft
$\Delta\psi$	change in average crossflow angle, deg
ΔC_l	increment of rolling-moment coefficient due to the application of power
ΔC_n	increment of yawing-moment coefficient due to the application of power

DESCRIPTION OF MISSILE AND APPARATUS

The geometric characteristics and basic dimensions of the missile are given in figure 2. The wing area and mean aerodynamic chord given are for the wing without either leading-edge or trailing-edge chord extensions. The coordinates of the airfoil sections on the basic wing,

parallel to the missile plane of symmetry, are given in table I. Table II gives the coordinates of the airfoil section at the inboard end of the leading-edge chord extension. Photographs of various configurations of the missile are shown in figure 3.

The missile was equipped with an Allison J-71 engine. For tests made without the engine operating, the engine inlet duct was covered by a faired plug and the tail pipe was closed by a flat plug. The inlet plug can be seen in figure 3(c). Engine rpm are given as percent of the engine's rated 6100 rpm.

A series of tests was made to measure the change in crossflow angle, in the vicinity of the vertical tail, due to power. The measurements were made by use of a rake having eight directional pitot-static tubes. The rake was mounted on the fuselage with the vertical tail removed as shown in figure 4. No attempt was made to determine the angles between the axis of the tubes and the plane of symmetry of the model since the only measurements obtained were the changes in crossflow angle which resulted from the addition of power.

TESTS AND RESULTS

The tests conducted and configurations tested are listed in table III. The majority of the tests were made with engine power off at a tunnel dynamic pressure of 25 pounds per square foot which resulted in a Reynolds number of 7.5×10^6 based on the mean aerodynamic chord. A number of tests were made at other dynamic pressures as indicated in table III. The variation of Reynolds number with dynamic pressure for all the tests is shown in figure 5. When tests were made with power on, the rise in tunnel temperature during the test resulted in a decreasing Reynolds number through the period of the test. This range of changes in Reynolds number is indicated in figure 5.

The missile dimensions used in the reduction of the data are those in figure 2. The moment data are referred to the moment center as indicated in figure 2.

The angles of attack and drag coefficients have been corrected for stream-angle inclination and wind-tunnel-wall effects. The corrections for wind-tunnel-wall effects are for an unswept wing with the same span as the subject wing and having elliptic loading. These corrections which were added are:

$$\alpha_T = 0.651\ C_L$$

$$C_{D_T} = 0.01137\ C_L^2$$

In addition, the drag and pitching-moment data were corrected for support-strut interference by the tares shown in figure 6. No tares were applied to the data to account for the drag of pressure tubing, wiring, fuel lines and so on, which were of necessity exposed to the air stream. A number of runs were made at the end of the test to determine the increments of drag due to these lines. These tests are discussed later.

All the force and moment data are presented in figures 7 to 34. Table III serves as an index to the figures.

In figures 10(a), (b), (e), and (f), it will be noted that the C_L, C_m, and C_l data for the case with power on are presented as dashed curves. During these runs, one of the two scales which record the lift forces failed to operate. The dashed curves were therefore calculated using the vertical component of thrust as an increment of lift which was added to the power-off lift data. This enabled the calculations of the trends of pitching-moment and rolling-moment curves as indicated. A check on the method made for the data of figures 10(c) and (d) indicated the following possible errors in the calculations:

$$\Delta C_L = \pm 0.01$$

$$\Delta C_m = \pm 0.03$$

$$\Delta C_l = \pm 0.0015$$

During the runs with power on, the thrust was held within ±200 pounds of the values shown in the figures.

DISCUSSION

On the first two flights a maximum of 7° of total aileron deflection was available for both roll stabilization and heading control. Telemetered data from the second flight indicated that the available amount of aileron deflection was insufficient for roll stabilization and, hence, no aileron deflection was available for heading control. Therefore, the neutral aileron position was altered so that 7° of aileron deflection was available for heading control beyond that required for roll stabilization. This system worked satisfactorily on the third flight, allowing the missile to trim out in a steady left sideslip and maintain heading.

Since the flights definitely indicated a directional out-of-trim condition, the purpose of the wind-tunnel tests was to determine whether such out-of-trim yawing and rolling moments actually existed and if so,

to determine their source. The results of the tests of the basic missile with power off as shown in figures 7 and 8 gave, in general, no indication of an out-of-trim condition. With power on (take-off thrust) however, an out-of-trim condition is readily apparent in figures 9 and 10.

A more detailed investigation of the effect of power on the yawing moments was made at a fixed attitude of the missile, that is, $\alpha = 6^\circ$, $\beta = 0^\circ$. The results of tests made with varying rpm at fixed values of dynamic pressure are shown in figure 11. These results indicate that the out-of-trim yawing moment varied with engine rpm, peaking at approximately 98-percent rpm. For these three values of dynamic pressures the variation of out-of-trim yawing moment with dynamic pressure appeared to decrease with the higher dynamic pressures used. Further tests, however, at a fixed 98-percent rpm at the fixed attitude of $\alpha = 6^\circ$, and $\beta = 0^\circ$ as shown in figure 12, indicated that the out-of-trim yawing moment tended to increase with increasing dynamic pressure after reaching a minimum at dynamic pressures of the order of 60-80 pounds per square foot.

In order to determine whether the out-of-trim condition was due to the direct engine characteristics or to aerodynamic loads induced by engine operation, tests were made with first the parachute box and then the parachute box and vertical tail removed. With the parachute box removed (fig. 13), no changes in the out-of-trim conditions were noted. With the vertical tail (including parachute box) removed (fig. 14), the major portion of the out-of-trim yawing moment was removed. A plot of the increment of yawing-moment coefficient due to the vertical tail with power off and power on (fig. 35) shows that at small angles of sideslip crossflow angles of the order of 0.8° at the vertical tail resulted from the application of power. To substantiate the existence of the crossflow, a series of tests were made to measure the change in crossflow angle due to application of power. The measurements were made using the directional rake described earlier. No attempt was made to measure absolute crossflow angles, only the increment of crossflow due to power. The average change in crossflow angle measured for the height of the rake is shown in figure 36 as a function of engine rpm, for three different dynamic pressures. At 98-percent rpm and 25 q the average crossflow angle is slightly over 0.8°, agreeing with the angle measured in the tests with the vertical tail on and off (see fig. 35). In general, the trends in $\Delta\psi$ check with the trends in C_n shown in figure 11.

A simplified calculation of the order of aileron deflection required to hold C_l and $C_n = 0$ at a given C_L was made to determine whether the out-of-trim yawing and rolling moments obtained during the tests were sufficient to result in saturation of the aileron control as obtained on the second flight. The following equation

$$\delta_a = \frac{C_{l_\beta}\Delta C_n - C_{n_\beta}\Delta C_l}{C_{n_\beta}C_{l_{\delta_a}} - C_{l_\beta}C_{n_{\delta_a}}}$$

was used for the calculation of the results which are presented in figure 37. The values of C_{l_β}, C_{n_β}, ΔC_n, and ΔC_l used were obtained from the force data with power on and at a dynamic pressure of approximately 25 pounds per square foot (fig. 10). The values of $C_{l_{\delta_a}}$ and $C_{n_{\delta_a}}$ were obtained from the power-off tests of aileron effectiveness at $q = 25$ pounds per square foot (fig. 15). As seen in figure 37, for the calculation at $q = 25$, the magnitude of yawing moment obtained during the test indicates that the required δ_a for trim could have exceeded the limits on the missile on the second flight. Although the yawing moments, as shown in figure 12, appeared to decrease with increasing q up to q of the order of 80 pounds per square foot, the rising trend of yawing moment above that q, indicates that the values of ΔC_n at the flight q's (order of 300 pounds per square foot) could again be sufficient to cause saturation of the aileron control. With the corrective action taken after flight 2 (i.e., changing the neutral aileron deflection to allow for roll stabilization) the missile could trim to a steady sideslip angle and maintain correct heading.

The remainder of the data obtained during the tests are presented without analysis. A number of tests were made to determine the increments of drag due to the instrumentation and fuel lines and pressure tubing which were exposed to the air stream. Two configurations of lines and tubing were used through the course of the tests. These are noted as X and Y in table III. At the end of the tests, all lines and tubing were removed and runs at 25 and 108 q were made. This is configuration Z. The increments of drag and effect of the tubing are indicated by the results given in figure 34.

Ames Aeronautical Laboratory
National Advisory Committee for Aeronautics
Moffett Field, Calif., Sept. 29, 1954

Approved: Lawrence A. Clousing for
Harry J. Goett
Chief, Full-Scale and Flight Research Division

FIGURE LEGENDS

Figure 1.- Sign convention for the standard NACA coefficients. The forces, moments, angles, and control-surface deflections are shown as positive.

Figure 2.- Three-view drawing of the Northrop XB-62 missile.

Figure 3.- Views of the XB-62 missile. (a) General view from above.

Figure 3.- Continued. (b) Three-quarter front view of basic model with air intake open.

Figure 3.- Concluded. (c) Three-quarter front view of modified model with landing skids extended.

Figure 4.- Position of sidewash rake on the fuselage.

Figure 5.- Variation of Reynolds number with dynamic pressure.

Figure 6.- Drag-coefficient and pitching-moment-coefficient tares applied to the data.

Figure 7.- Aerodynamic characteristics of the basic model in pitch. Power off; q_n = 25 lb/sq ft; $\beta = 0^\circ$. (a) C_L vs. α, C_D, C_m.

Figure 7.- Concluded. (b) C_L vs. C_l, C_n, C_Y.

Figure 8.- Aerodynamic characteristics of the basic model in sideslip. Power off; q_n = 25 lb/sq ft. (a) C_L, C_D, C_m vs. β.

Figure 8.- Concluded. (b) C_Y, C_n, C_l vs. β.

Figure 9.- Effect of the application of power on the aerodynamic characteristics of the basic model in pitch; q_n = 25 lb/sq ft; $\beta = 0^\circ$. (a) C_L vs. α, C_D, C_m.

Figure 9.- Concluded. (b) C_L vs. C_l, C_n, C_Y.

Figure 10.- Effect of application of power on the aerodynamic characteristics of the basic model in sideslip; q_n = 25 lb/sq ft. (a) $\alpha = 0.1^\circ$; C_L, C_D, C_m vs. β.

Figure 10.- Continued. (b) $\alpha = 0.1^\circ$; C_Y, C_n, C_l vs. β.

Figure 10.- Continued. (c) $\alpha = 6.3^\circ$; C_L, C_D, C_m vs. β.

Figure 10.- Continued. (d) $\alpha = 6.3^\circ$; C_Y, C_n, C_l vs. β.

Figure 10.- Continued. (e) $\alpha = 12.6^\circ$; C_L, C_D, C_m vs. β.

Figure 10.- Concluded. (f) $\alpha = 12.6^\circ$; C_Y, C_n, C_l vs. β.

Figure 11.- Variation of the aerodynamic characteristics of the basic model with change in engine rpm at given values of dynamic pressure; $\alpha = 6.3^\circ$; $\beta = 0^\circ$. (a) C_L, C_D, C_m vs. percent rpm.

Figure 11.- Concluded. (b) C_Y, C_n, C_l vs. percent rpm.

Figure 12.- Variation of the aerodynamic characteristics of the basic model with change in dynamic pressure at 98-percent rpm; $\alpha = 6.3^\circ$; $\beta = 0^\circ$. (a) C_L, C_D, C_m vs. q.

Figure 12.- Concluded. (b) C_Y, C_n, C_l vs. q.

Figure 13.- Effect of the removal of the parachute box on the aerodynamic characteristics of the model in sideslip; $q_n = 25$ lb/sq ft; $\alpha = 6.3^\circ$. (a) C_L, C_D, C_m vs. β.

Figure 13.- Concluded. (b) C_Y, C_n, C_l vs. β.

Figure 14.- Effect of the removal of the vertical tail on the aerodynamic characteristics of the model in sideslip; $q_n = 25$ lb/sq ft; $\alpha = 6.3^\circ$. (a) C_L, C_D, C_m vs. β.

Figure 14.- Concluded. (b) C_Y, C_n, C_l vs. β.

Figure 15.- Characteristics of the basic model in pitch with elevon deflected for lateral control; $q_n = 25$ lb/sq ft; $\beta = 0^\circ$. (a) C_L vs. α, C_D, C_m.

Figure 15.- Concluded. (b) C_L vs. C_l, C_n, C_Y.

Figure 16.- Characteristics of the basic model in pitch with elevon deflected as lateral control; $q_n = 25$ lb/sq ft; $\beta = -4^\circ$. (a) C_L vs. α, C_D, C_m.

Figure 16.- Concluded. (b) C_L vs. C_l, C_n, C_Y.

Figure 17.- Characteristics of the basic model in sideslip with elevon deflected as lateral control; $q_n = 25$ lb/sq ft; $\alpha = 6.3^\circ$. (a) C_L, C_D, C_m vs. β.

Figure 17.- Concluded. (b) C_Y, C_n, C_l vs. β.

Figure 18.- Characteristics of the basic model in pitch with elevons deflected as longitudinal controls; $q_n = 25$ lb/sq ft; $\beta = 0^\circ$. (a) C_L vs. α, C_D, C_m.

Figure 18.- Concluded. (b) C_L vs. C_l, C_n, C_Y.

Figure 19.- Characteristics of the basic model in sideslip with elevons deflected as longitudinal controls; q_n = 25 lb/sq ft. (a) $\alpha = 0.1^\circ$; C_L, C_D, C_m vs. β.

Figure 19.- Continued. (b) $\alpha = 0.1^\circ$; C_Y, C_n, C_l vs. β.

Figure 19.- Continued. (c) $\alpha = 6.3^\circ$; C_L, C_D, C_m vs. β.

Figure 19.- Concluded. (d) $\alpha = 6.3^\circ$; C_Y, C_n, C_l vs. β.

Figure 20.- Characteristics of the basic model in pitch with elevons deflected as combined lateral and longitudinal controls; q_n = 25 lb/sq ft; $\beta = 0^\circ$. (a) C_L vs. α, C_D, C_m.

Figure 20.- Concluded. (b) C_L vs. C_l, C_n, C_Y.

Figure 21.- Characteristics of the basic model in pitch with elevons deflected as combined lateral and longitudinal controls; q_n = 25 lb/sq ft; $\beta = -4^\circ$. (a) C_L vs. α, C_D, C_m.

Figure 21.- Concluded. (b) C_L vs. C_l, C_n, C_Y.

Figure 22.- Characteristics of the basic model in sideslip with elevons deflected as combined lateral and longitudinal controls; q_n = 25 lb/sq ft; $\alpha = 6.3^\circ$. (a) C_L, C_D, C_m vs. β.

Figure 22.- Concluded. (b) C_Y, C_n, C_l vs. β.

Figure 23.- Characteristics of the basic model in sideslip with the rudder deflected; q_n = 25 lb/sq ft. (a) $\alpha = 0.1^\circ$; C_L, C_D, C_m vs. β.

Figure 23.- Continued. (b) $\alpha = 0.1^\circ$; C_Y, C_n, C_l vs. β.

Figure 23.- Continued. (c) $\alpha = 6.3^\circ$; C_L, C_D, C_m vs. β.

Figure 23.- Concluded. (d) $\alpha = 6.3^\circ$; C_Y, C_n, C_l vs. β.

Figure 24.- Effect of the addition of the trailing-edge chord extension on the characteristics of the model in pitch; q_n = 25 lb/sq ft; $\beta = 0^\circ$. (a) C_L vs. α, C_D, C_m.

Figure 24.- Concluded. (b) C_L vs. C_l, C_n, C_Y.

Figure 25.- Effect of the addition of the trailing-edge chord extension on the characteristics of the model in sideslip; q_n = 25 lb/sq ft. (a) $\alpha = 0.1^\circ$; C_L, C_D, C_m vs. β.

Figure 25.- Continued. (b) $\alpha = 0.1^\circ$; C_Y, C_n, C_l vs. β.

Figure 25.- Continued. (c) $\alpha = 6.3^\circ$; C_L, C_D, C_m vs. β.

Figure 25.- Continued. (d) $\alpha = 6.3^\circ$; C_Y, C_n, C_l vs. β.

Figure 25.- Continued. (e) $\alpha = 12.6^\circ$; C_L, C_D, C_m vs. β.

Figure 25.- Concluded. (f) $\alpha = 12.6^\circ$; C_Y, C_n, C_l vs. β.

Figure 26.- Characteristics of the modified model in pitch with elevons used as longitudinal controls; $q_n = 25$ lb/sq ft; $\beta = 0^\circ$. (a) C_L vs. α, C_D, C_m.

Figure 26.- Concluded. (b) C_L vs. C_l, C_n, C_Y.

Figure 27.- Characteristics of the modified model in sideslip with elevons used as longitudinal controls; $q_n = 25$ lb/sq ft; $\alpha = 6.3^\circ$. (a) C_L, C_D, C_m vs. β.

Figure 27.- Concluded. (b) C_Y, C_n, C_l vs. β.

Figure 28.- Characteristics of the modified model in pitch with elevons used as combined lateral and longitudinal controls; $q_n = 25$ lb/sq ft; $\beta = 0^\circ$. (a) C_L vs. α, C_D, C_m.

Figure 28.- Concluded. (b) C_L vs. C_l, C_n, C_Y.

Figure 29.- Characteristics of the modified model in sideslip with elevons used as combined lateral and longitudinal controls; $q_n = 25$ lb/sq ft; $\alpha = 6.3^\circ$. (a) C_L, C_D, C_m vs. β.

Figure 29.- Concluded. (b) C_Y, C_n, C_l vs. β.

Figure 30.- Effect of extending the landing skids on the characteristics of the modified model in pitch; $\beta = 0^\circ$. (a) C_L vs. α, C_D, C_m.

Figure 30.- Concluded. (b) C_L vs. C_l, C_n, C_Y.

Figure 31.- Effect of extending the landing skids on the characteristics of the modified model in sideslip; $q_n = 25$ lb/sq ft. (a) $\alpha = 6.3^\circ$; C_L, C_D, C_m vs. β.

Figure 31.- Continued. (b) $\alpha = 6.3^\circ$; C_Y, C_n, C_l vs. β.

Figure 31.- Continued. (c) $\alpha = 12.6^\circ$; C_L, C_D, C_m vs. β.

Figure 31.- Concluded. (d) $\alpha = 12.6^\circ$; C_Y, C_n, C_l vs. β.

Figure 32.- Effect of the addition of power on the characteristics of the modified model in pitch with landing skids extended; $\beta = 0^{\circ}$. (a) C_L vs. α, C_D, C_m.

Figure 32.- Concluded. (b) C_L vs. C_l, C_n, C_Y.

Figure 33.- Effect of the addition of power on the characteristics of the modified model in sideslip with landing skids extended; $q_n = 25$ lb/sq ft. (a) $\alpha = 6.3^{\circ}$; C_L, C_D, C_m vs. β.

Figure 33.- Continued. (b) $\alpha = 6.3^{\circ}$; C_Y, C_n, C_l vs. β.

Figure 33.- Continued. (c) $\alpha = 12.6^{\circ}$; C_L, C_D, C_m vs. β.

Figure 33.- Concluded. (d) $\alpha = 12.6^{\circ}$; C_Y, C_n, C_l vs. β.

Figure 34.- Effect of the various drag configurations on the longitudinal characteristics of the model; $\beta = 0^{\circ}$. (a) C_L vs. C_D; $q_n = 25$ lb/sq ft.

Figure 34.- Continued. (b) C_L vs. α, C_m; $q_n = 25$ lb/sq ft.

Figure 34.- Continued. (c) C_L vs. C_D; configuration Z.

Figure 34.- Concluded. (d) C_L vs. α, C_m; configuration Z.

Figure 35.- Increment of yawing moment due to the vertical tail with power off and power on; $q_n = 25$ lb/sq ft.

Figure 36.- Variation of change in average sidewash angle with change in engine rpm at given values of dynamic pressure; $\alpha = 6.3^{\circ}$; $\beta = 0^{\circ}$.

Figure 37.- Computed aileron deflections required to hold C_L and $C_n = 0$ at given values of C_L and ΔC_n.

TABLE I.- COORDINATES OF THE STREAMWISE AIRFOIL SECTIONS OF THE WING WITHOUT CHORD EXTENSIONS

Station, percent chord	Upper-surface ordinate, percent chord	Lower-surface ordinate, percent chord
0	-0.846	-0.846
.116	-.533	-1.158
.234	-.410	-1.267
.351	-.314	-1.345
.585	-.150	-1.446
.878	.018	-1.543
1.461	.267	-1.685
2.915	.681	-1.937
5.806	1.240	-2.275
6.851	1.397	-2.363
8.672	1.631	-2.485
11.514	1.932	-2.646
14.587	2.177	-2.769
17.126	2.344	-2.847
22.647	2.625	-2.958
26.565	2.775	-3.004
28.076	2.822	-3.015
28.616	2.838	-3.018
33.417	2.946	-3.023
37.209	2.987	-3.012
38.672	2.996	-3.006
40.562	2.998	-2.998
41.268	2.996	-2.996
42.843	2.977	-2.977
47.007	2.926	-2.926
47.920	2.904	-2.904
48.931	2.876	-2.876
52.300	2.759	-2.759
53.940	2.686	-2.692
54.436	2.662	-2.672
56.415	2.561	-2.591
58.870	2.423	-2.493
63.724	2.109	-2.297
65.644	1.974	-2.219
68.502	1.757	-2.103
69.363	1.688	-2.069
Straight line to T.E. radius		
100.000	-.778	-.778

L.E. radius: 0.444 percent
T.E. radius: 0.05 inch (constant)

TABLE II.- COORDINATES OF THE AIRFOIL SECTIONS AT THE INBOARD END OF THE LEADING-EDGE CHORD EXTENSION

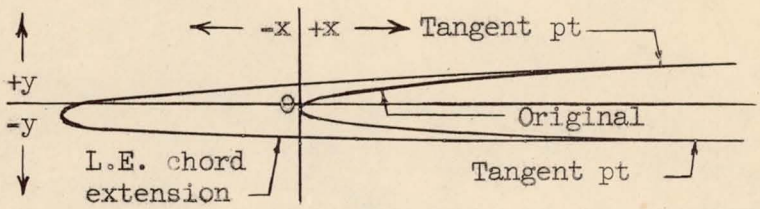

x, in.	y_u, in.	y_L, in.	Remarks
-15.534	-0.740	-0.740	L.E.
-15.234		-1.142	
-15.074	-.266		
-14.744		-1.315	
-14.514	-.082		
-12.734		-1.558	
-12.164	.230		
-9.534		-1.770	
-7.684	.644		
-3.614		-2.032	
-.364	1.215		
3.786		-2.290	
4.976	1.573		
9.496		-2.428	
10.236	1.873		
14.786		-2.508	
15.226	2.098		
23.738	2.387		Tan. pt.
25.596		-2.560	Tan. pt.
L.E. radius: 0.335 inch			

TABLE III.- SUMMARY OF CONFIGURATIONS TESTED

Figure no.	Configuration (1)	Nominal angle of attack, α, deg	Angle of sideslip, β, deg	Elevator deflection, δ_e, deg	Aileron deflection, δ_a, deg	Rudder deflection, δ_r, deg	Approximate dynamic pressure, q_n, lb/sq ft	Power	Drag configuration (2)	Data presented
7	B	variable	0	0	0	0	25	off	X	(3)
8	B	0,6,12	variable	0	0	0	25	off	X	(4)
9	B	variable	0	0	0	0	25	off; on at constant thrust	X	(3)
10	B	0,6,12	variable	0	0	0	25	off; on at constant thrust	X	(4)
11	B	6	0	0	0	0	25,48,107	on at varying rpm	X	$C_L, C_D, C_m, C_Y, C_n, C_l$ vs. rpm
12	B	6	0	0	0	0	variable	on at 98-percent rpm	X	$C_L, C_D, C_m, C_Y, C_n, C_l$ vs. q
13	B minus parachute box	6	variable	0	0	0	25	off; on at constant thrust	X	(4)
14	B minus vertical tail	6	variable	0	0	0	25	off; on at constant thrust	X	(4)
15	B	variable	0	0	0,10,20,30	0	25	off	X	(3)
16	B	variable	-4	0	10,20,30	0	25	off	X	(3)
17	B	6	variable	0	0,10,20,30	0	25	off	X	(4)
18	B	variable	0	-10,0,+10	0	0	25	off	X	(3)
19	B	0,6	variable	-10,0,+10	0	0	25	off	X	(4)
20	B	variable	0	+5	10,20	0	25	off	X	(3)
21	B	variable	-4	+5	10,20	0	25	off	X	(3)
22	B	6	variable	+5	10,20	0	25	off	X	(4)
23	B	0,6	variable	0	0	-5,0,+10,+20, +25	25	off	X	(4)
24	B, T	variable	0	0	0	0	25	off	Y	(3)
25	B, T	0,6,12	variable	0	0	0	25	off	Y	(4)
26	T	variable	0	+15,+10,0, -10,-25	0	0	25	off	Y	(3)
27	T	6	variable	+15,+10,0, -10,-25	0	0	25	off	Y	(4)
28	T	variable	0	+7.5	-15	0	25	off	Y	(3)
				+5	-10					
				0	0					
				-5	+10					
				-12.5	+25					
29	T	6	variable	+7.5	-15	0	25	off	Y	(4)
				+5	-10					
				0	0					
				-5	+10					
				-12.5	+25					
30	T, T+S	variable	0	0	0	0	25,108	off	Y	(3)
31	T, T+S	6,12	variable	0	0	0	25	off	Y	(4)
32	T+S	variable	0	0	0	0	25,108	off; on at constant thrust	Y	(3)
33	T+S	6,12	variable	0	0	0	25	off; on at constant thrust	Y	(4)
34	T	variable	0	0	0	0	25,108	off	X,Y,Z	C_L vs. C_D, α, C_m

[1]Configurations: B Basic model
T Modified model (Model with wing-trailing-edge extension)
S Configuration "T" with landing skids extended.

[2]See Text for explanation of drag configuration.

[3]C_L vs. α, C_D, C_m, C_l, C_n, C_Y.

[4]C_L, C_D, C_m, C_Y, C_n, C_l vs. β.

NATIONAL ADVISORY COMMITTEE FOR AERONAUTICS
AMES AERONAUTICAL LABORATORY
MOFFETT FIELD, CALIF.

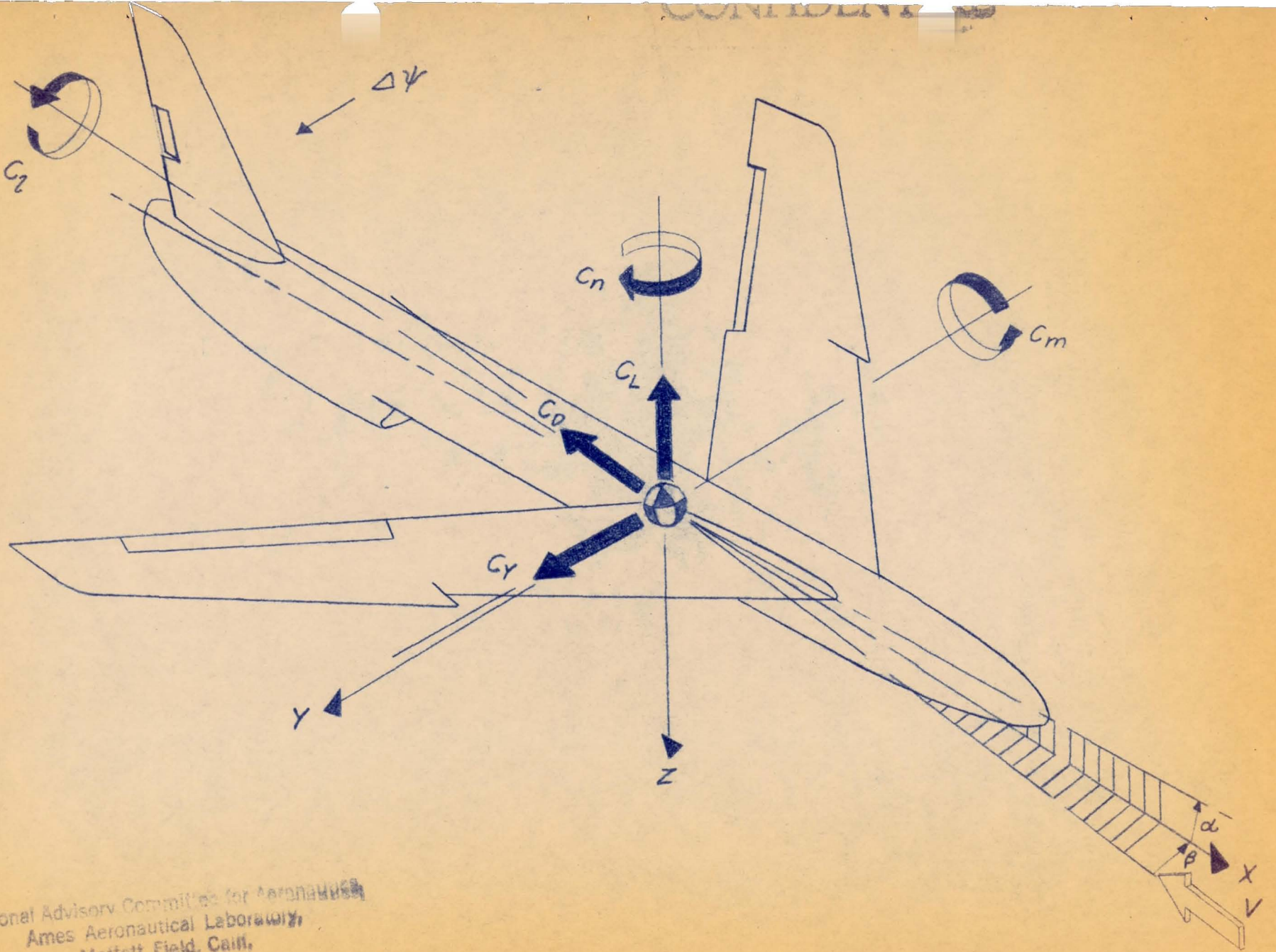

Figure 1.- Sign convention for the standard NACA coefficients. The forces, moments, angles, and control-surface deflections are shown as positive.

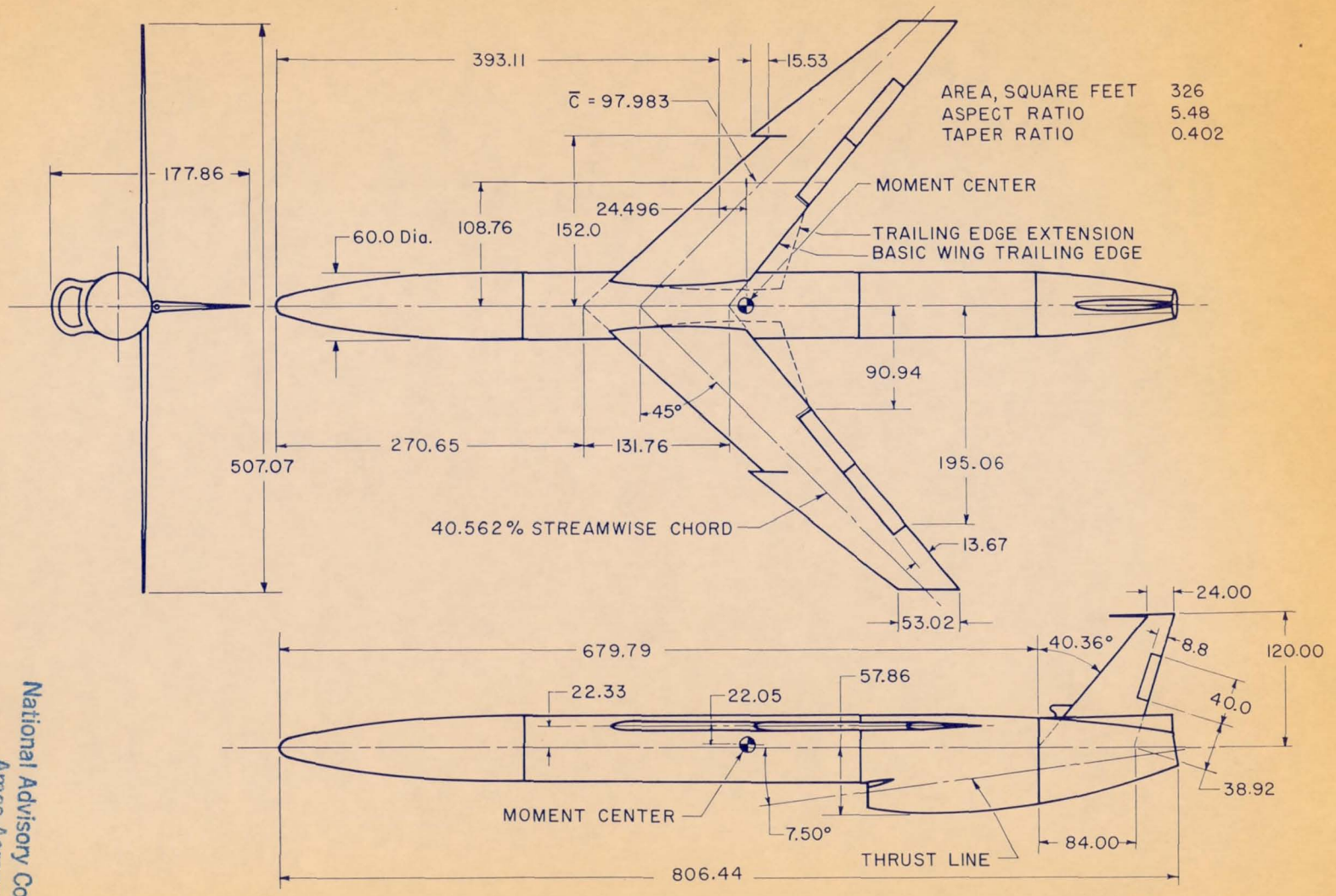

NOTE:
ALL DIMENSIONS IN INCHES UNLESS OTHERWISE NOTED.

Figure 2.- Three-view drawing of the Northrop XB-62 missile.

NACA A-19154

(a) General view from above.

Figure 3.- Views of the XB-62 missile.

(b) Three-quarter front view of basic model with air intake open.

Figure 3.- Continued.

NATIONAL ADVISORY COMMITTEE FOR AERONAUTICS
AMES AERONAUTICAL LABORATORY, MOFFETT FIELD, CALIF.

(c) Three-quarter front view of modified model with landing skids extended.

Figure 3.- Concluded.

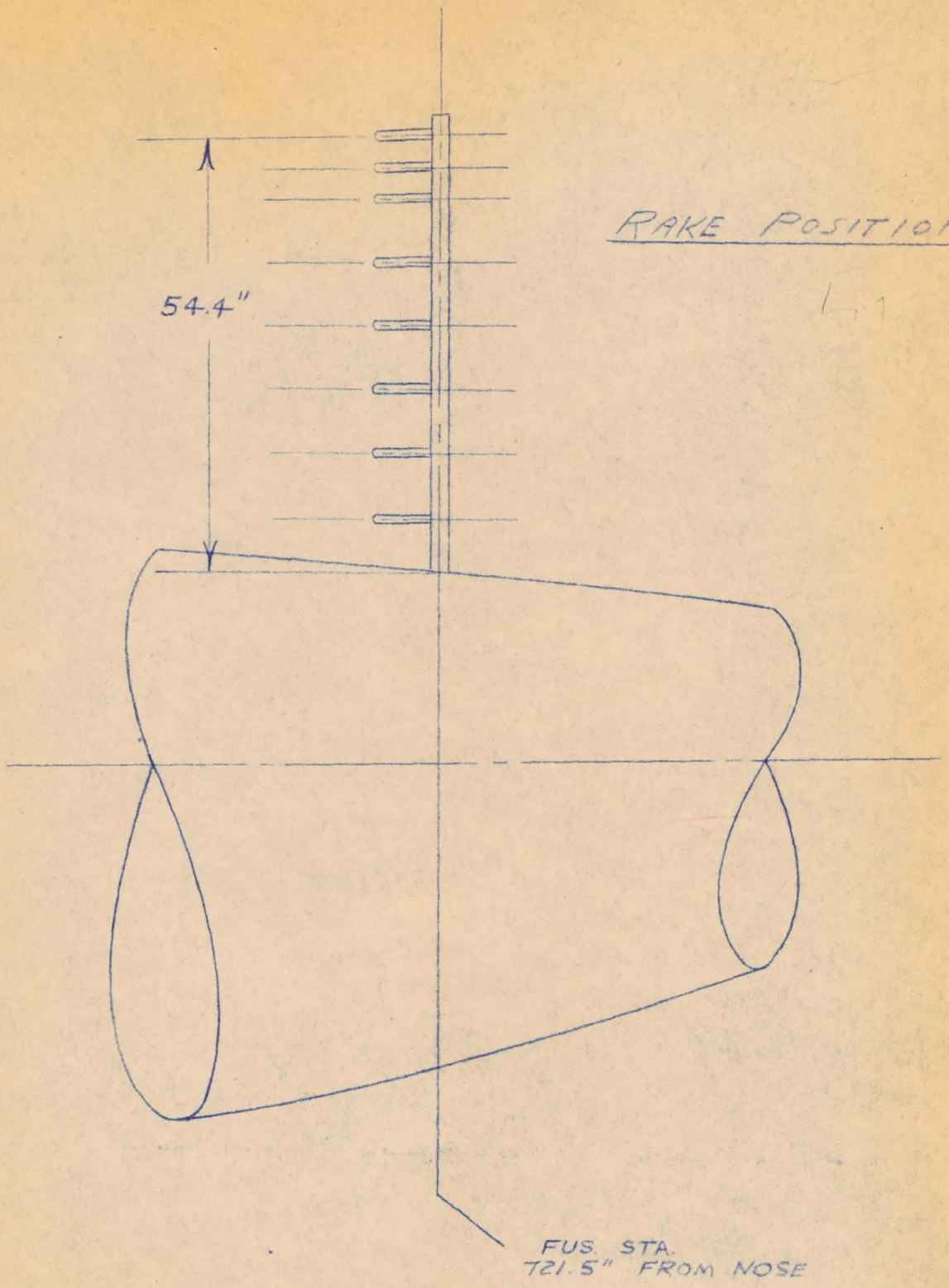

Figure 4.- Position of sidewash rake on the fuselage.

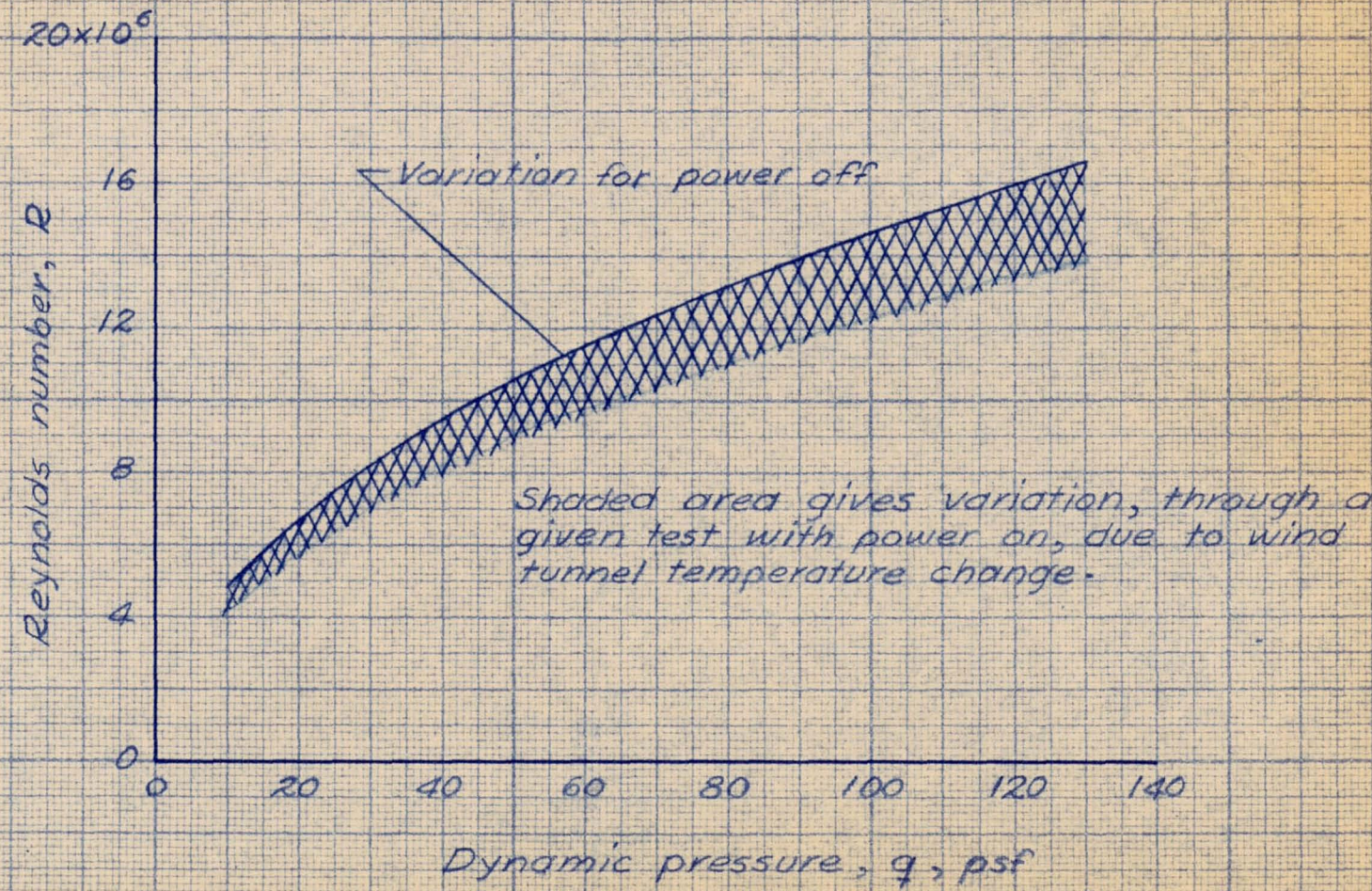

Figure 5.- Variation of Reynolds number with dynamic pressure.

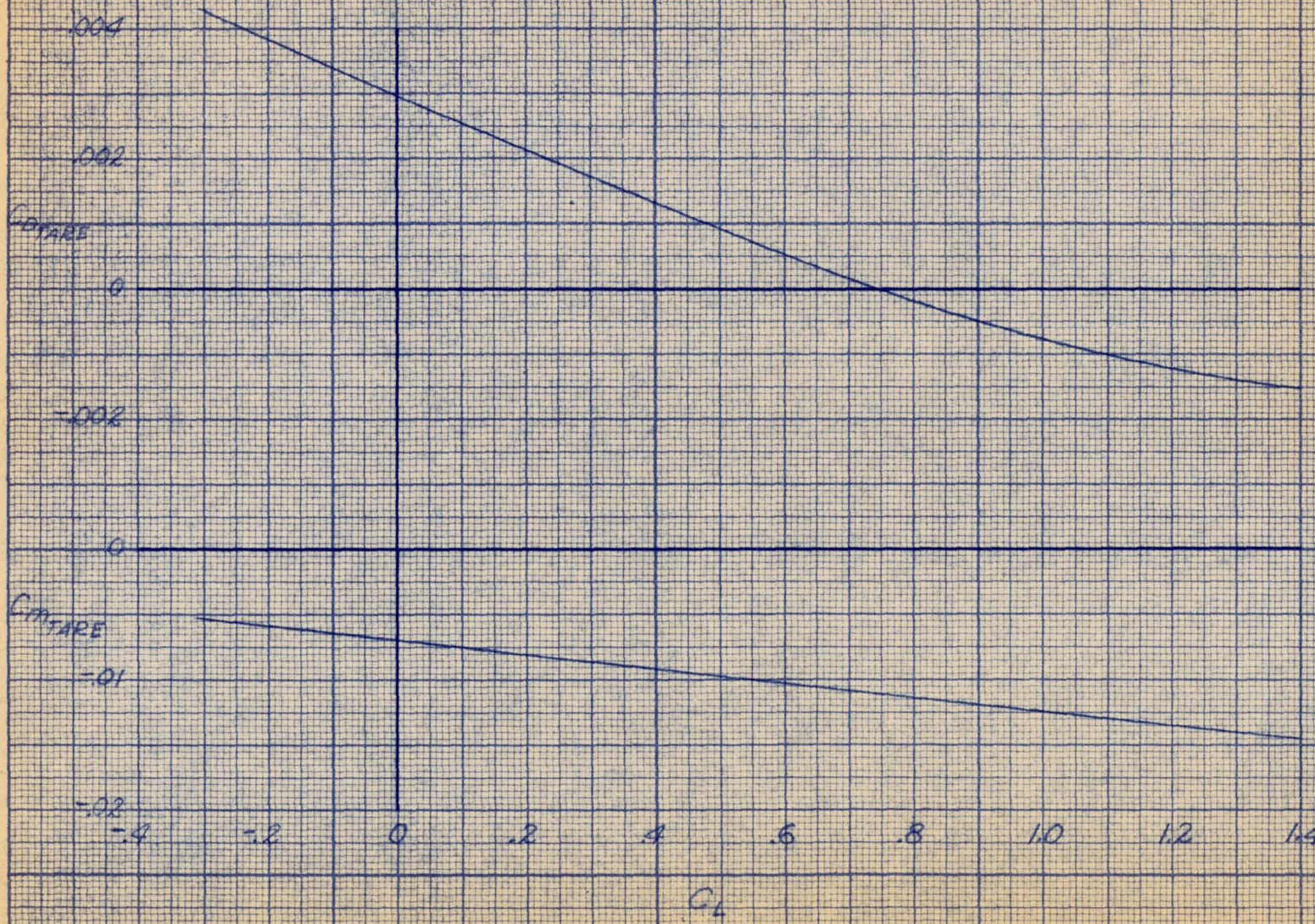

Figure 6.- Drag-coefficient and pitching-moment-coefficient tares applied to the data.

AD-82 Fig 6

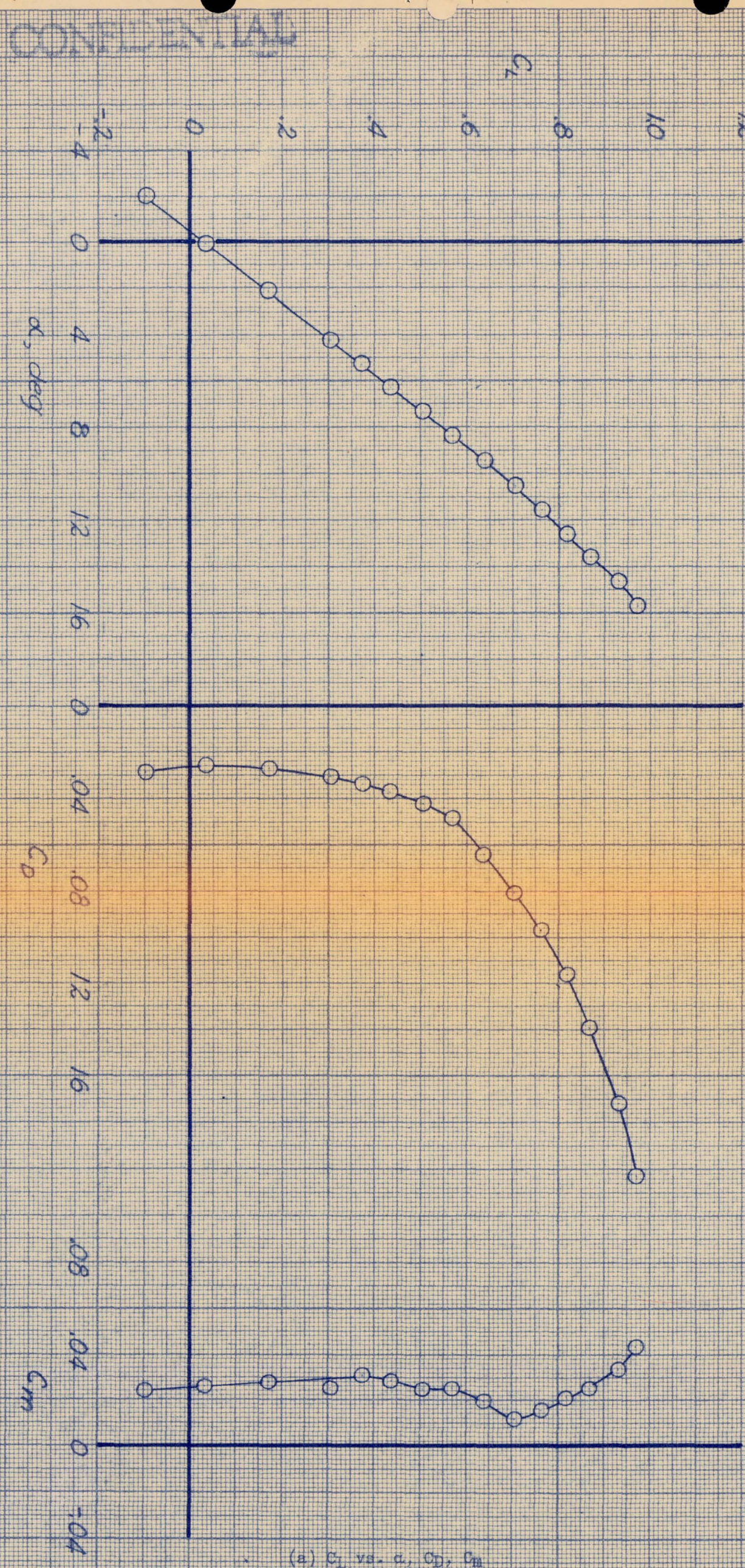

(a) C_L vs. α, C_D, C_m

Figure 7.- Aerodynamic characteristics of the basic model in pitch. Power off; q_m = 25 lb/sq ft; β = 0°.

National Advisory Committee for Aeronautics,
Ames Aeronautical Laboratory,
Moffett Field, Calif.

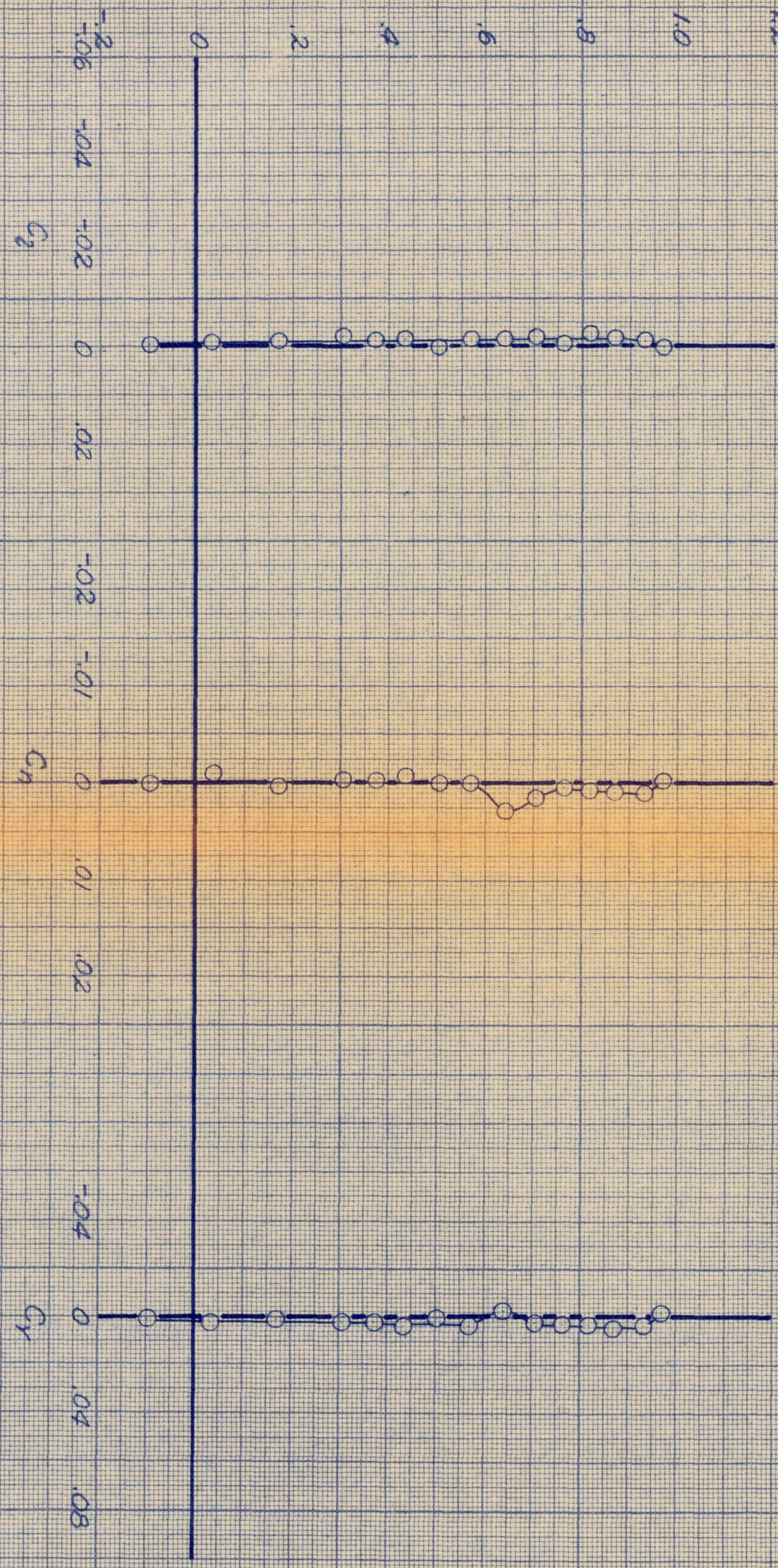

(b) C_L vs. C_l, C_n, C_Y

Figure 7.- Concluded.

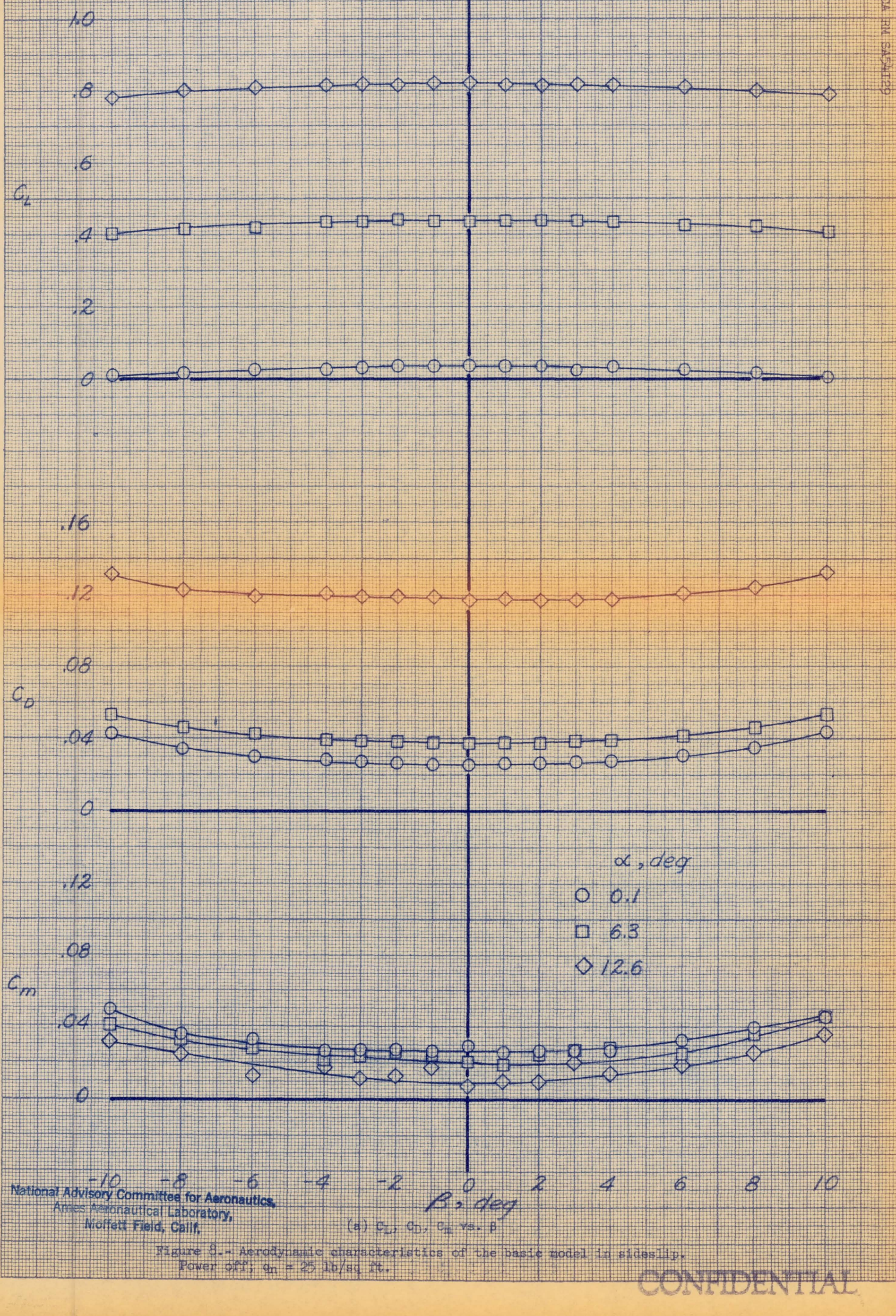

(a) C_L, C_D, C_m vs. β

Figure 8.- Aerodynamic characteristics of the basic model in sideslip. Power off; q_m = 25 lb/sq ft.

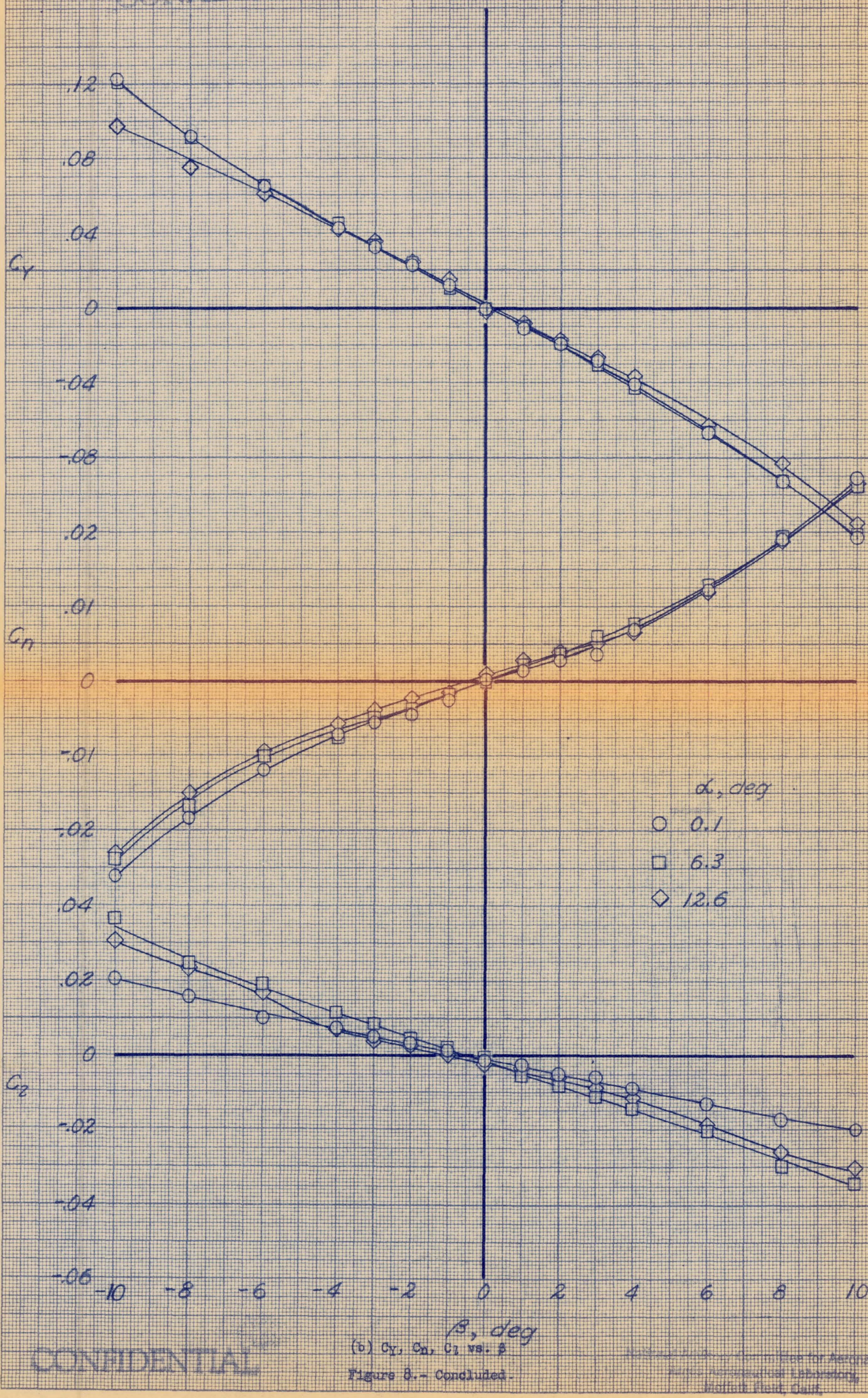

(b) C_Y, C_n, C_l vs. β

Figure 8.- Concluded.

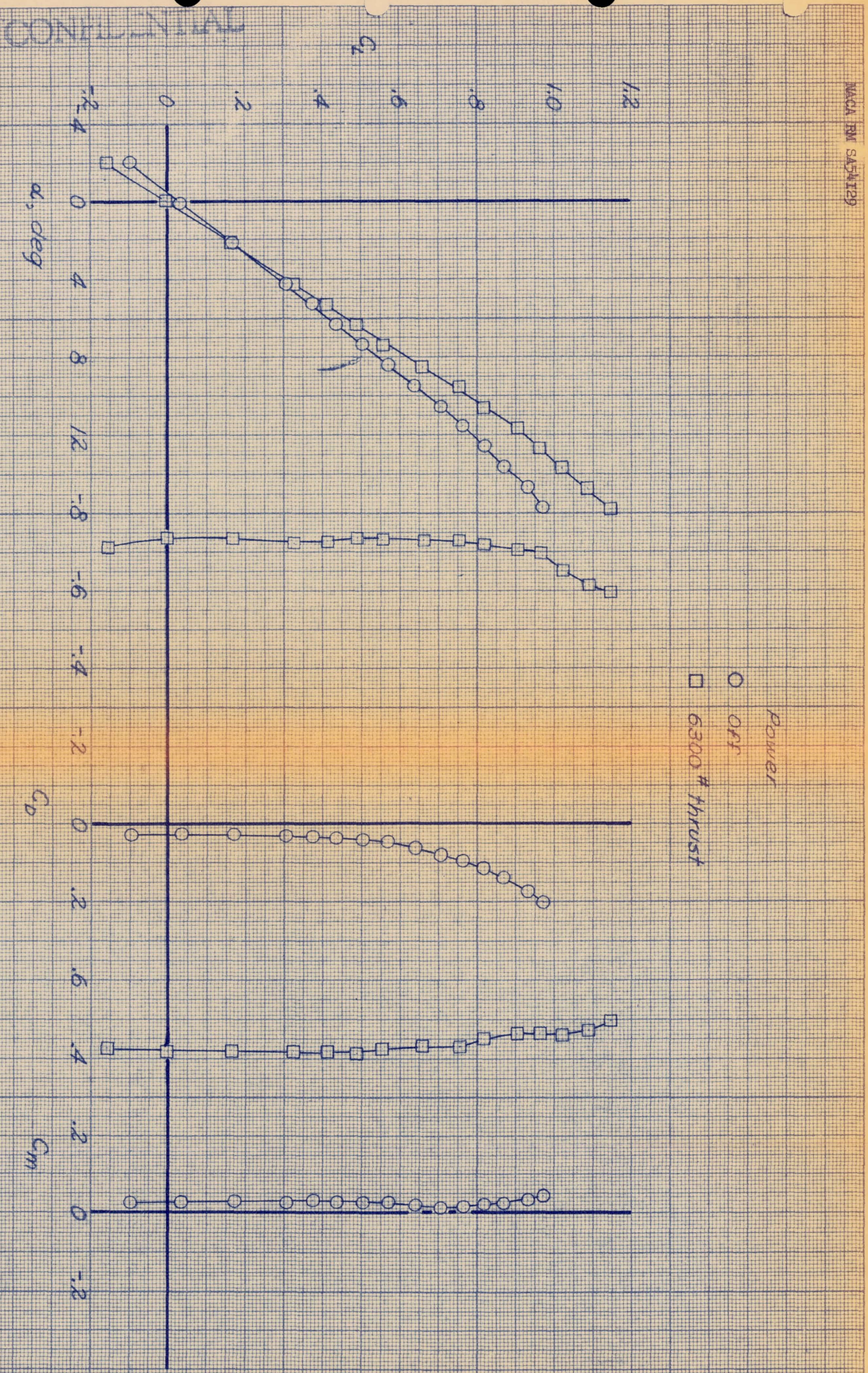

(a) C_L vs. α, C_D, C_m

Figure 9.- Effect of the application of power on the aerodynamic characteristics of the basic model in pitch; q_m = 25 lb/sq ft; $\beta = 0^\circ$.

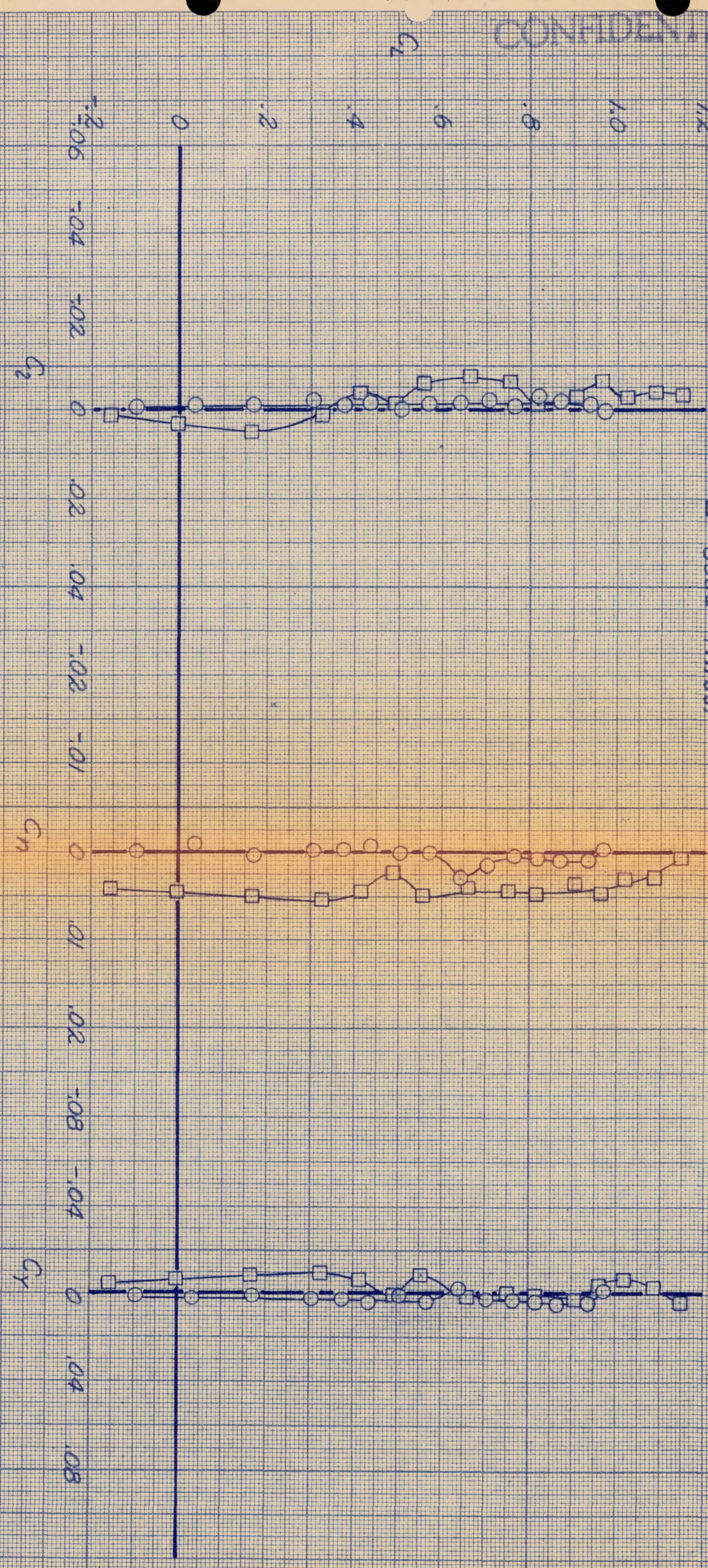

(b) C_L vs. C_l, C_n, C_Y

Figure 9.- Concluded.

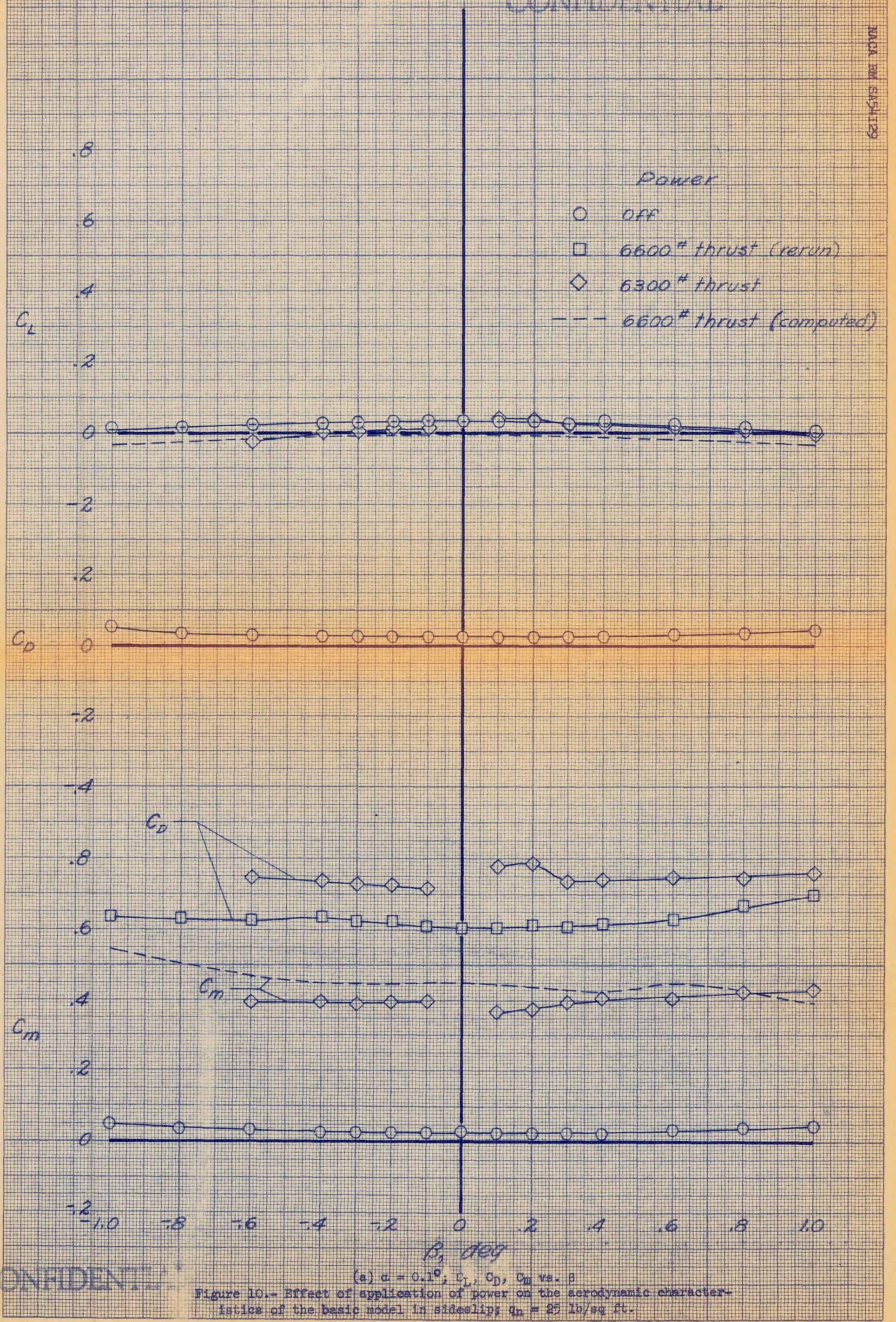

(a) $\alpha = 0.1^\circ$; C_L, C_D, C_m vs. β

Figure 10.- Effect of application of power on the aerodynamic characteristics of the basic model in sideslip; q_m = 25 lb/sq ft.

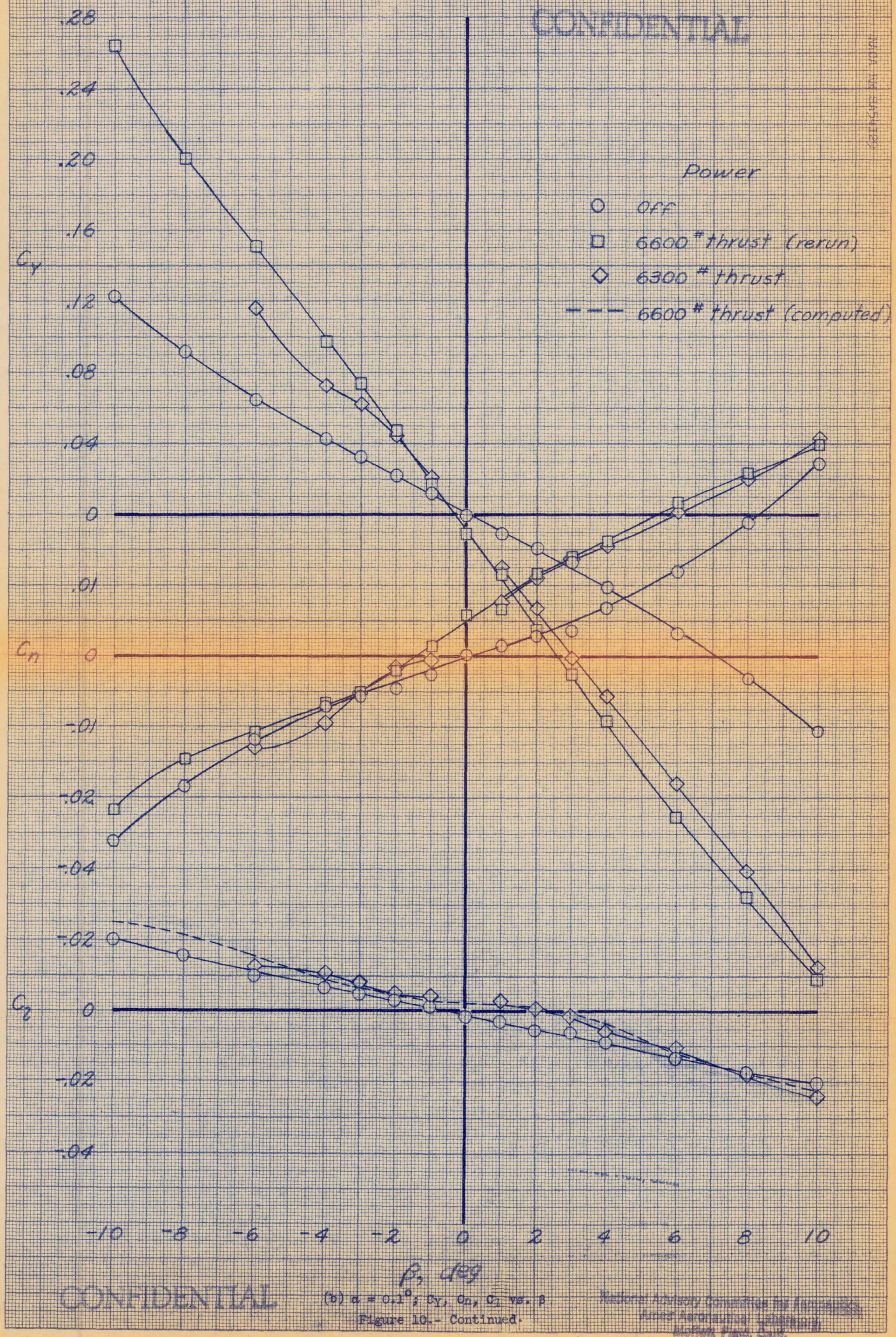

(b) $\alpha = 0.1^\circ$; C_Y, C_n, C_l vs. β

Figure 10.- Continued.

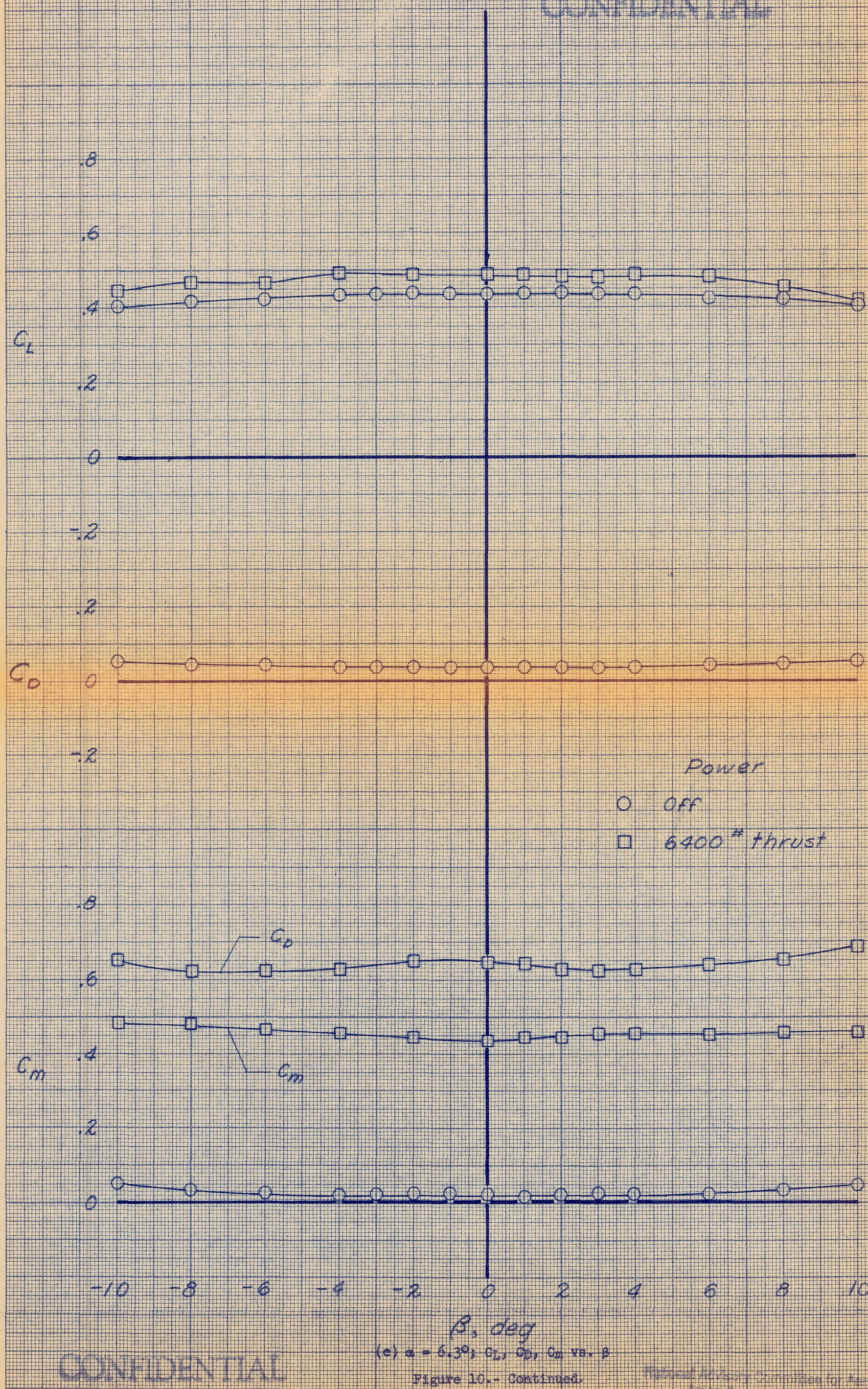

(e) $\alpha = 6.3°$; C_L, C_D, C_m vs. β

Figure 10.- Continued.

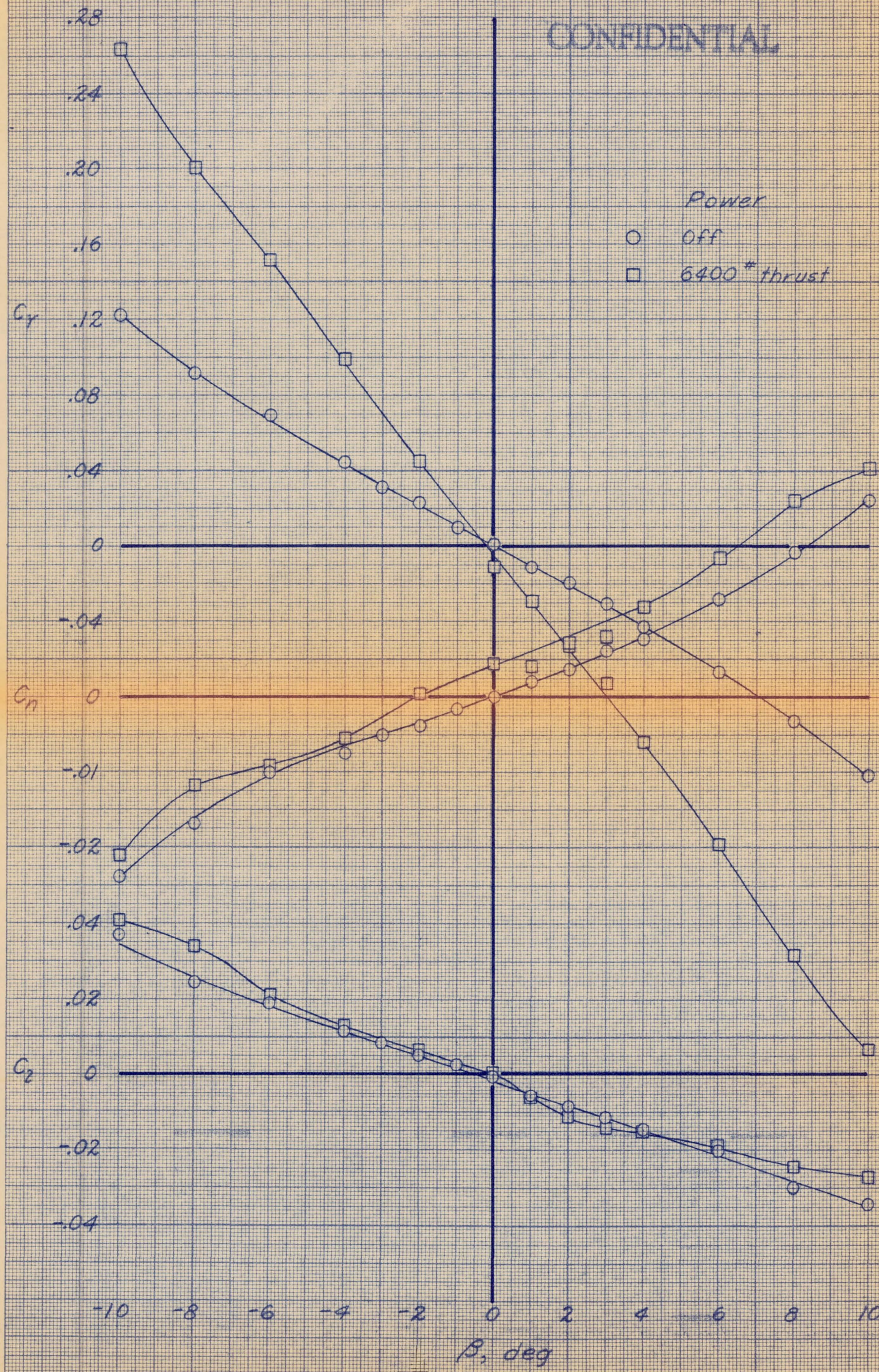

(d) $\alpha = 6.3^\circ$; C_Y, C_n, C_l vs. β

Figure 10.- Continued.

Power
○ Off
□ 6400 # thrust
– – – 6400 # thrust (computed)

C_L
C_D
C_m

1.0
.8
.6
.4
.2
0
-.2

-10 -8 -6 -4 -2 0 2 4 6 8 10

β, deg

(e) $\alpha = 12.6^\circ$; C_L, C_D, C_m vs. β

Figure 10.- Continued.

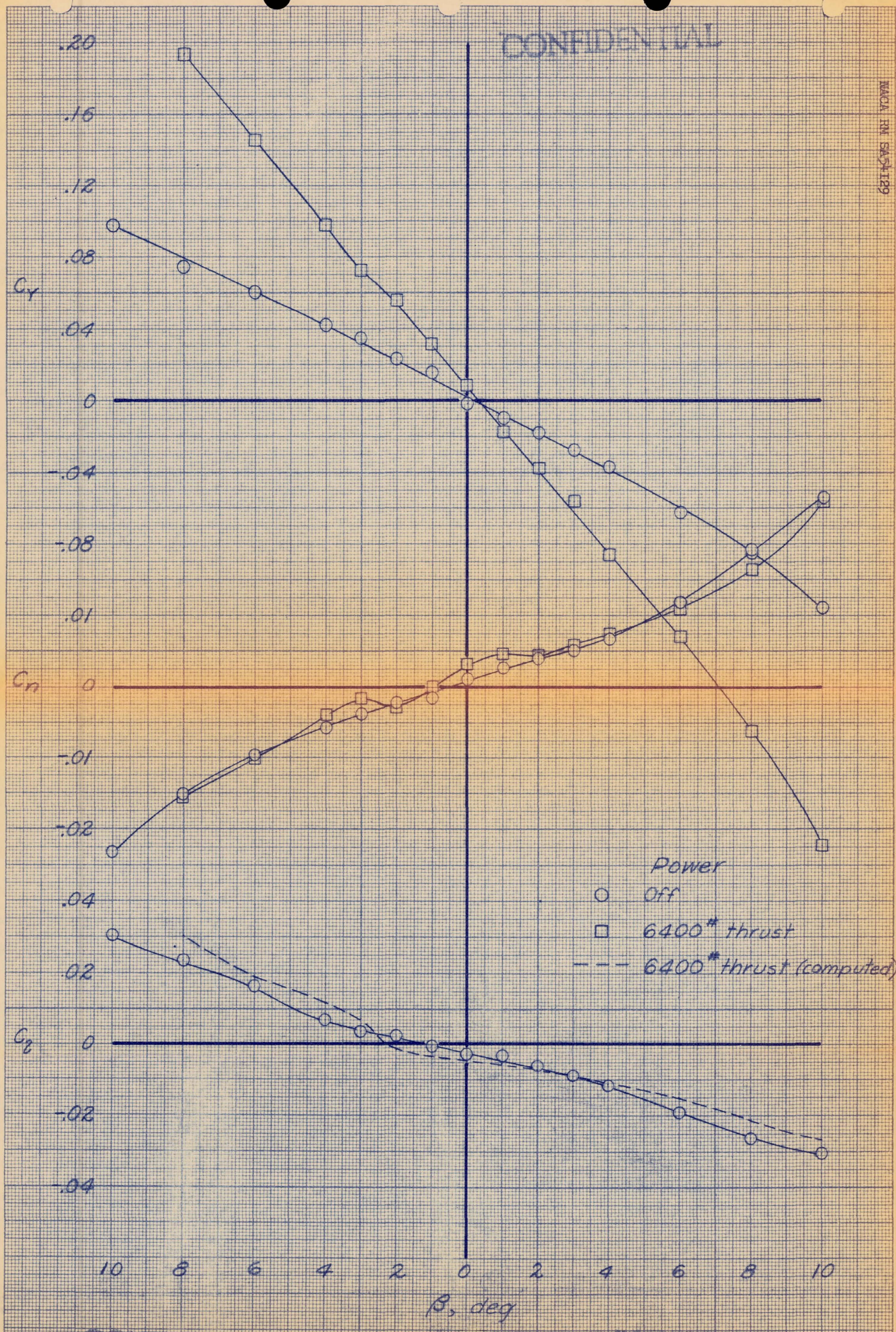

(f) $\alpha = 12.6°$; C_Y, C_n, C_l vs. β

Figure 10.- Concluded.

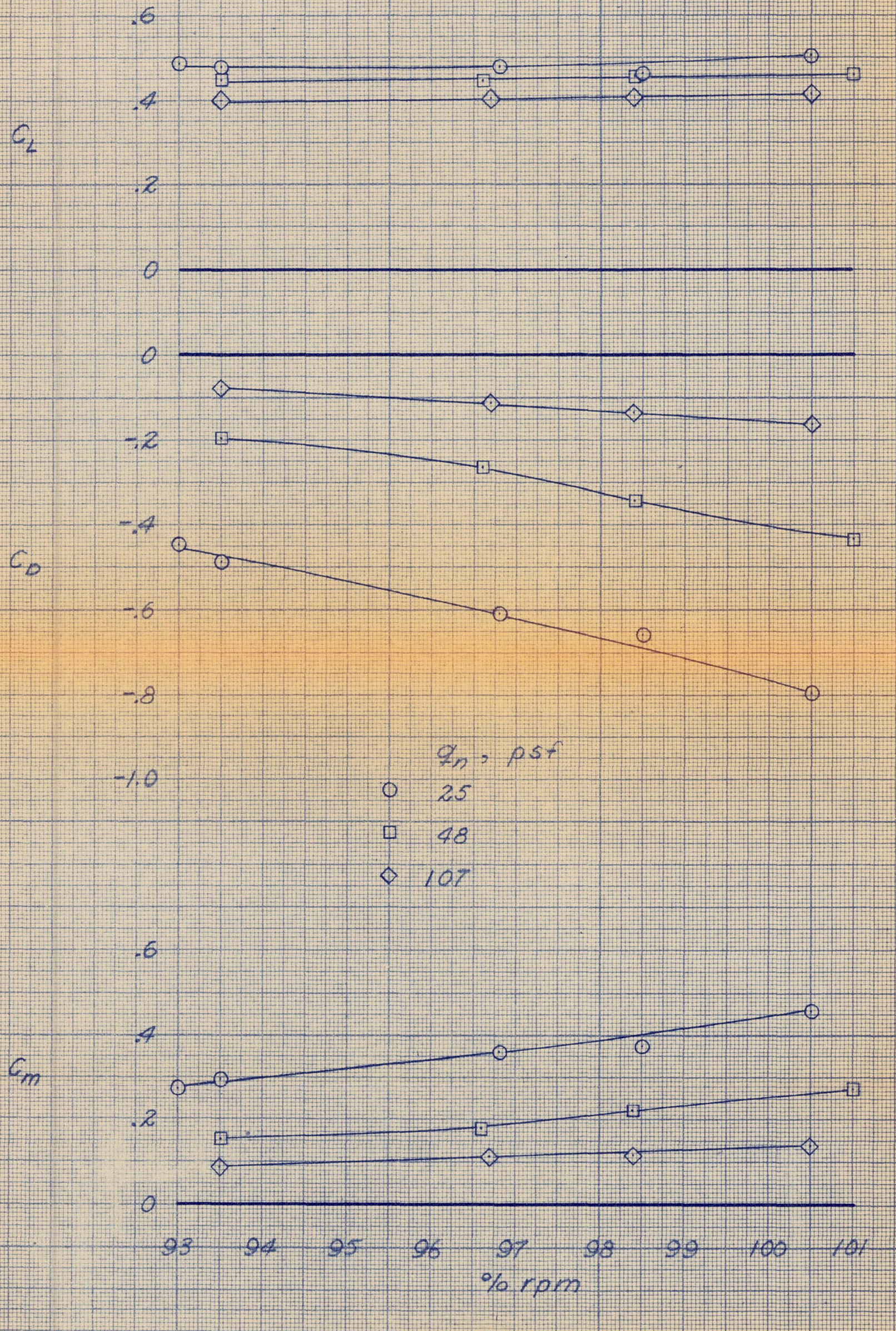

(a) C_L, C_D, C_m vs. percent rpm

Figure 11.- Variation of the aerodynamic characteristics of the basic model with change in engine rpm at given values of dynamic pressure; $\alpha = 6.3^\circ$; $\beta = 0^\circ$.

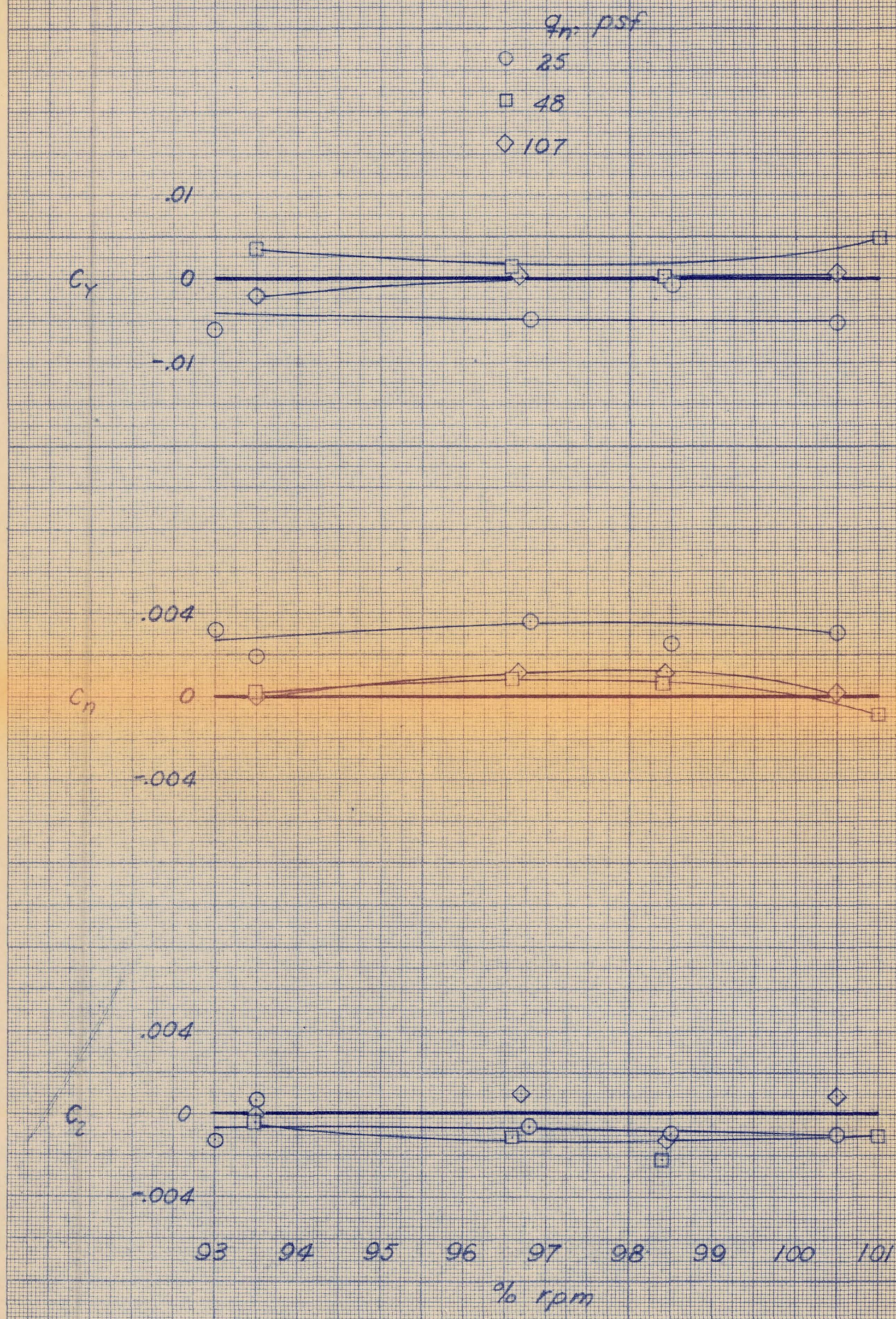

(b) C_Y, C_n, C_l vs. percent rpm.

Figure 11.- Concluded.

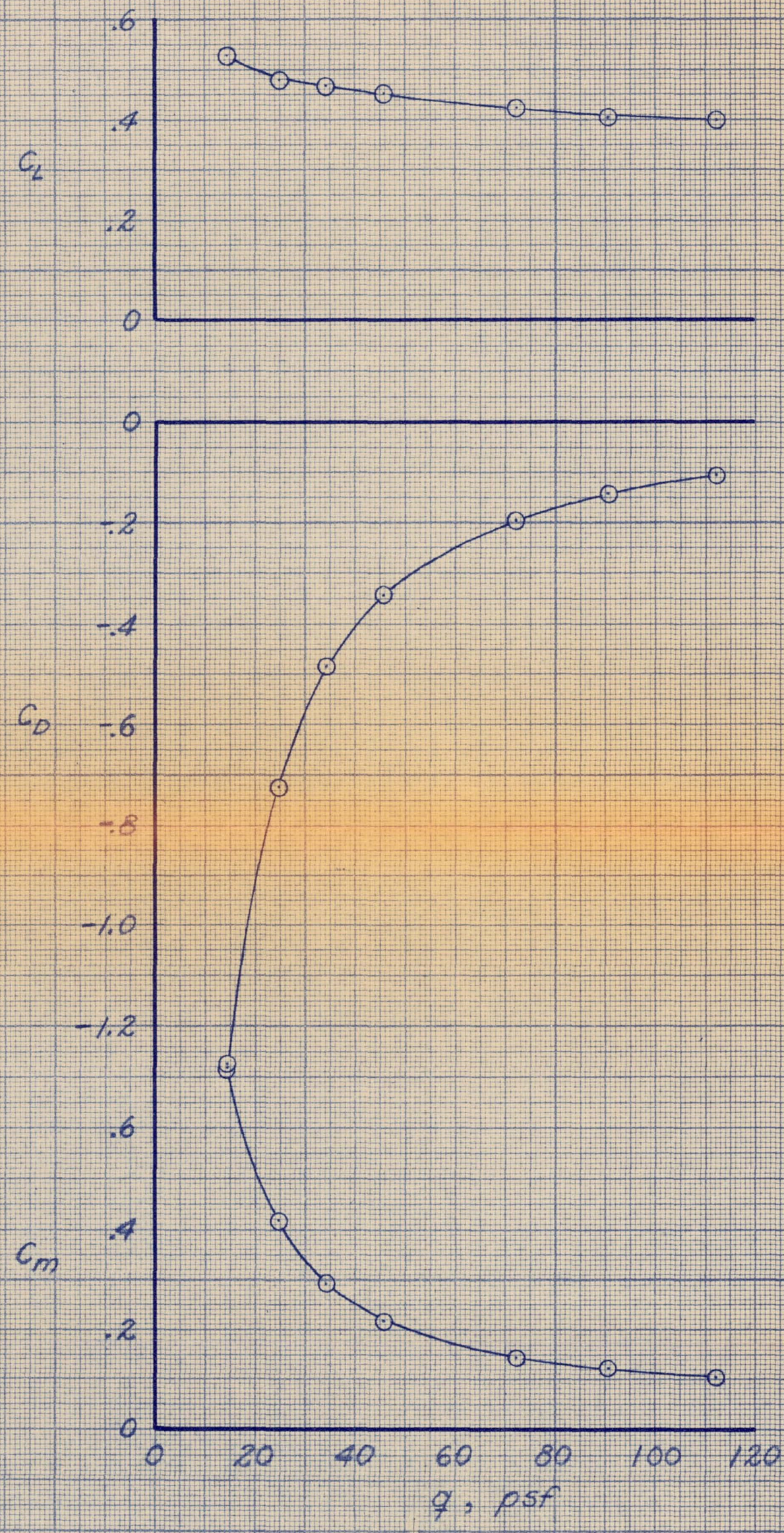

(a) C_L, C_D, C_m vs. q

Figure 12.- Variation of the aerodynamic characteristics of the basic model with change in dynamic pressure at 98-percent rpm; $\alpha = 6.3^\circ$; $\beta = 0^\circ$.

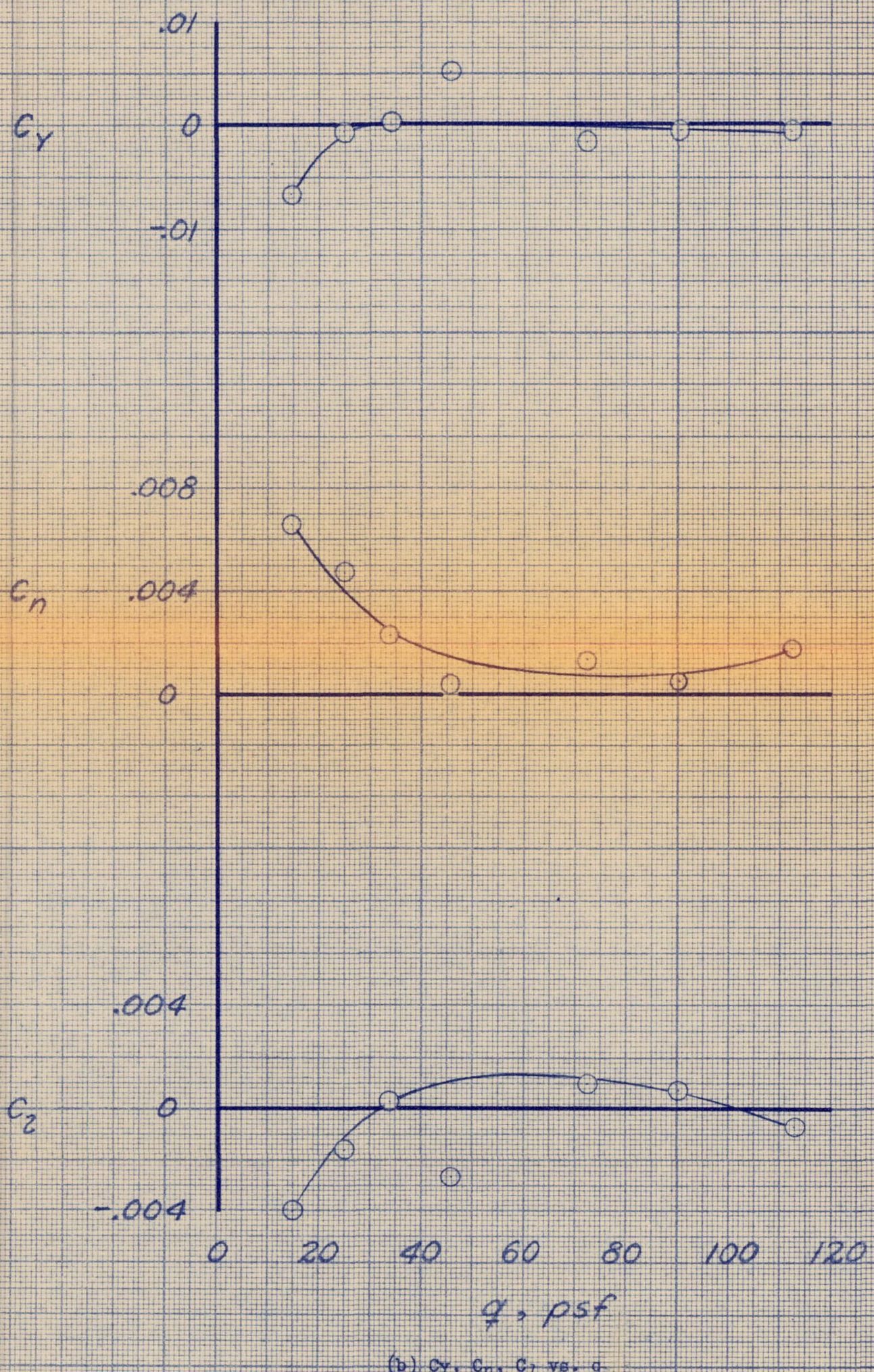

(b) C_Y, C_n, C_l vs. q

Figure 12.- Concluded.

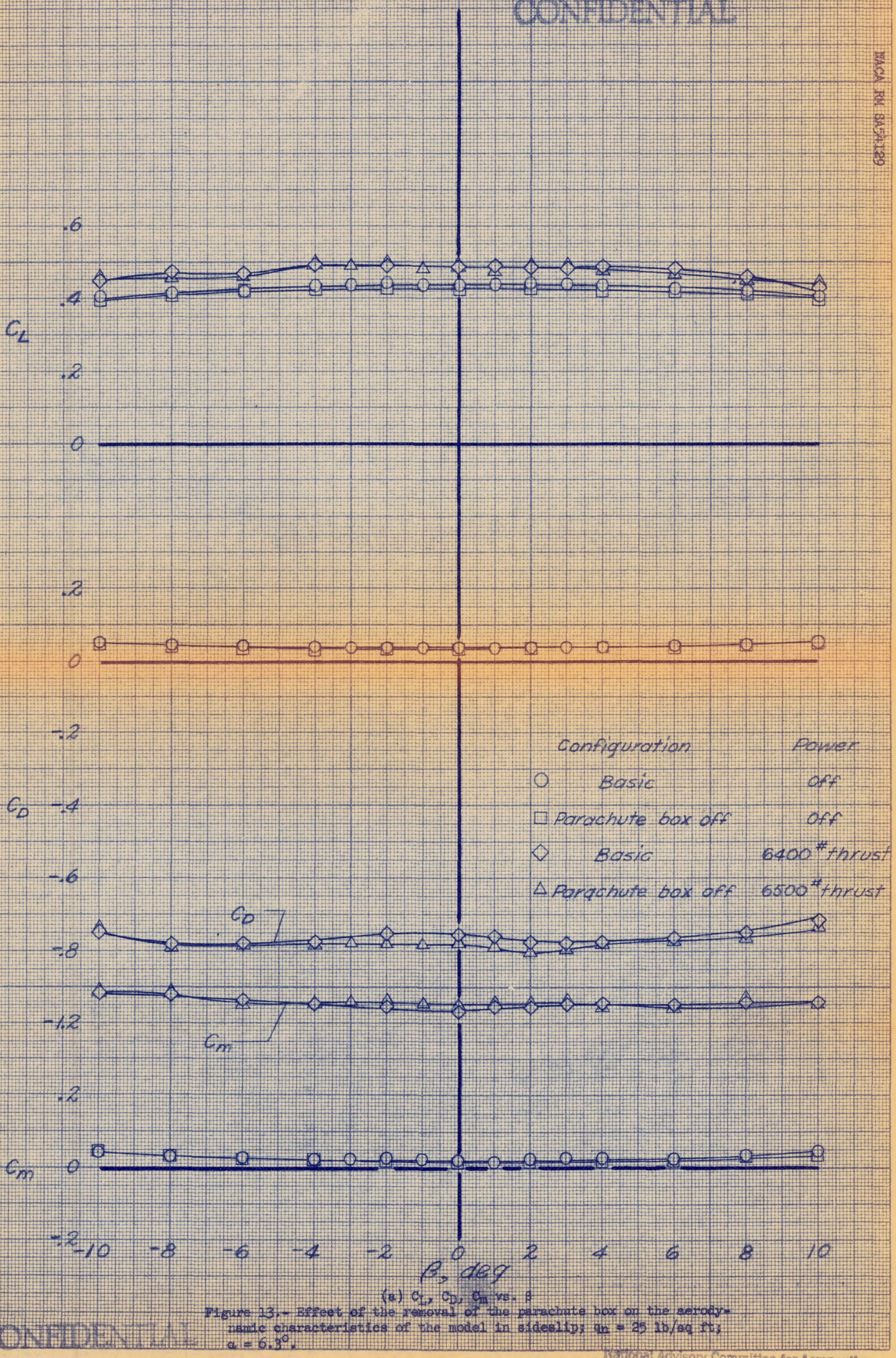

(a) C_L, C_D, C_m vs. β

Figure 13.- Effect of the removal of the parachute box on the aerodynamic characteristics of the model in sideslip; q_n = 25 lb/sq ft; α = 6.3°.

Configuration	Power
○ Basic	Off
□ Parachute box off	Off
◇ Basic	6400# thrust
△ Parachute box off	6500# thrust

C_Y: .28, .24, .20, .16, .12, .08, .04, 0, -.01

C_n: 0, -.01, -.02, .04, .02, 0, -.02, -.04, -.06

C_l: .04, .02, 0, -.02, -.04

-10 -8 -6 -4 -2 0 2 4 6 8 10

β, deg

(b) C_Y, C_n, C_l vs. β

Figure 13.- Concluded.

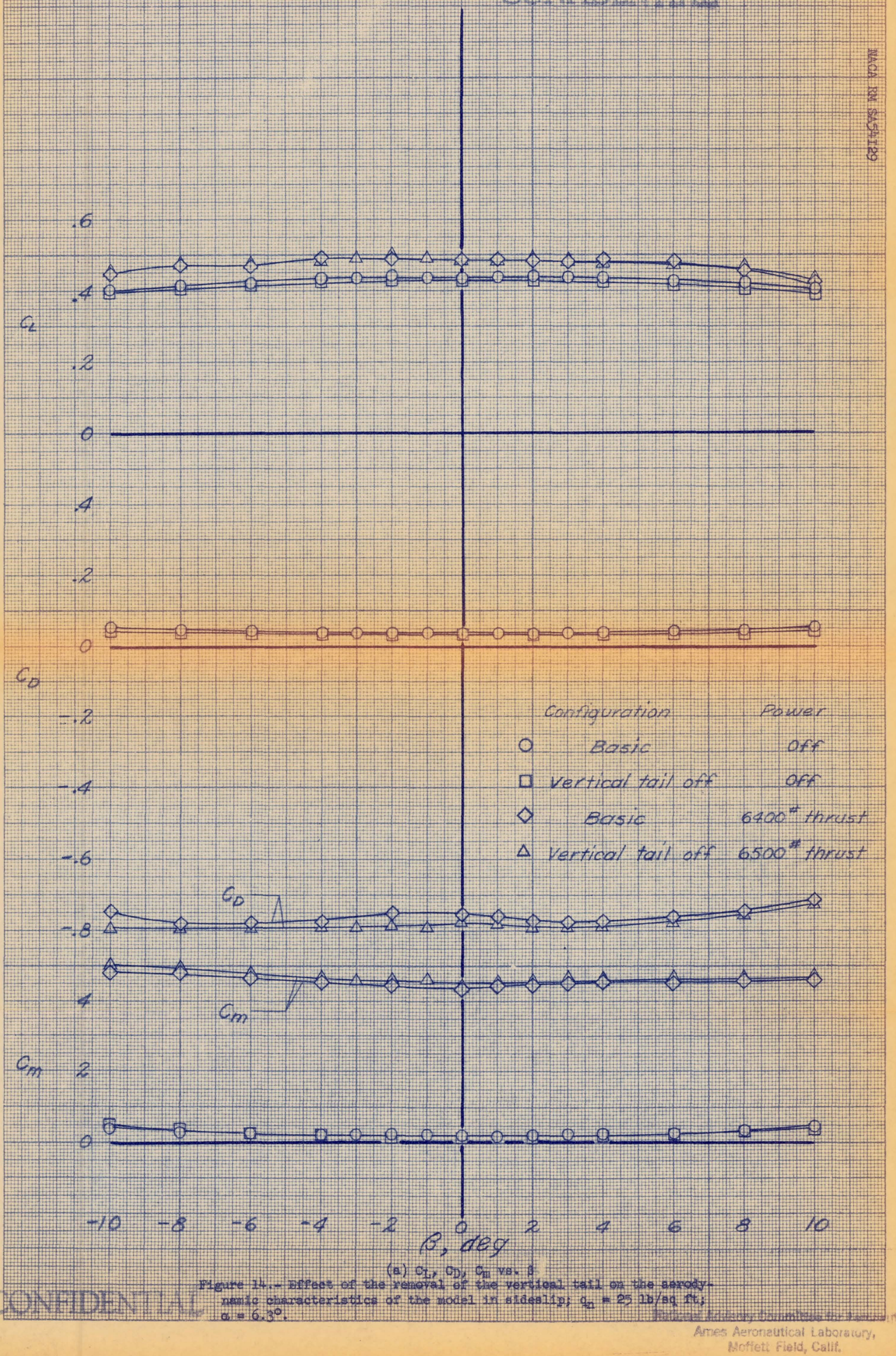

(a) C_L, C_D, C_m vs. β

Figure 14.- Effect of the removal of the vertical tail on the aerodynamic characteristics of the model in sideslip; q_m = 25 lb/sq ft; α = 6.3°.

	Configuration	Power
○	Basic	Off
□	Vertical tail off	Off
◇	Basic	6400 # thrust
△	Vertical tail off	6500 # thrust

C_Y: .28, .24, .20, .16, .12, .08, .04, 0, .01, 0

C_n: -.01, -.02, .04, .02, 0, -.02, -.04

C_l

-10 -8 -6 -4 -2 0 2 4 6 8 10

β, deg

(b) C_Y, C_n, C_l vs. β

Figure 14.- Concluded.

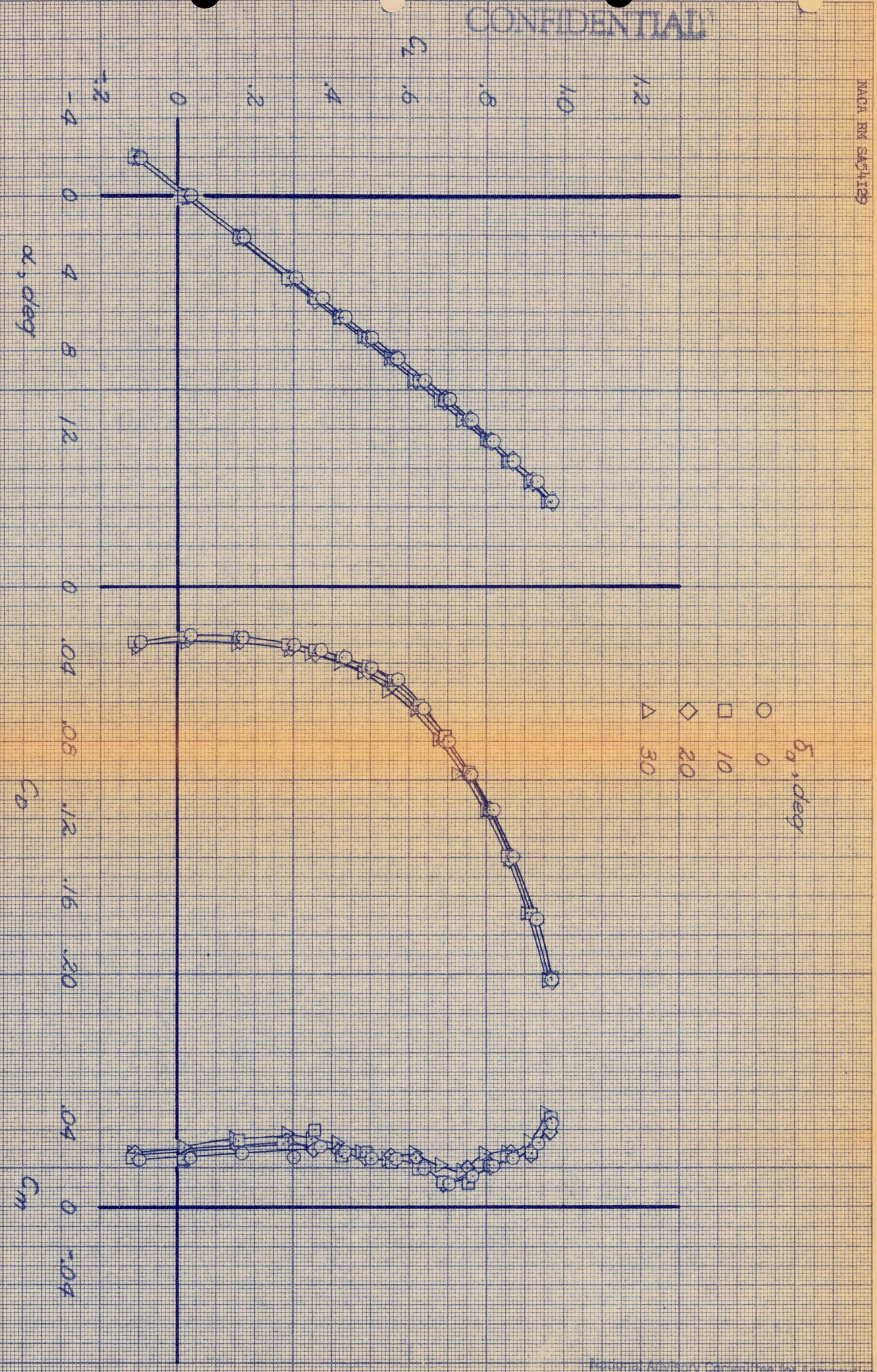

(a) C_L vs. α, C_D, C_m

Figure 15.- Characteristics of the basic model in pitch with elevon deflected for lateral control; q_m = 25 lb/sq ft; $\beta = 0^\circ$.

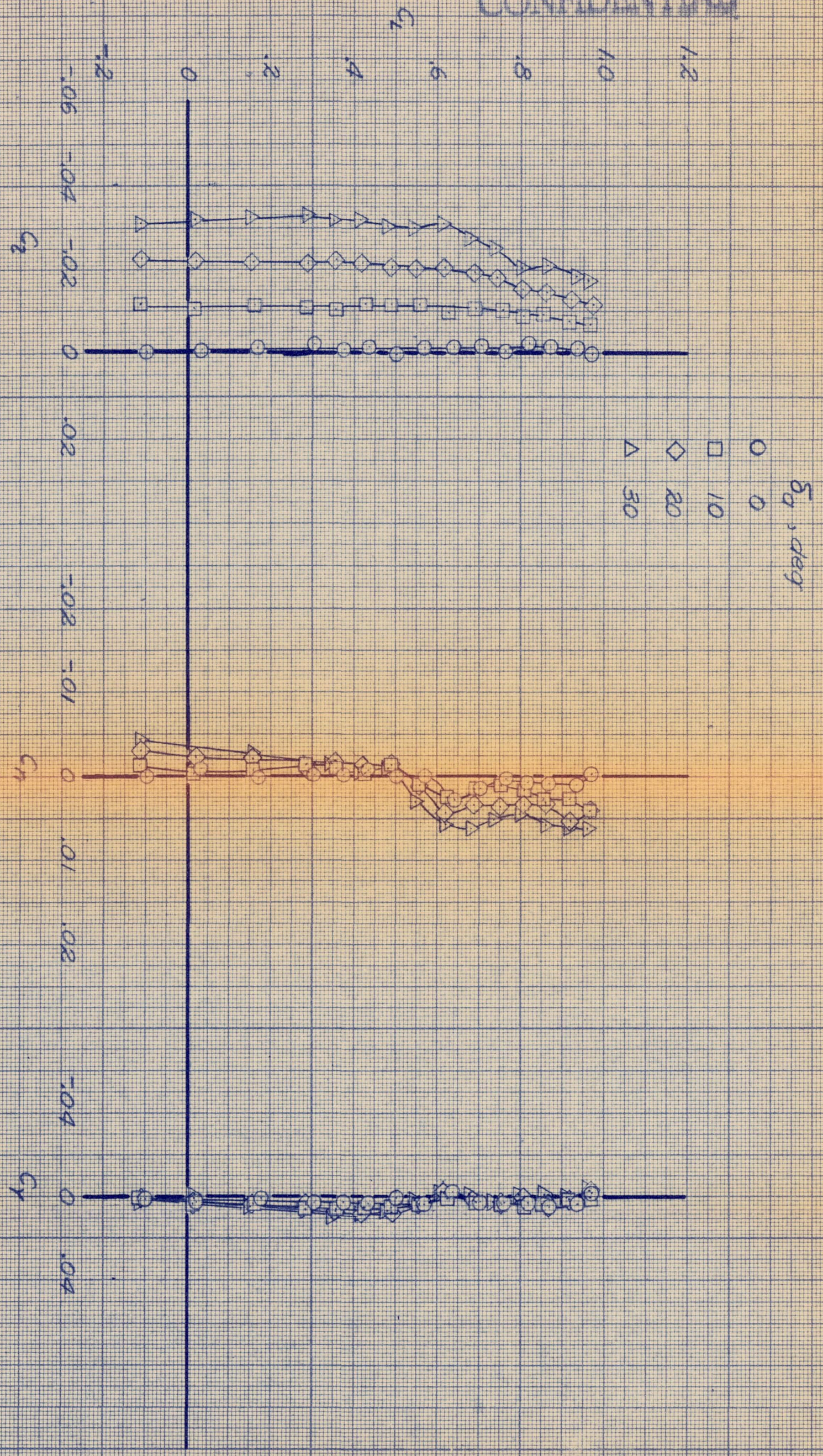

(b) C_L vs. C_l, C_n, C_Y

Figure 15.- Concluded.

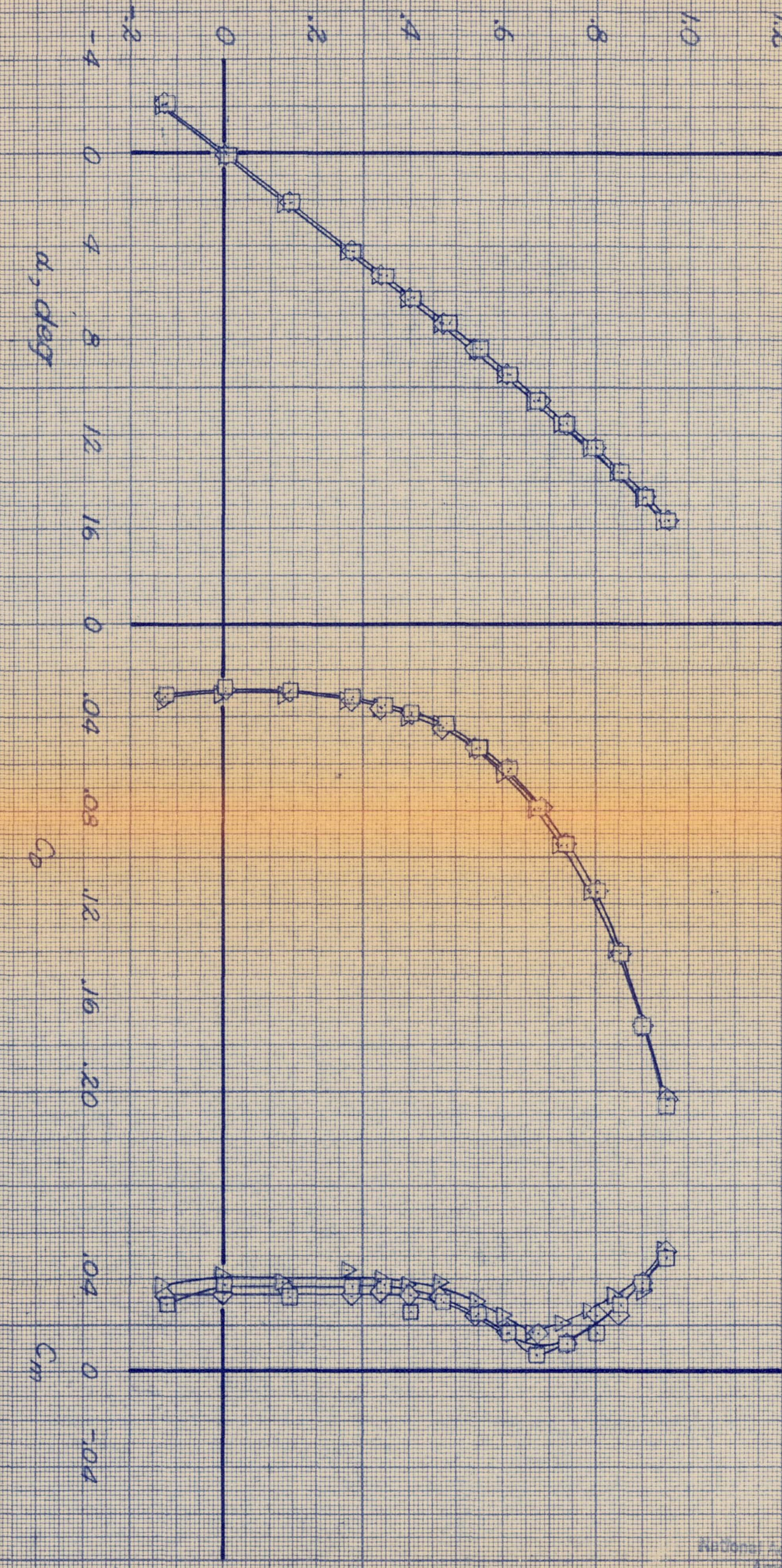

(a) C_L vs. α, C_D, C_m

Figure 16.- Characteristics of the basic model in pitch with elevon deflected as lateral controls; q_m = 25 lb/sq ft; β = -4°.

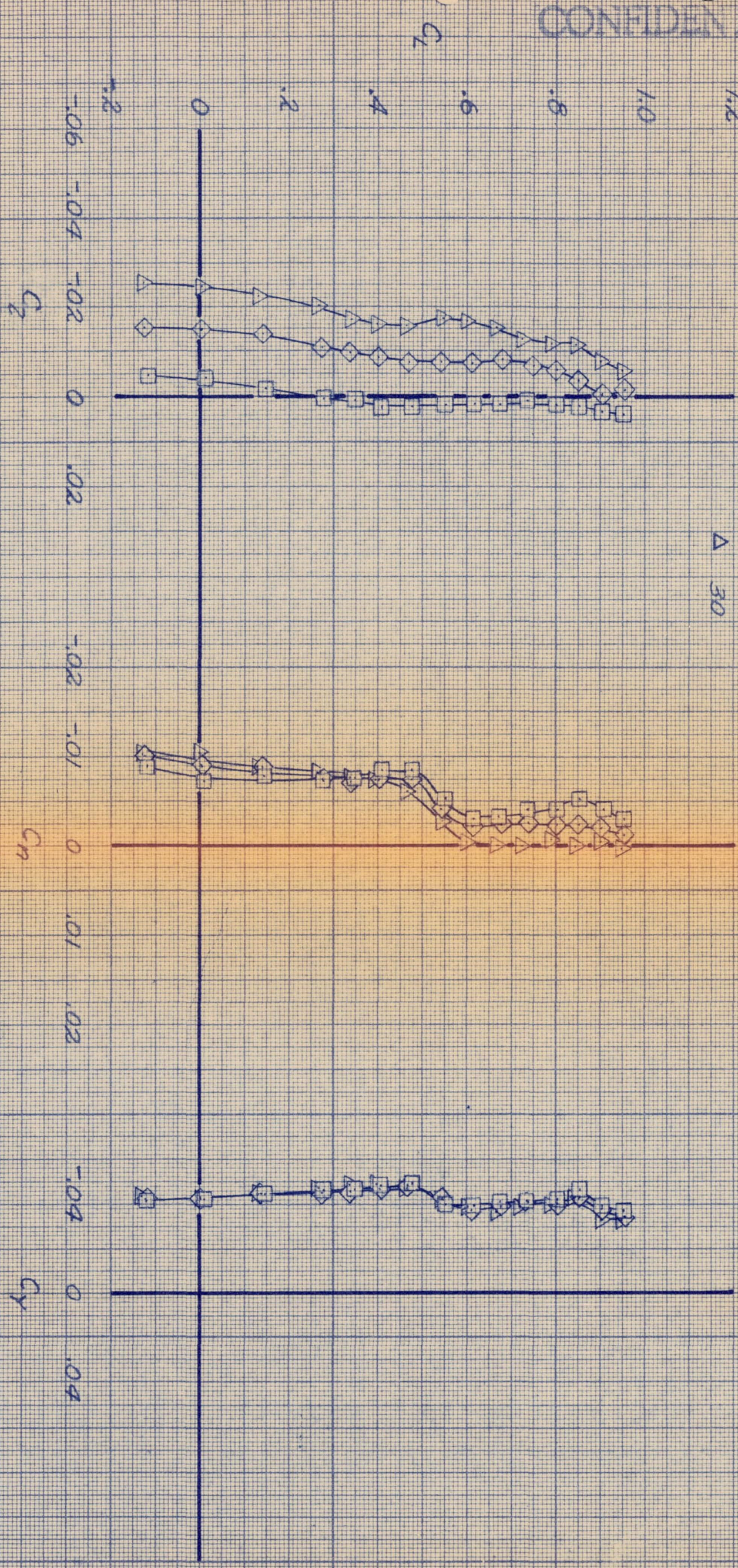

(b) C_L vs. C_l, C_n, C_Y

Figure 16.- Concluded.

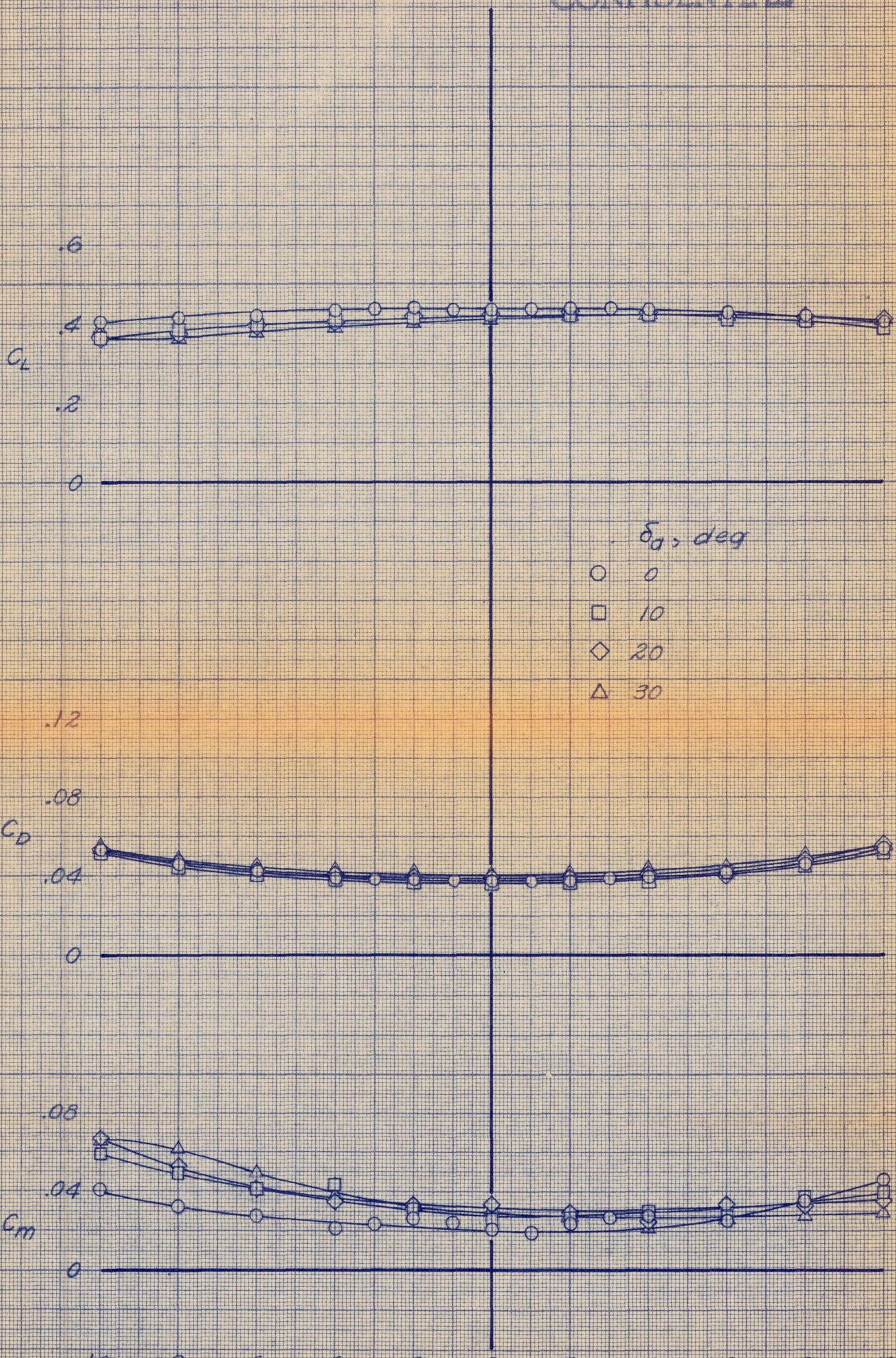

(a) C_L, C_D, C_m vs. β.

Figure 17.- Characteristics of the basic model in sideslip with elevon deflected as lateral control; q_m = 25 lb/sq ft; α = 6.3°.

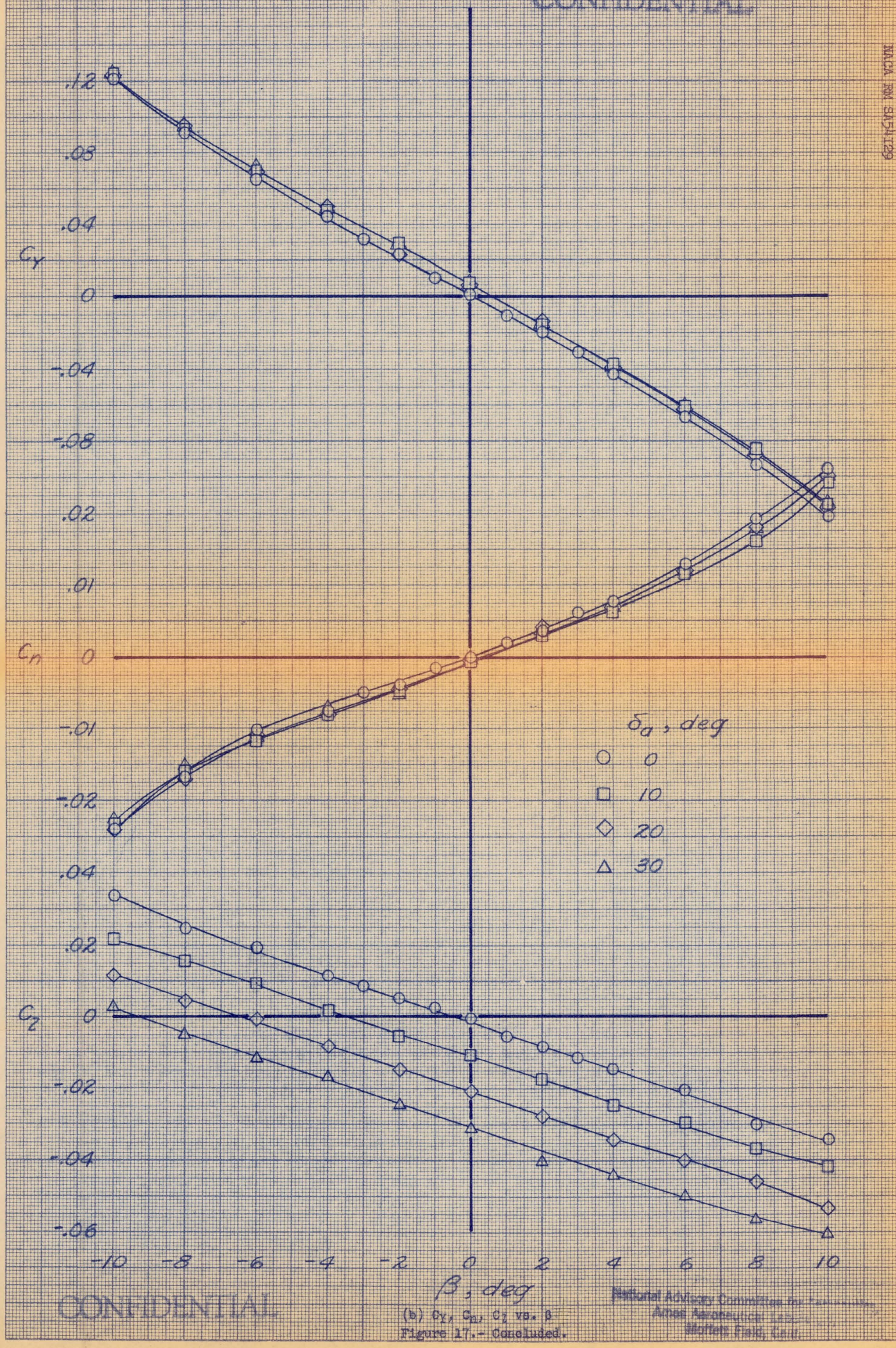

(b) C_Y, C_n, C_l vs. β

Figure 17.- Concluded.

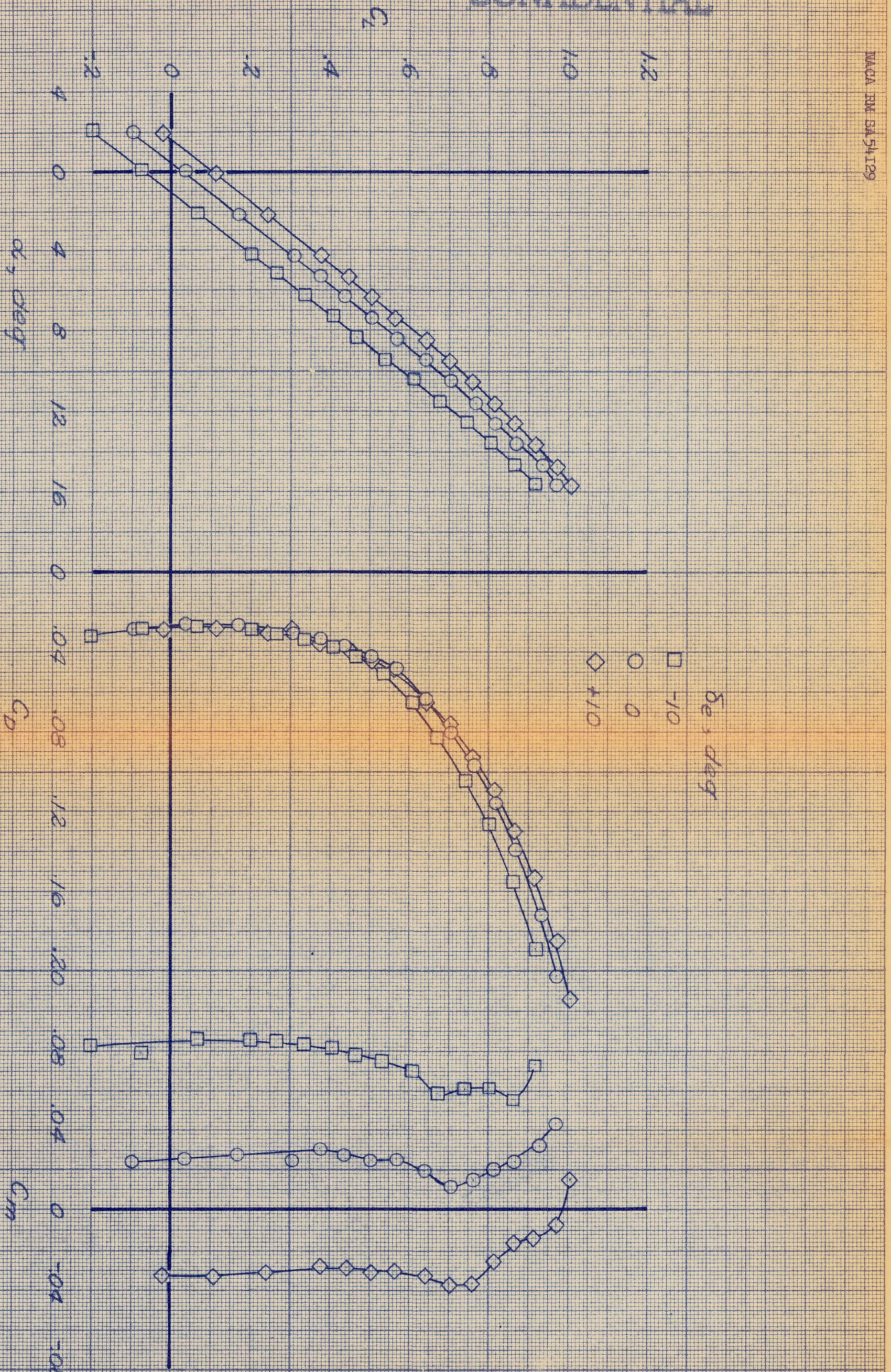

(a) C_L vs. α, C_D, C_m

Figure 18.- Characteristics of the basic model in pitch with elevons deflected as longitudinal controls; q_m = 25 lb/sq ft; $\beta = 0^\circ$.

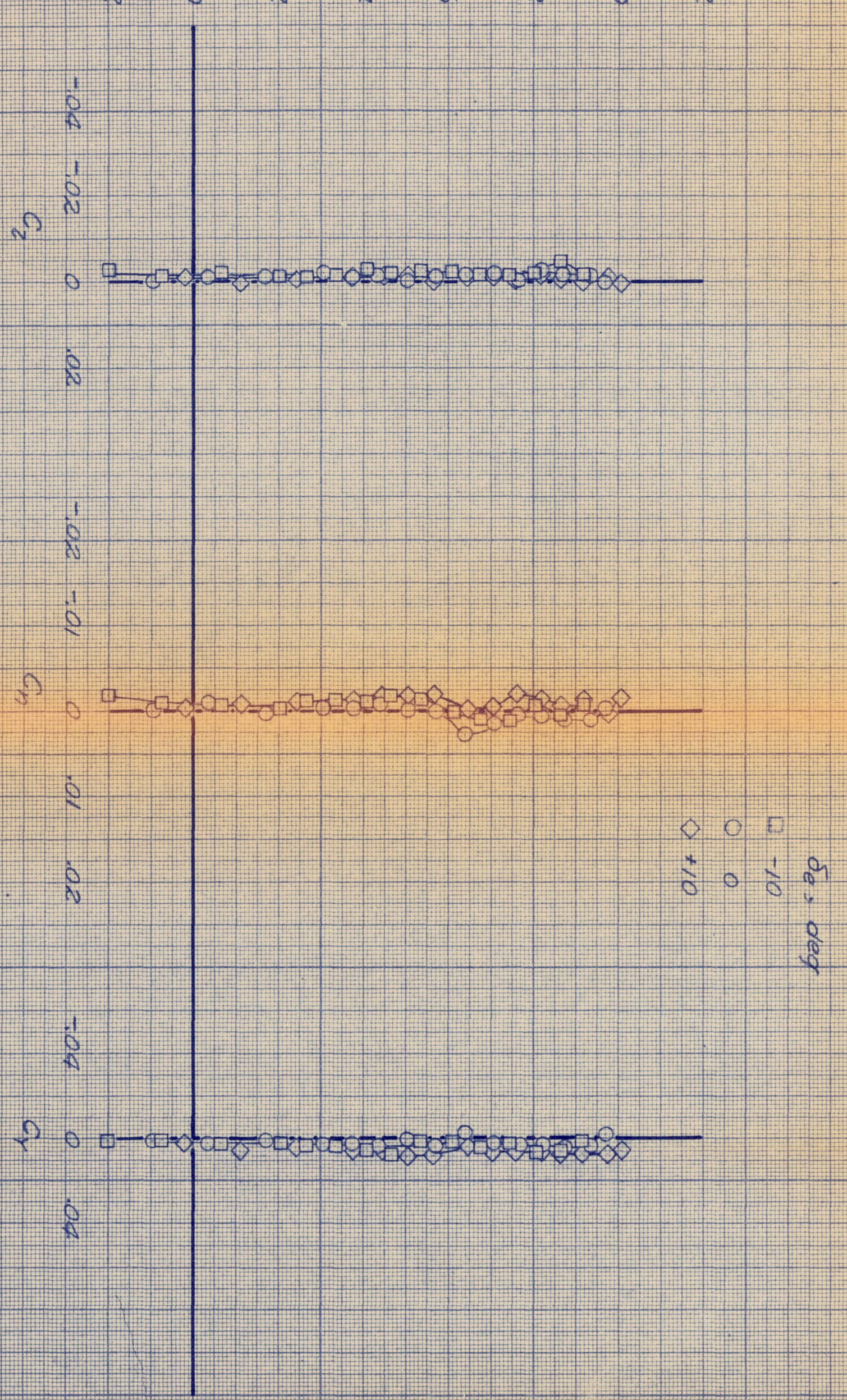

(b) C_L vs. C_l, C_n, C_Y

Figure 18.- Concluded.

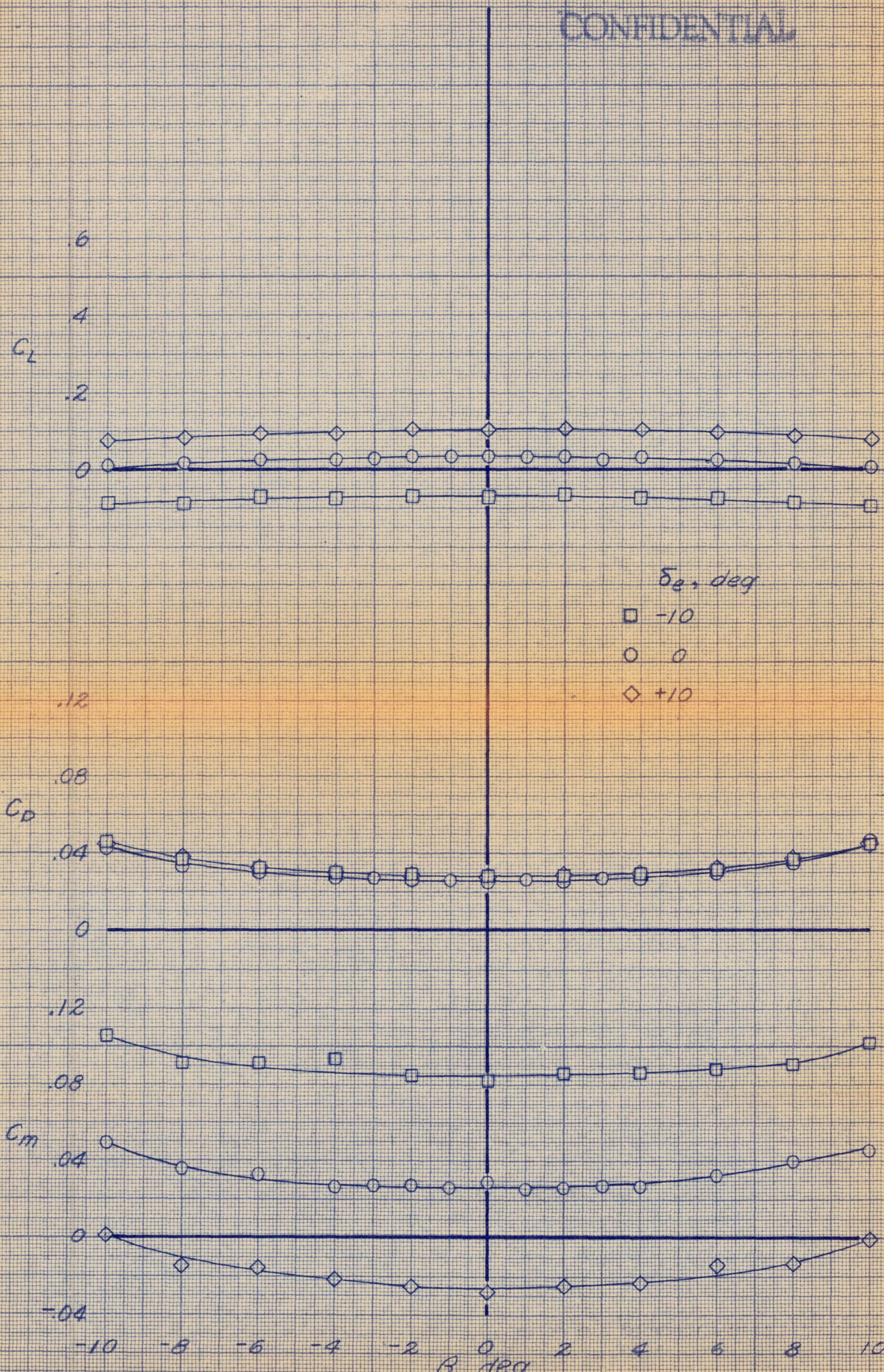

(a) $\alpha = 0.1^\circ$; C_L, C_D, C_m vs. β

Figure 19.- Characteristics of the basic model in sideslip with elevons deflected as longitudinal controls; q_m = 25 lb/sq ft.

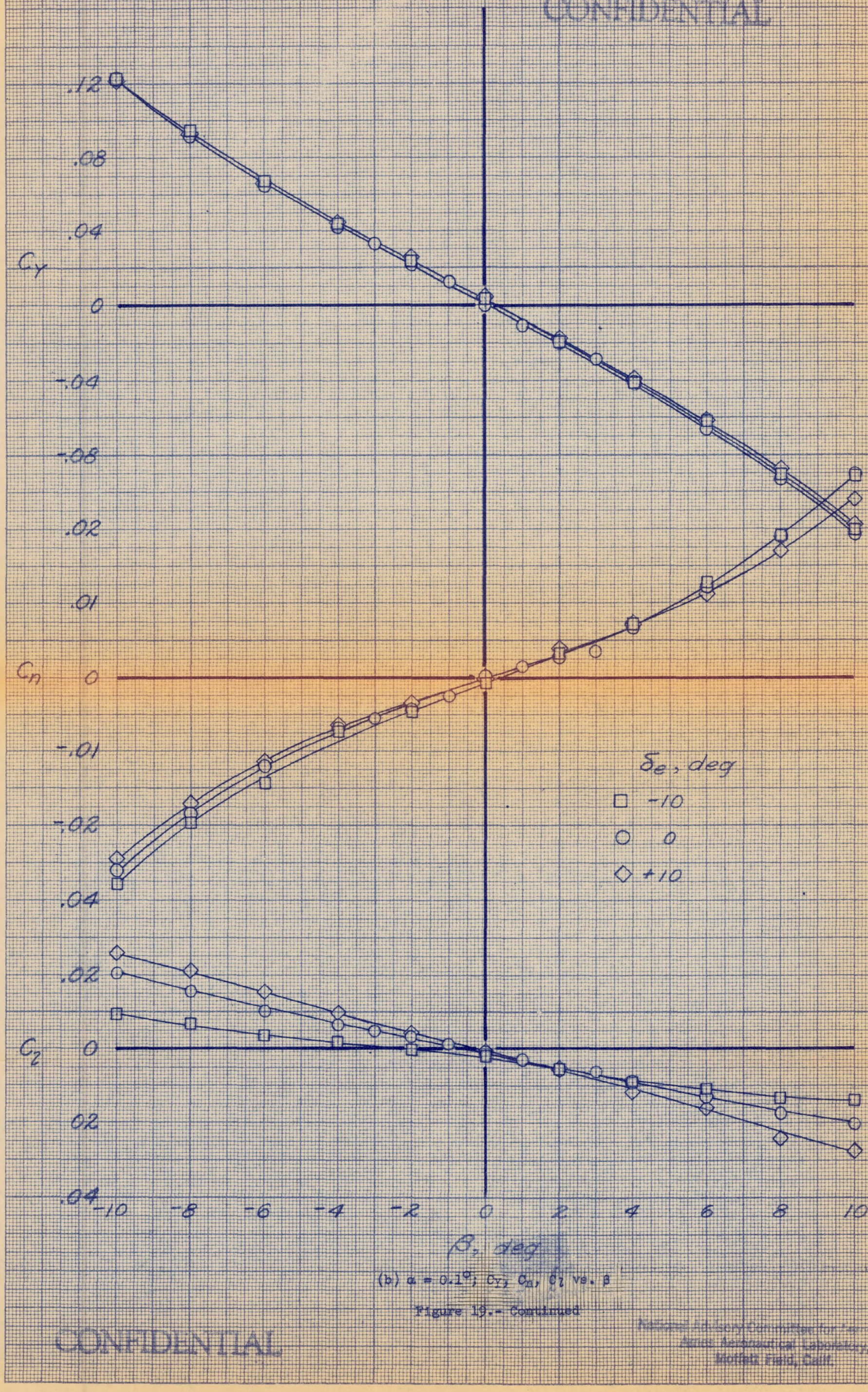

(b) $\alpha = 0.1^\circ$; C_Y, C_n, C_l vs. β

Figure 19.- Continued

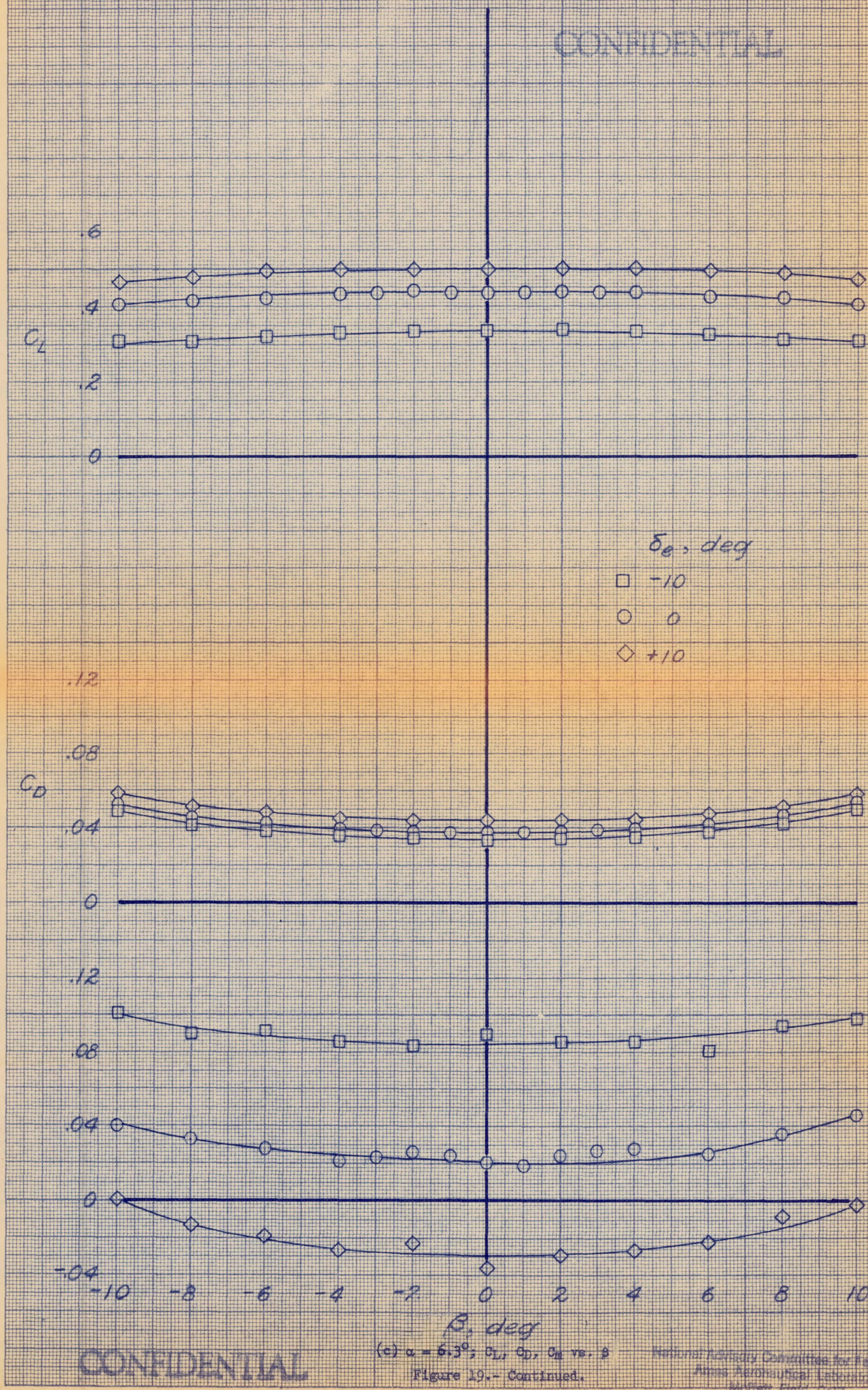

(c) $\alpha = 6.3^\circ$; C_L, C_D, C_m vs. β

Figure 19.- Continued.

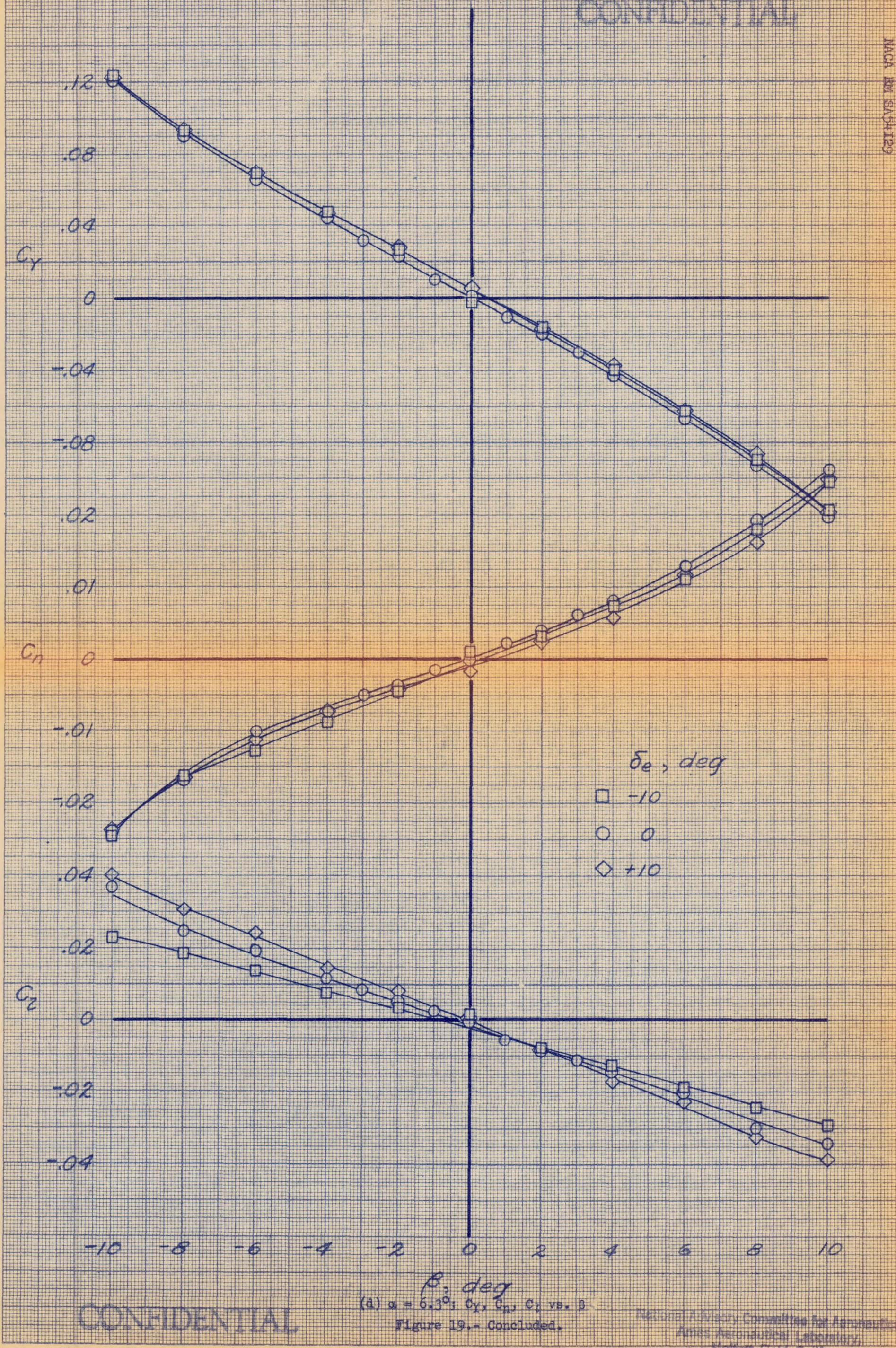

(d) $\alpha = 6.3^\circ$; C_Y, C_n, C_l vs. β

Figure 19.- Concluded.

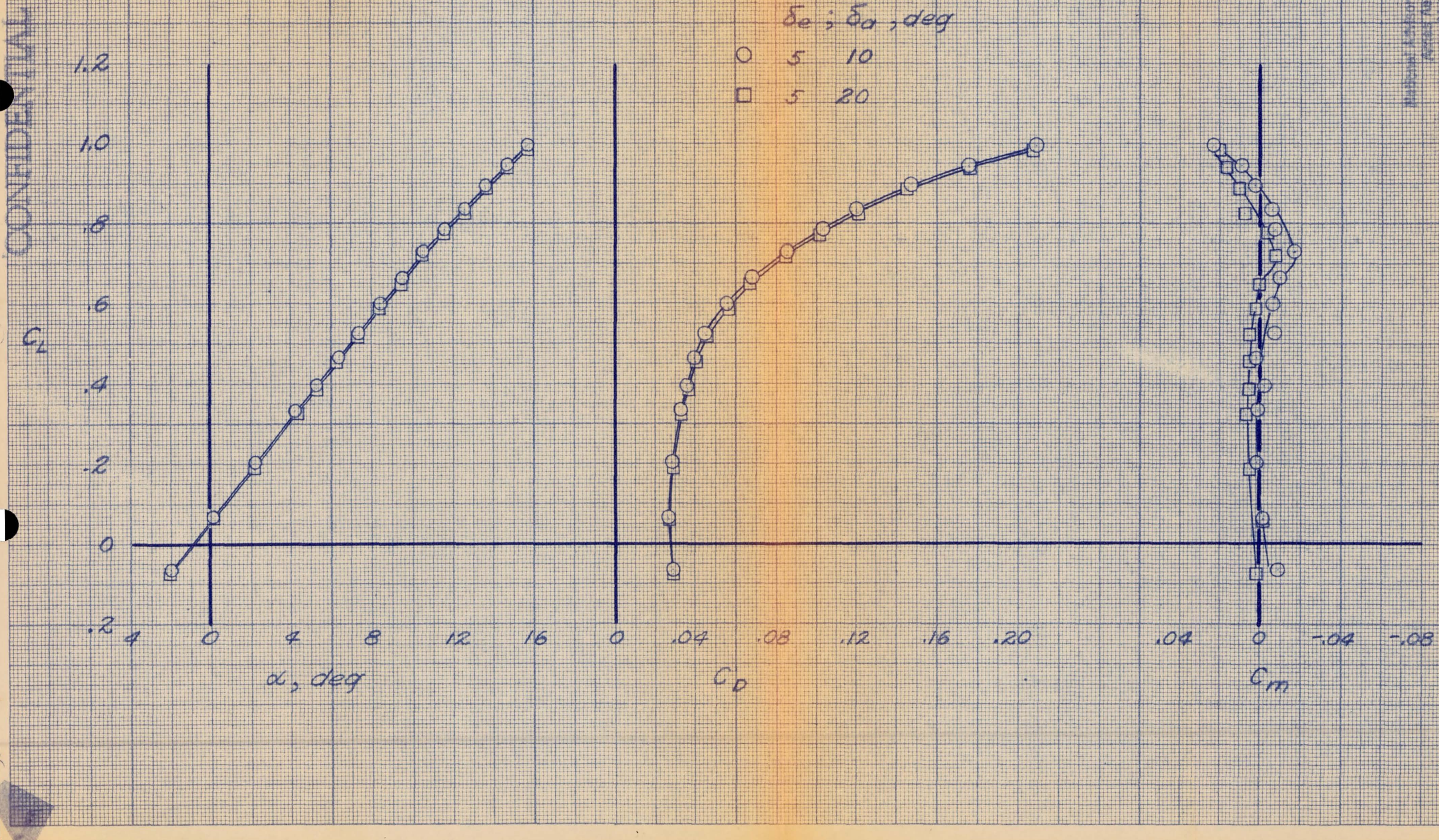

Figure 20.- Characteristics of the basic model in pitch with elevons deflected as combined lateral and longitudinal controls; q_p = 25 lb/sq ft, β = 0°.

(a) C_L vs. α, C_D, C_m.

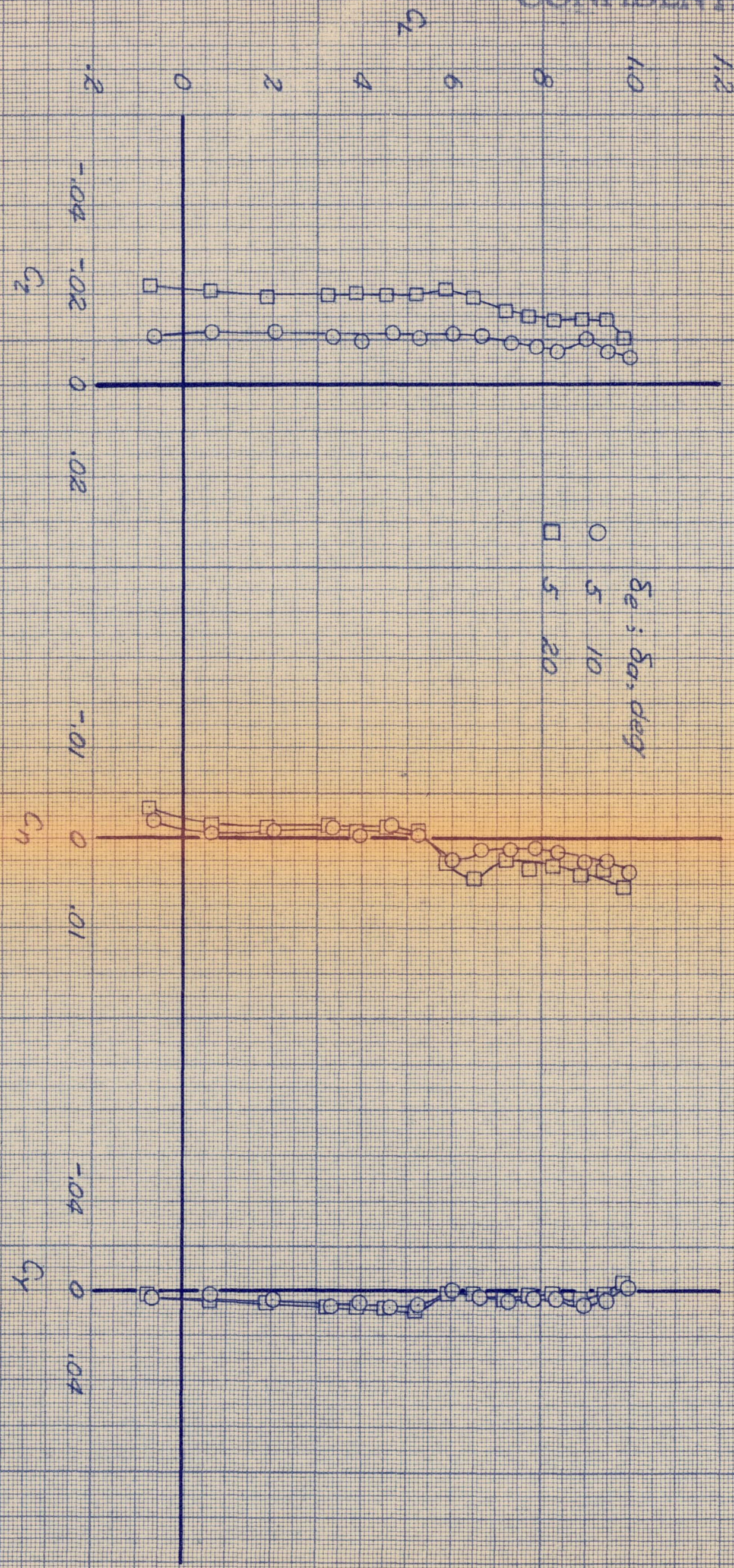

(b) C_L vs. C_l, C_n, C_Y

Figure 20.- Concluded.

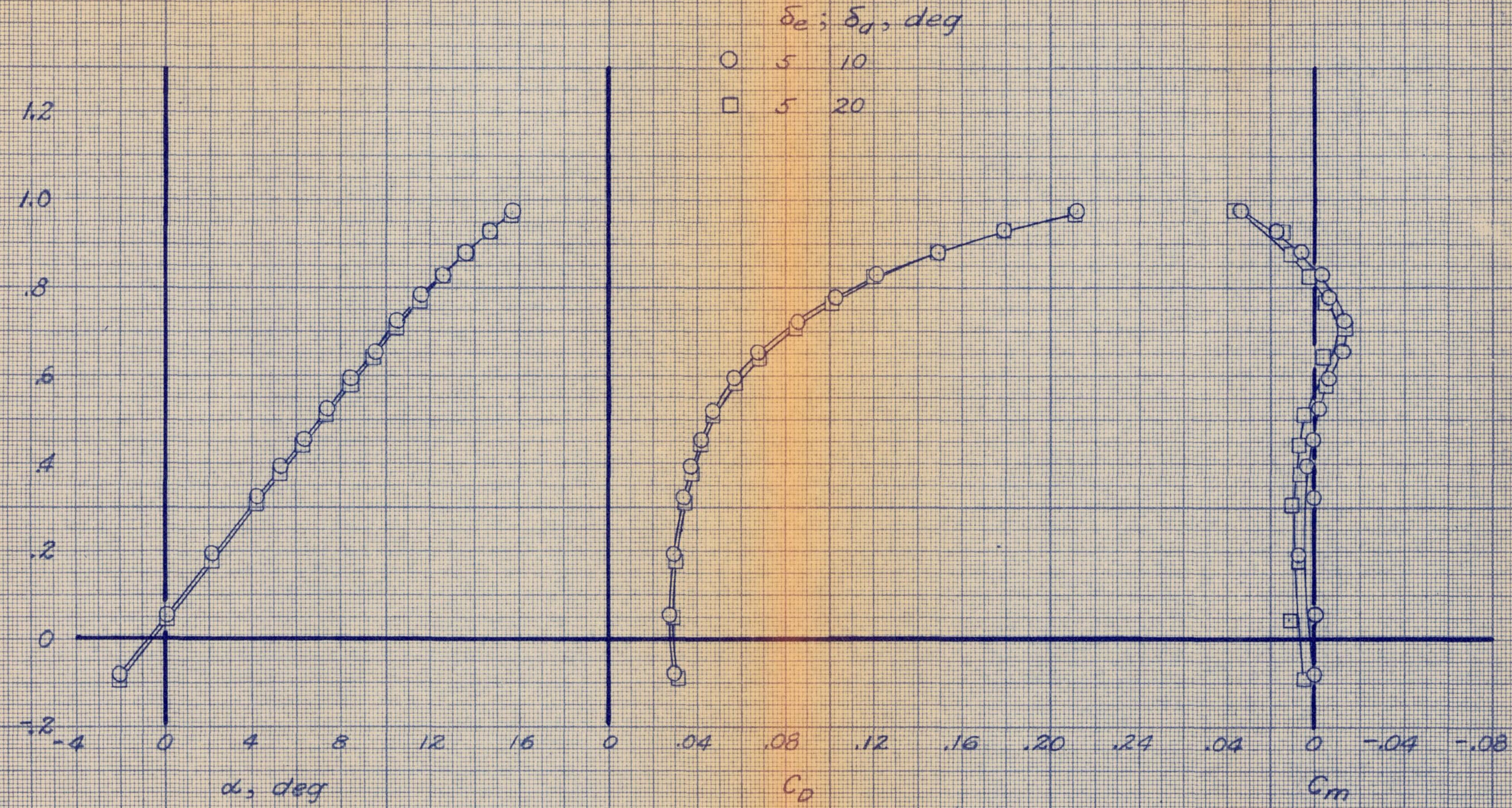

Figure 21.- Characteristics of the basic model in pitch with elevons deflected as combined lateral and longitudinal controls; q_a = 25 lb/sq ft; $\beta = 4^\circ$.

(a) C_L vs. α, C_D, C_m

D-82 Fig 21a

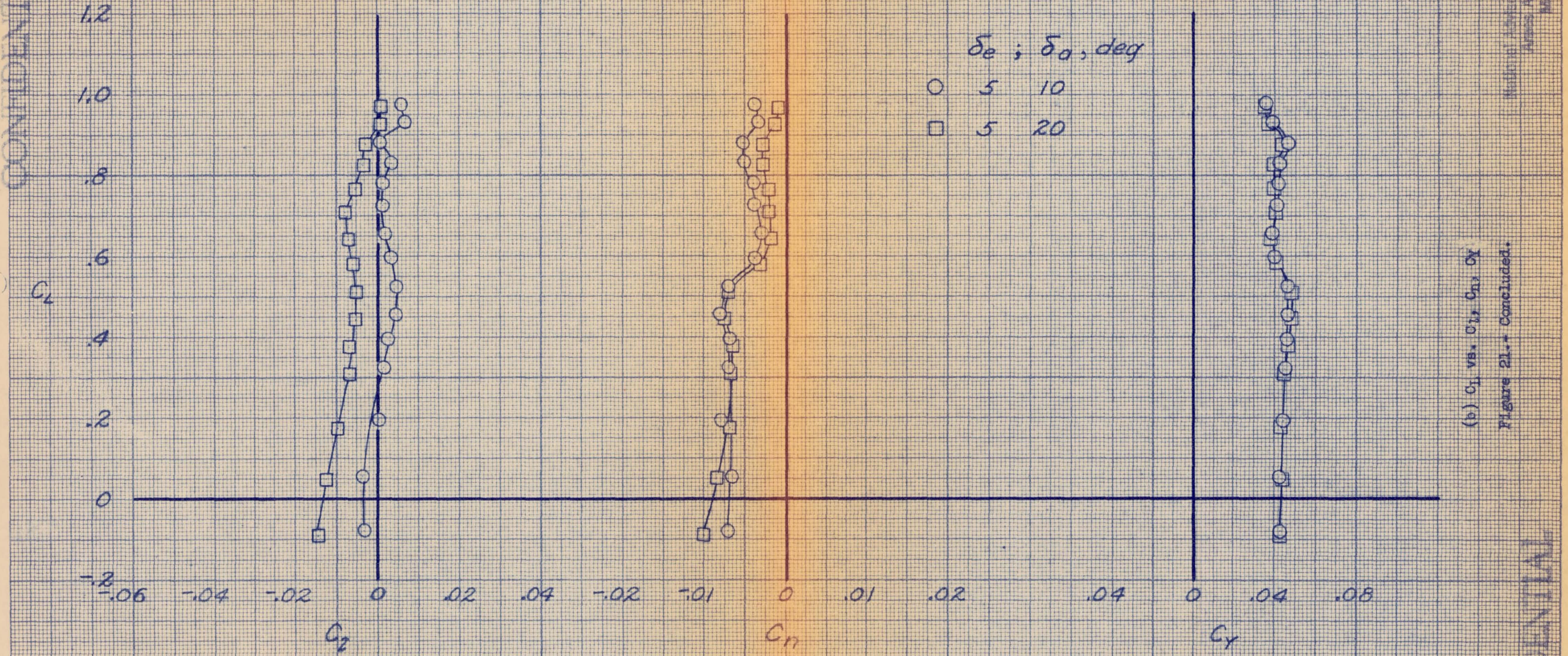

(b) C_l vs. C_L, C_n, C_Y.

Figure 21.- Concluded.

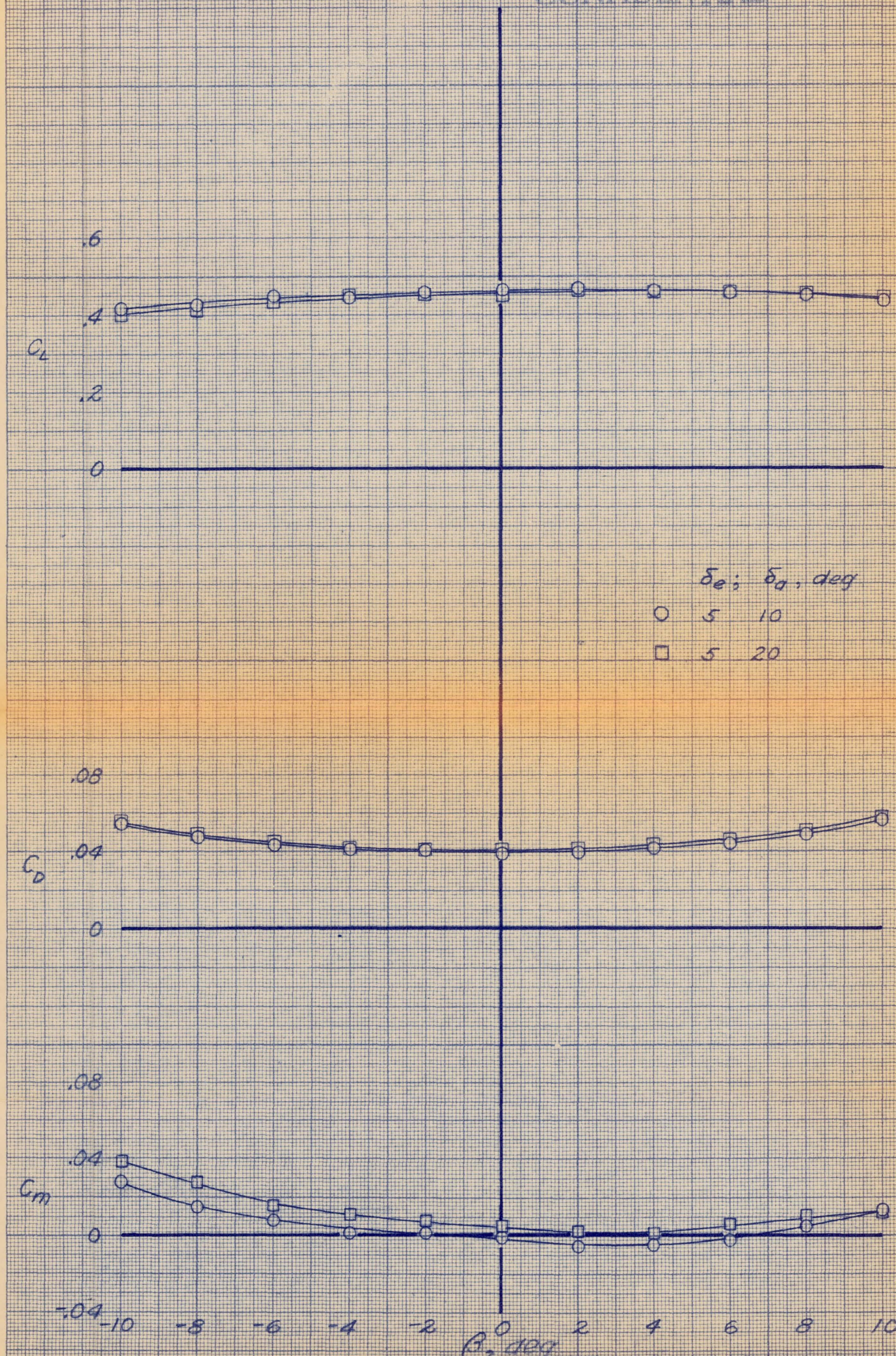

(a) C_L, C_D, C_m vs. β

Figure 22.- Characteristics of the basic model in sideslip with elevons deflected as combined lateral and longitudinal controls; q_n = 25 lb/sq ft; α = 6.3°.

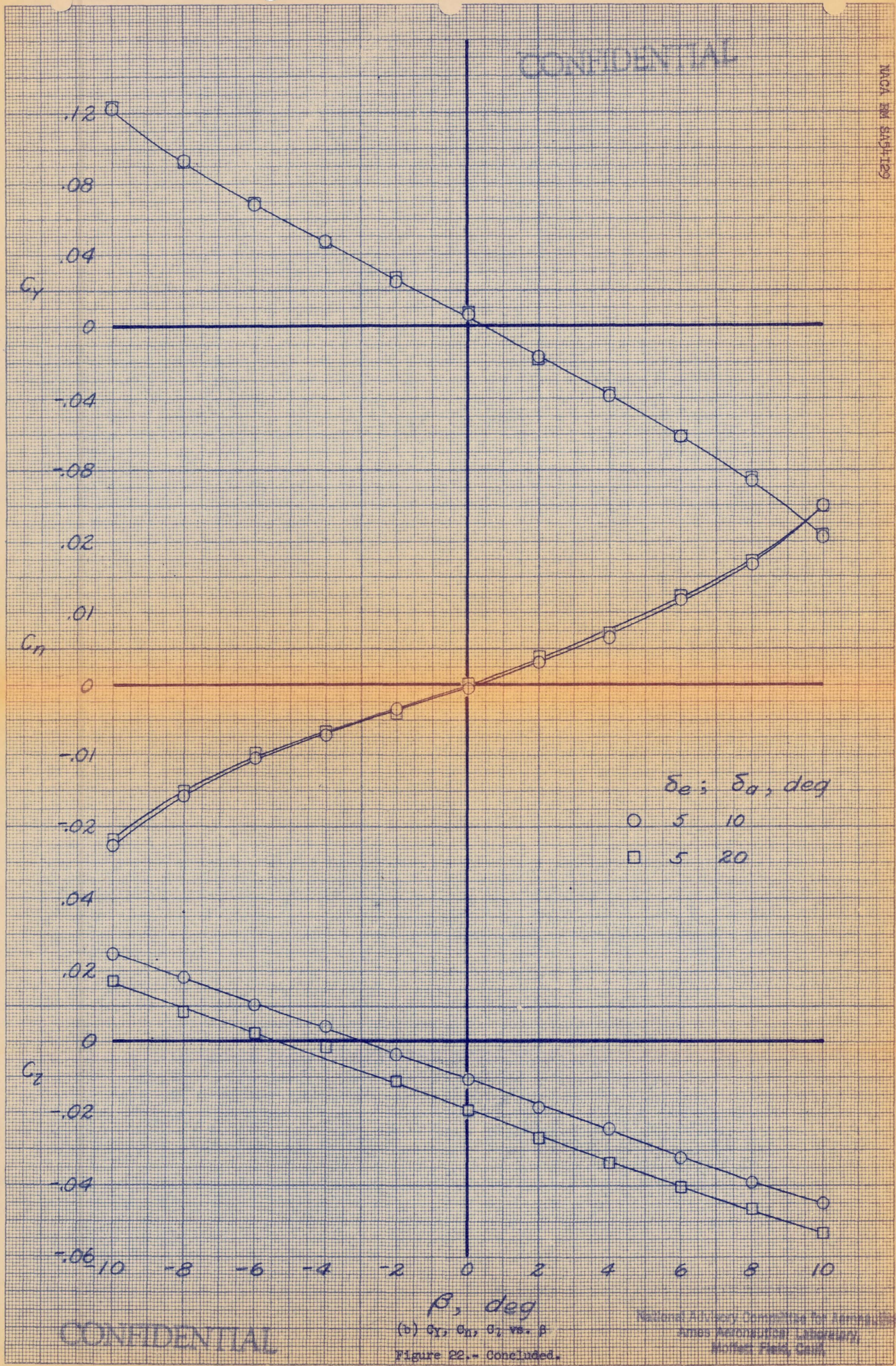

(b) C_Y, C_n, C_l vs. β

Figure 22.- Concluded.

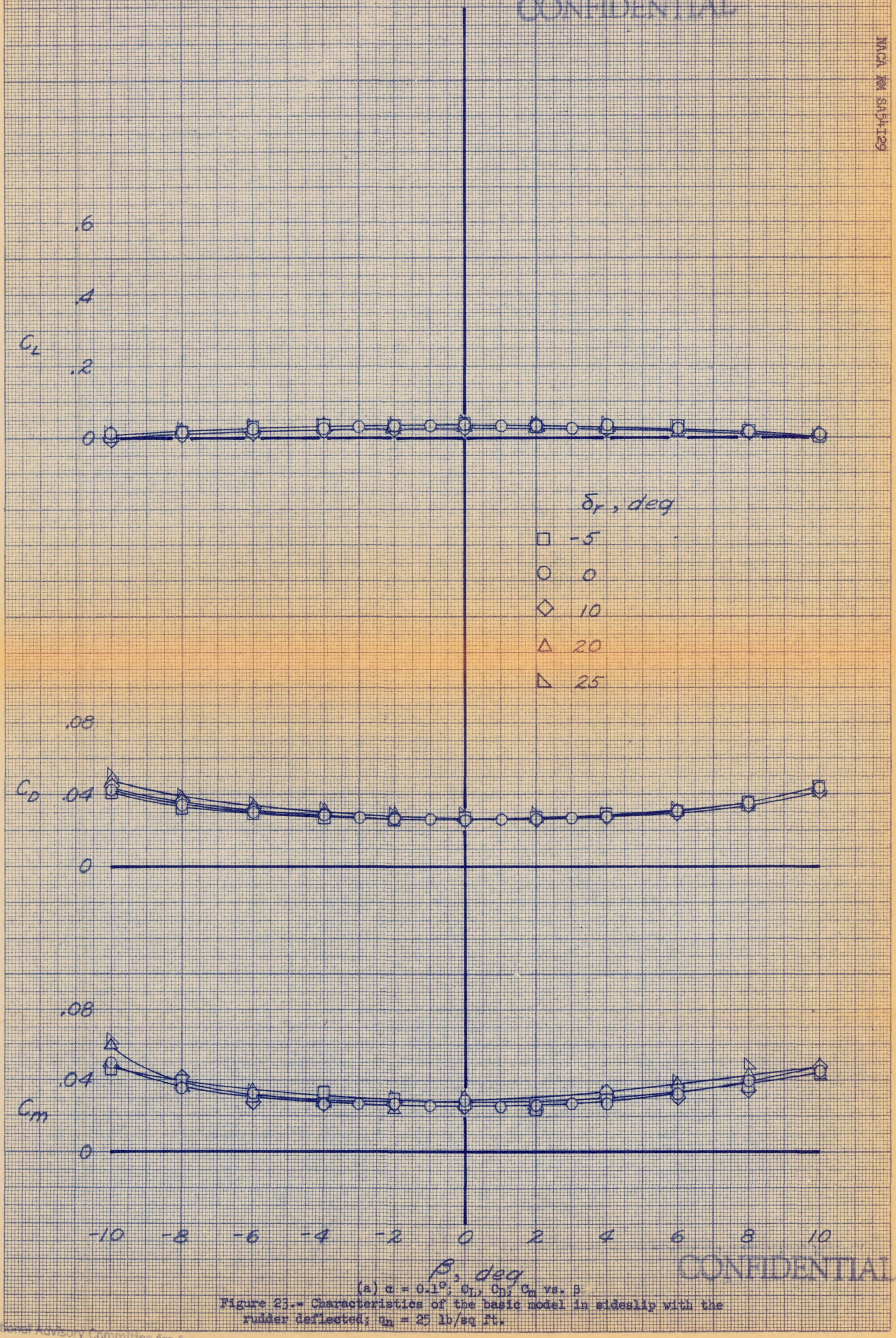

(a) $\alpha = 0.1^\circ$; C_L, C_D, C_m vs. β

Figure 23.- Characteristics of the basic model in sideslip with the rudder deflected; q_m = 25 lb/sq ft.

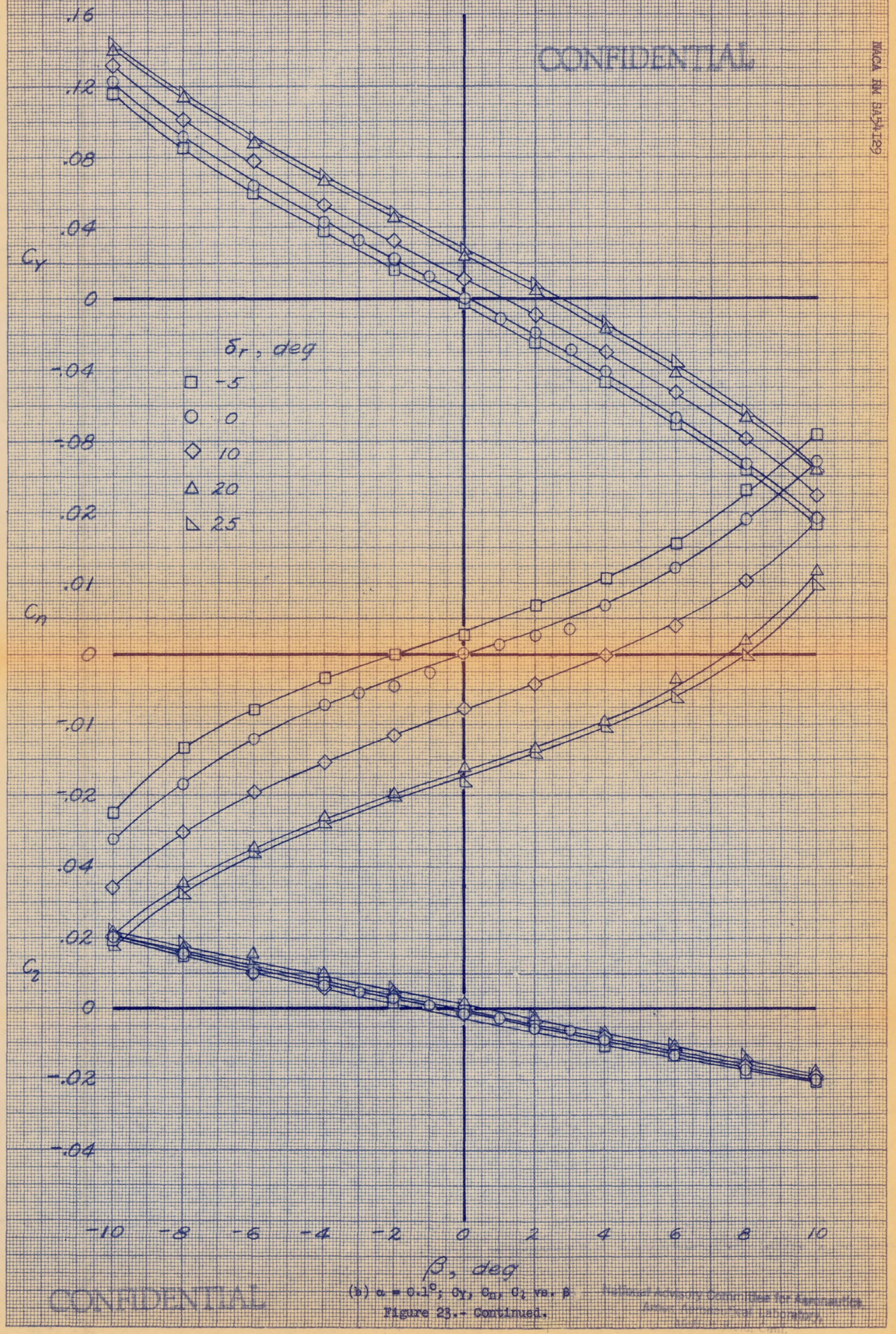

(b) $\alpha = 0.1^\circ$; C_Y, C_n, C_l vs. β

Figure 23.- Continued.

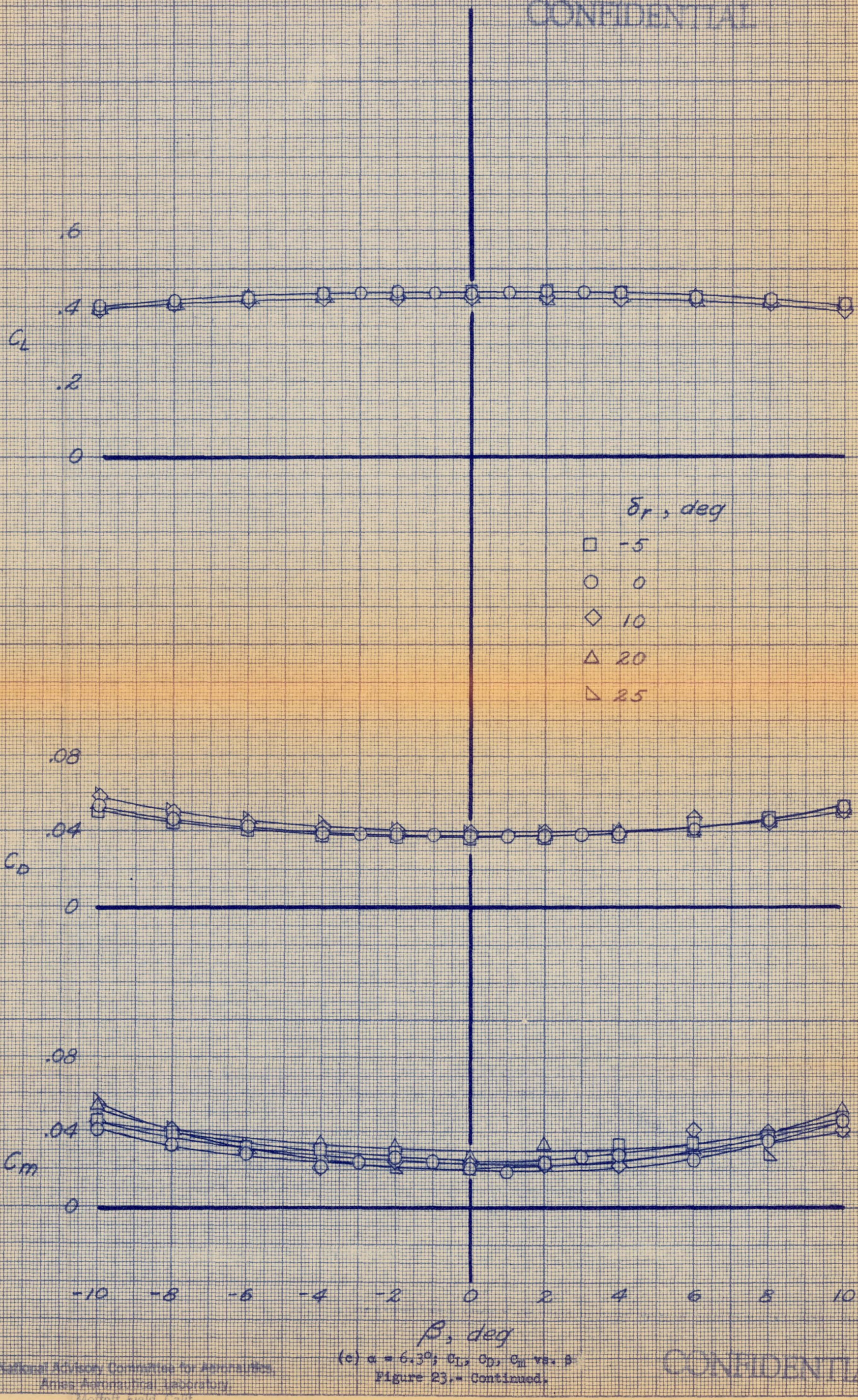

(c) $\alpha = 6.3°$; C_L, C_D, C_m vs. β

Figure 23.- Continued.

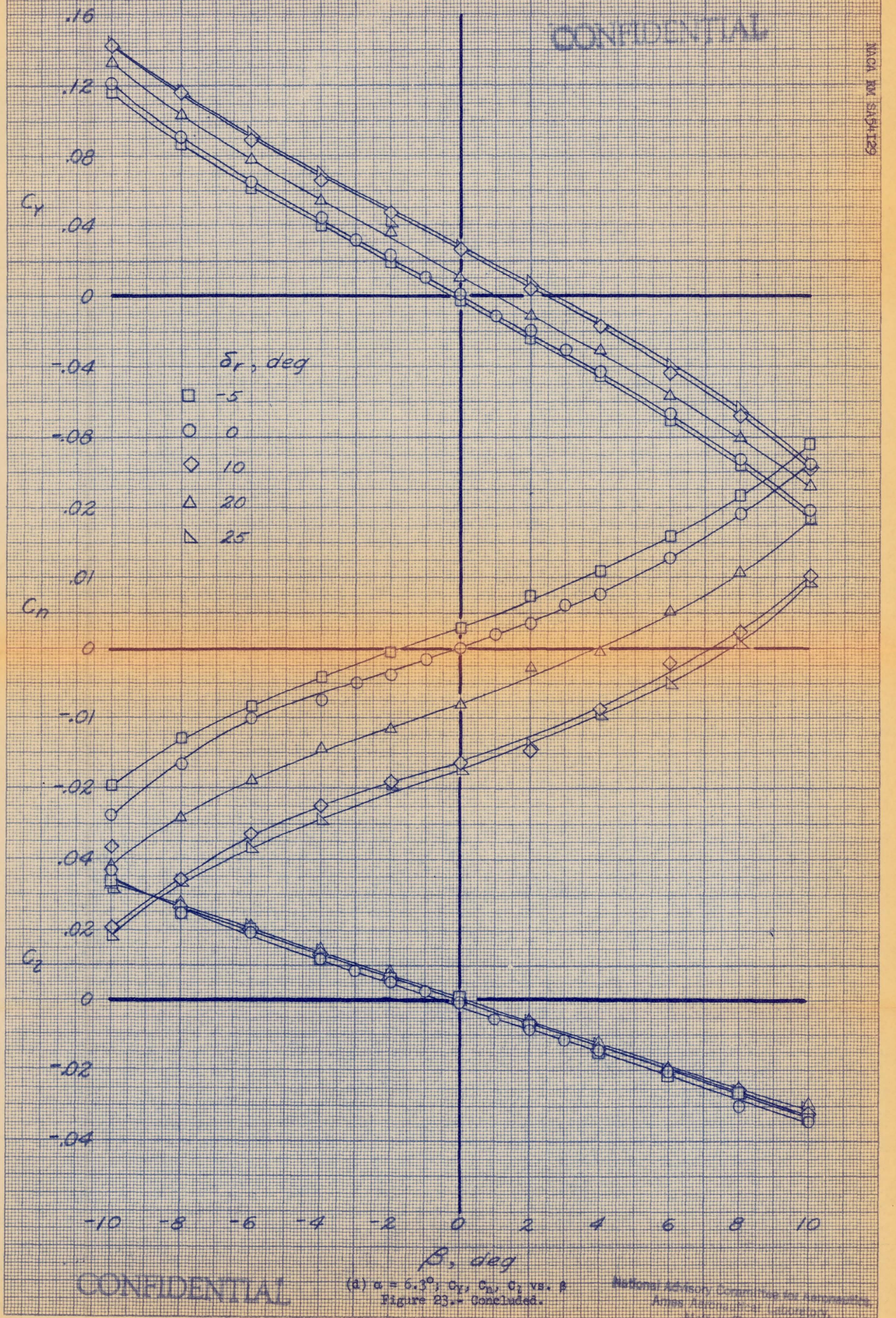

(d) $\alpha = 6.3°$; C_Y, C_n, C_l vs. β

Figure 23.- Concluded.

○ Model with trailing-edge extension

□ Model with trailing-edge extension, wing-body junction sealed

◇ Basic model

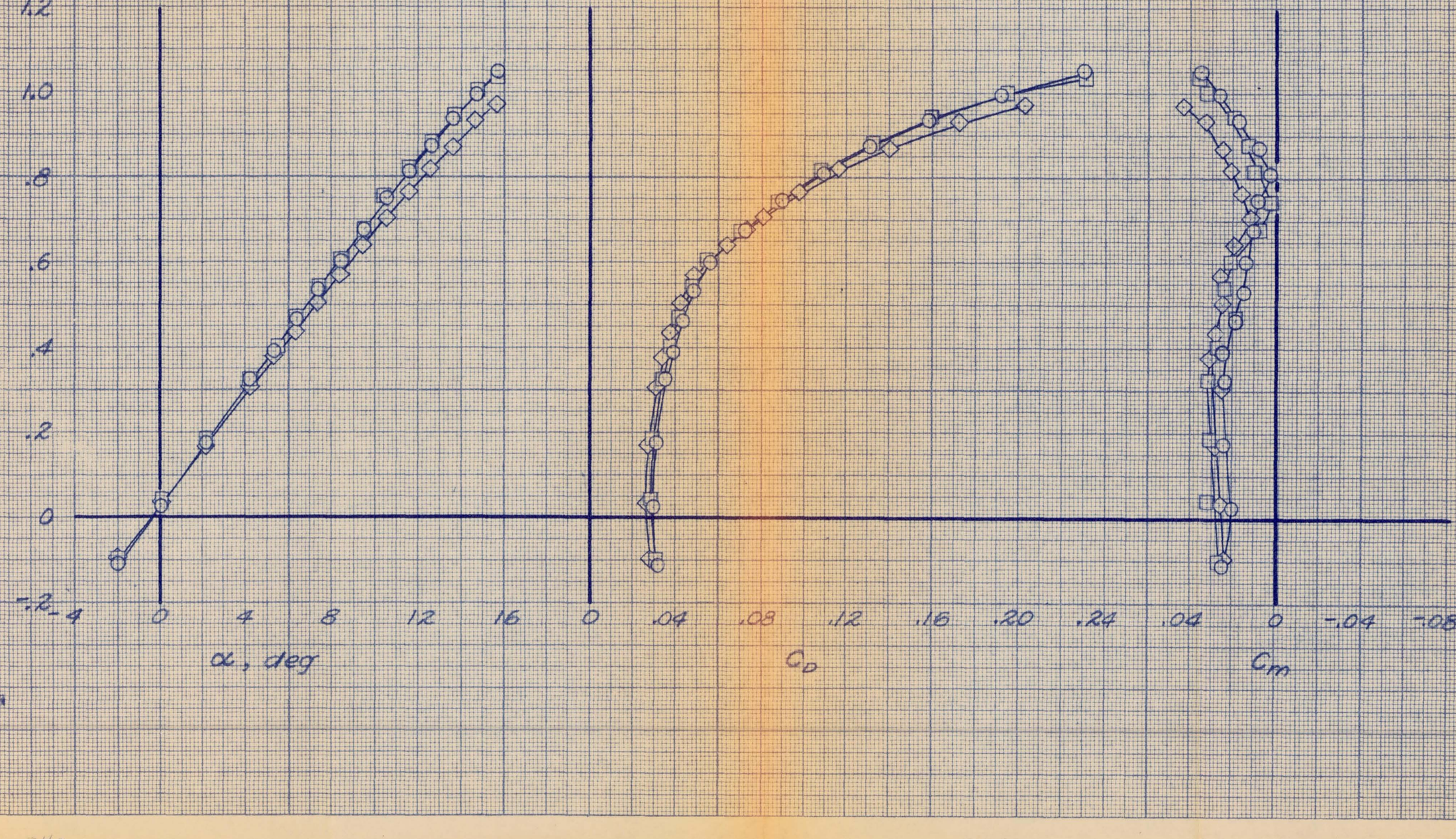

Figure 24.- Effect of the addition of the trailing-edge chord extension on the characteristics of the model. (a) C_L vs. α, C_D, C_m. M_a = 2.5 lb/sq ft; β = 0°.

CONFIDENTIAL

○ Model with trailing-edge extension

□ Model with trailing-edge extension, wing-body junction sealed

◇ Basic model

(b) C_l vs. C_l, C_n, C_Y

Figure 24.- Concluded.

National Advisory Committee for Aeronautics
Ames Aeronautical Laboratory
Moffett Field, Calif.

CONFIDENTIAL

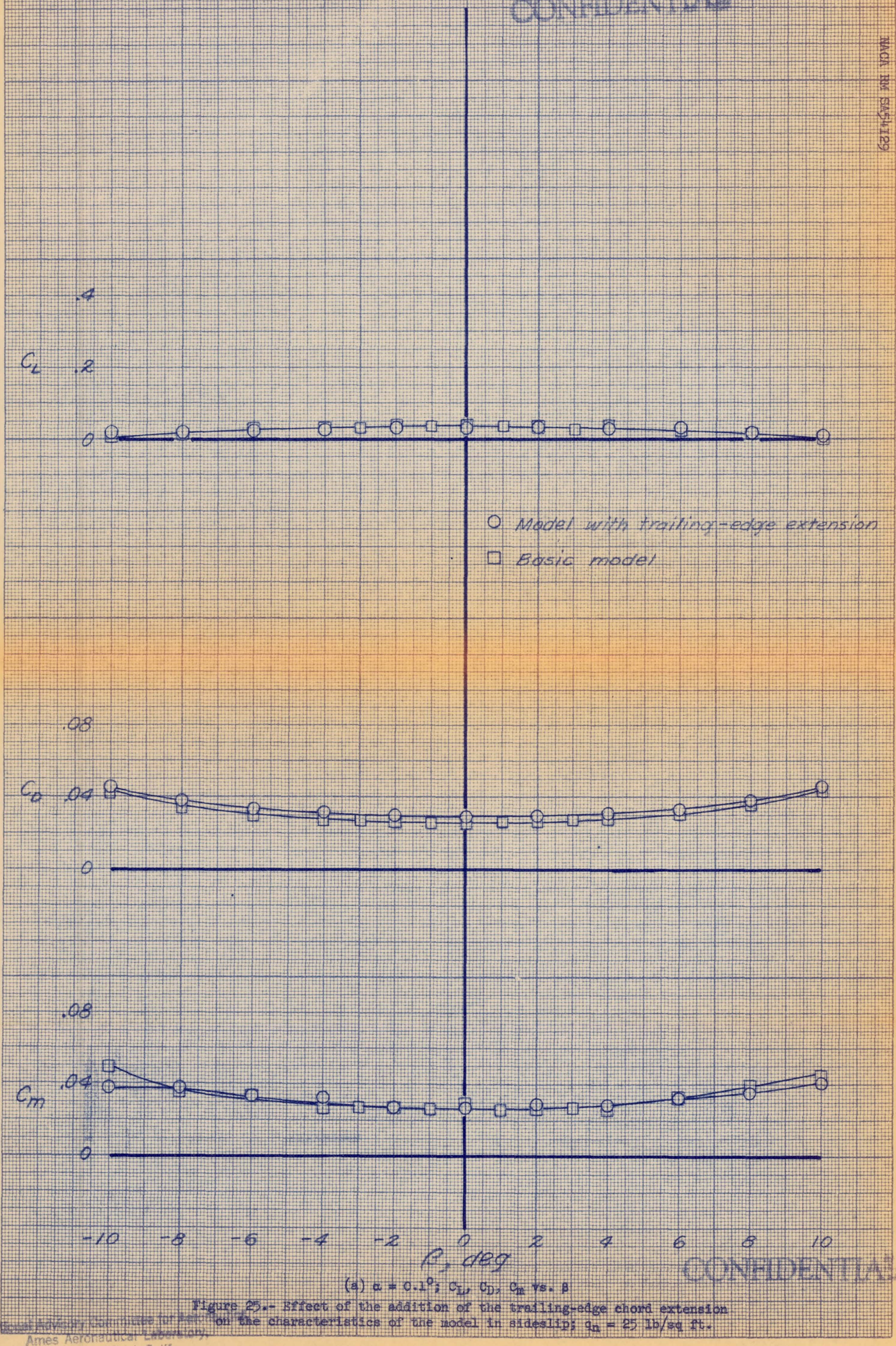

(a) $\alpha = 0.1^\circ$; C_L, C_D, C_m vs. β

Figure 25.- Effect of the addition of the trailing-edge chord extension on the characteristics of the model in sideslip; q_m = 25 lb/sq ft.

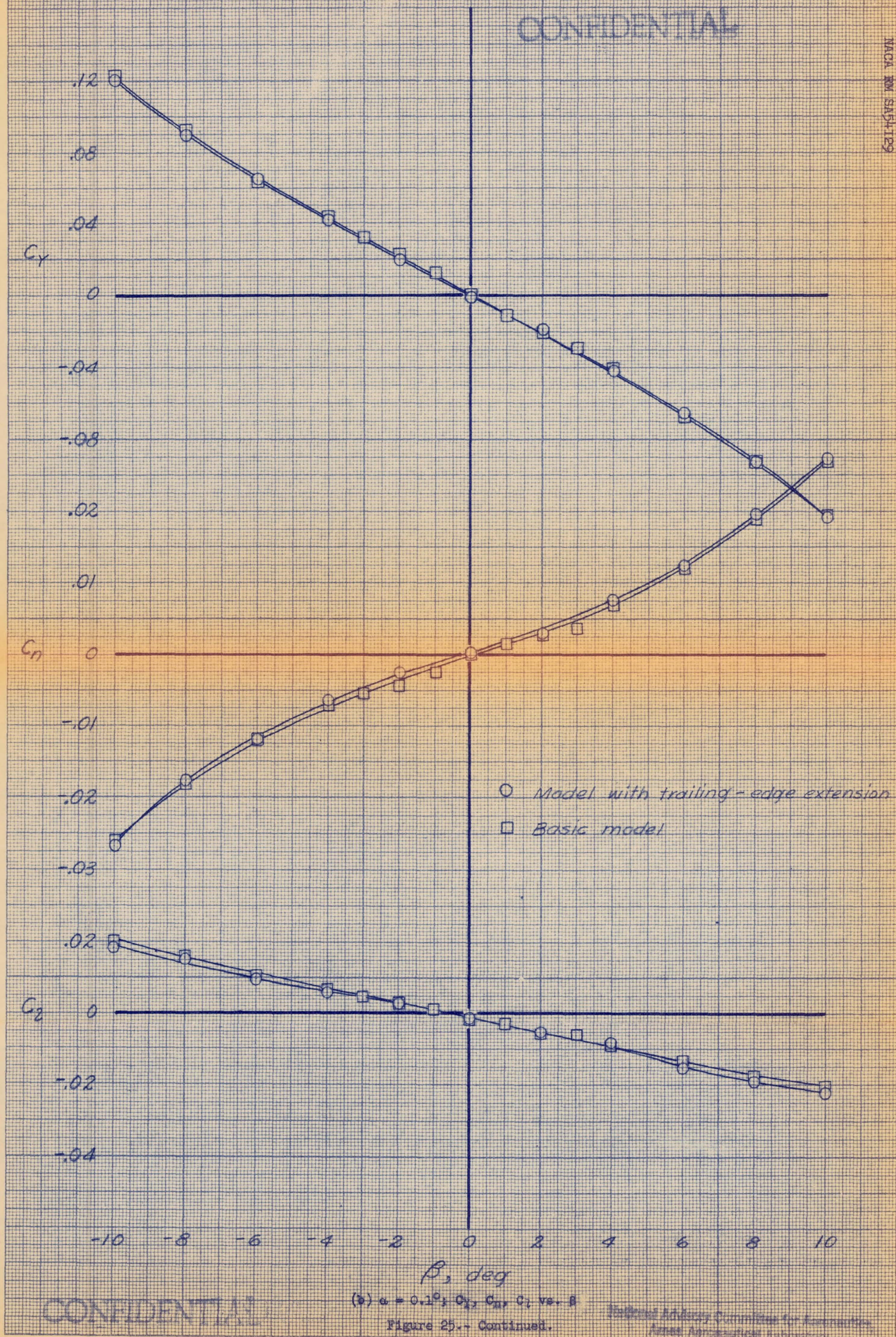

(b) $\alpha = 0.1^\circ$; C_Y, C_n, C_l vs. β

Figure 25.- Continued.

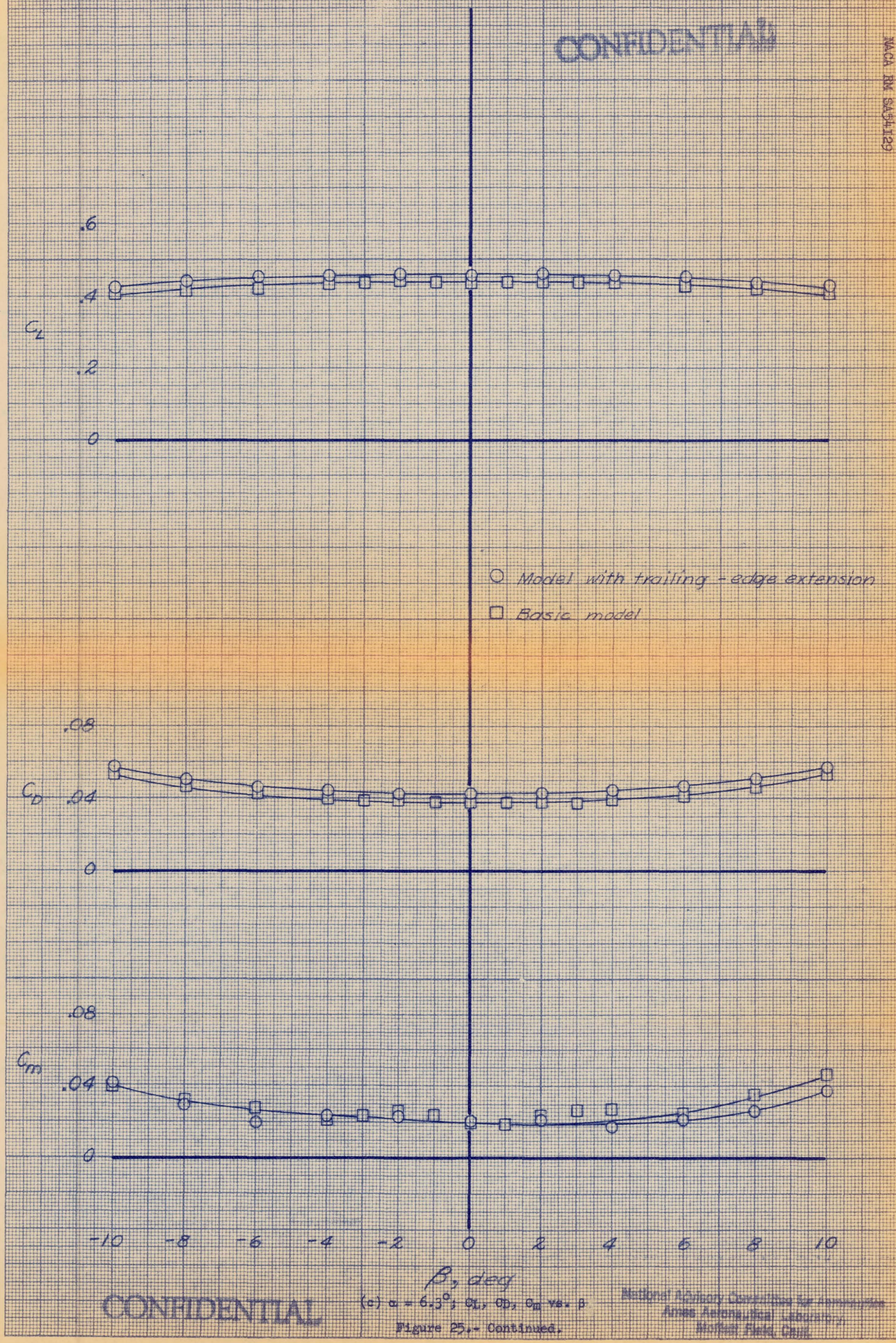

(c) $\alpha = 6.3°$; C_L, C_D, C_m vs. β

Figure 25.- Continued.

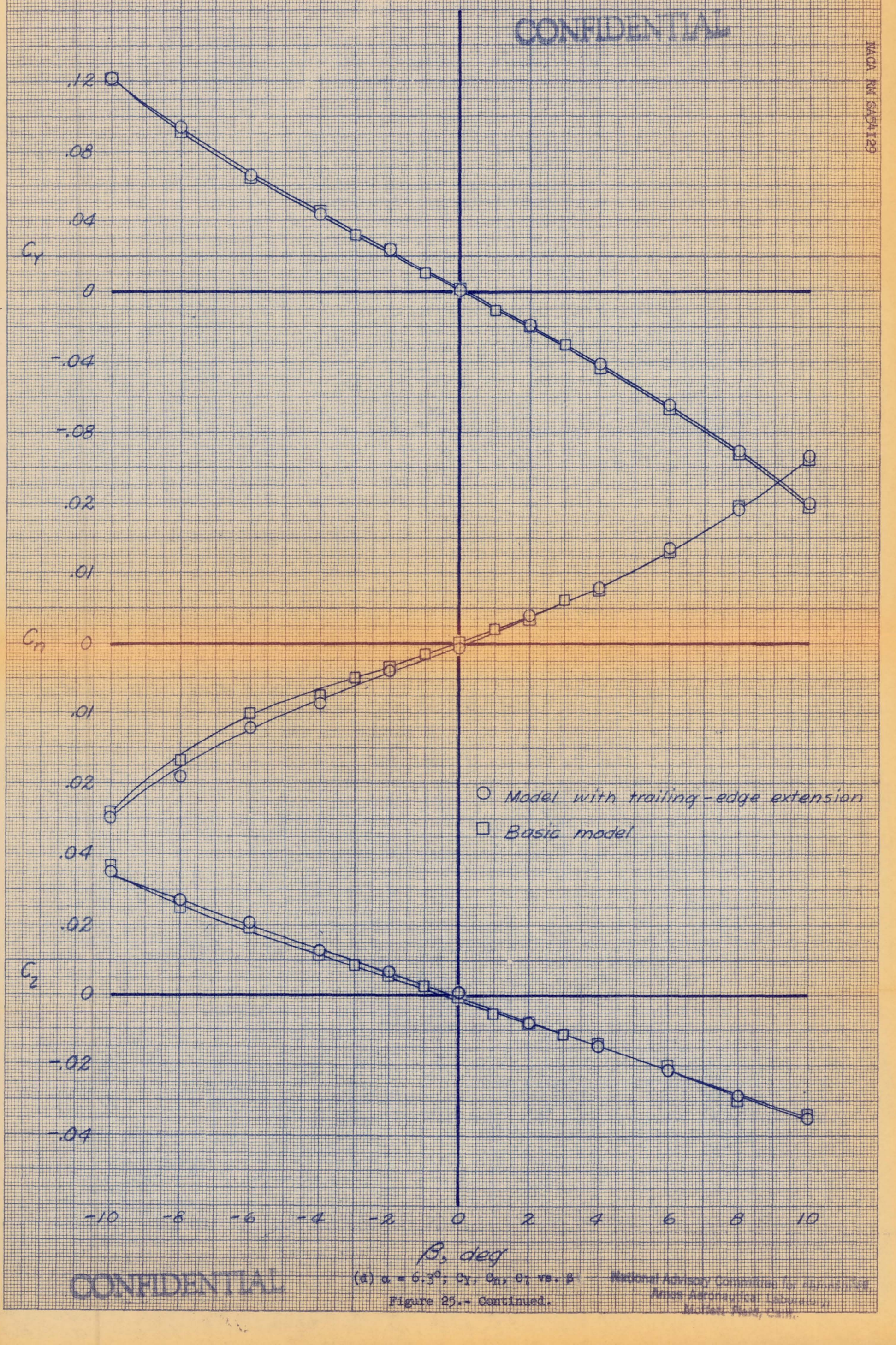

(d) $\alpha = 6.3°$; C_Y, C_n, C_l vs. β

Figure 25.- Continued.

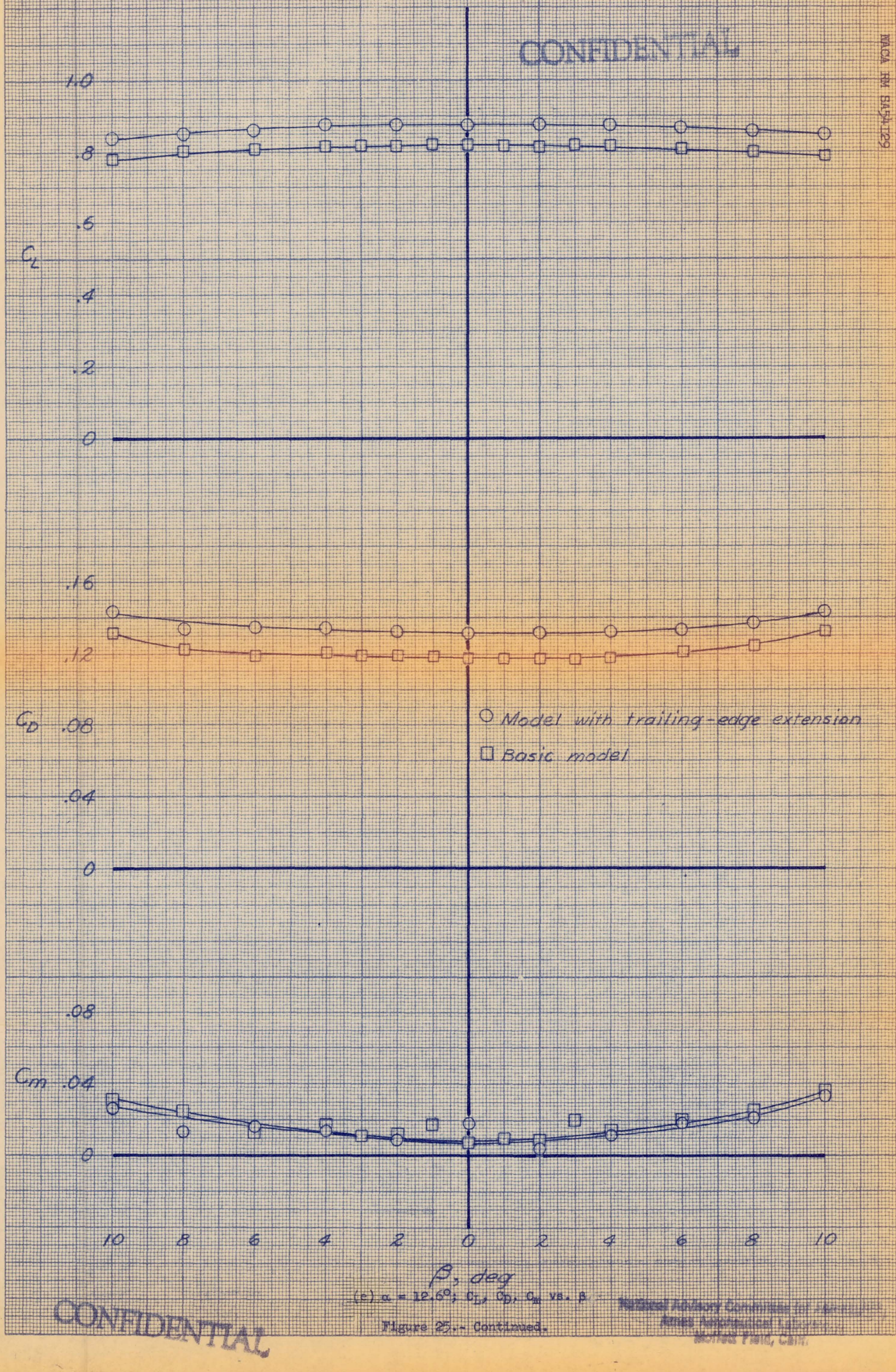

(e) $\alpha = 12.6°$; C_L, C_D, C_m vs. β

Figure 25.- Continued.

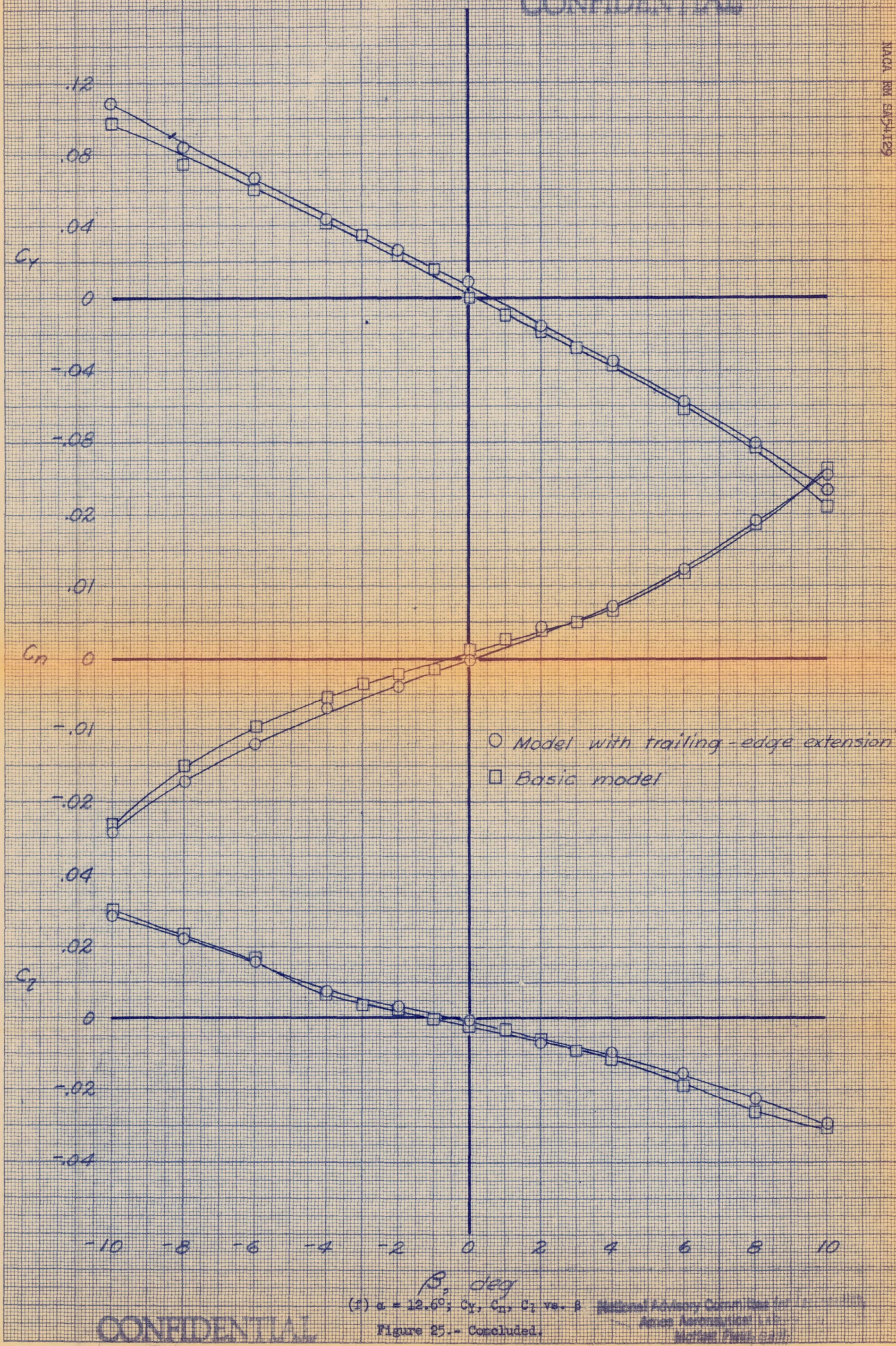

(f) $\alpha = 12.6^{\circ}$; C_Y, C_n, C_l vs. β

Figure 25.- Concluded.

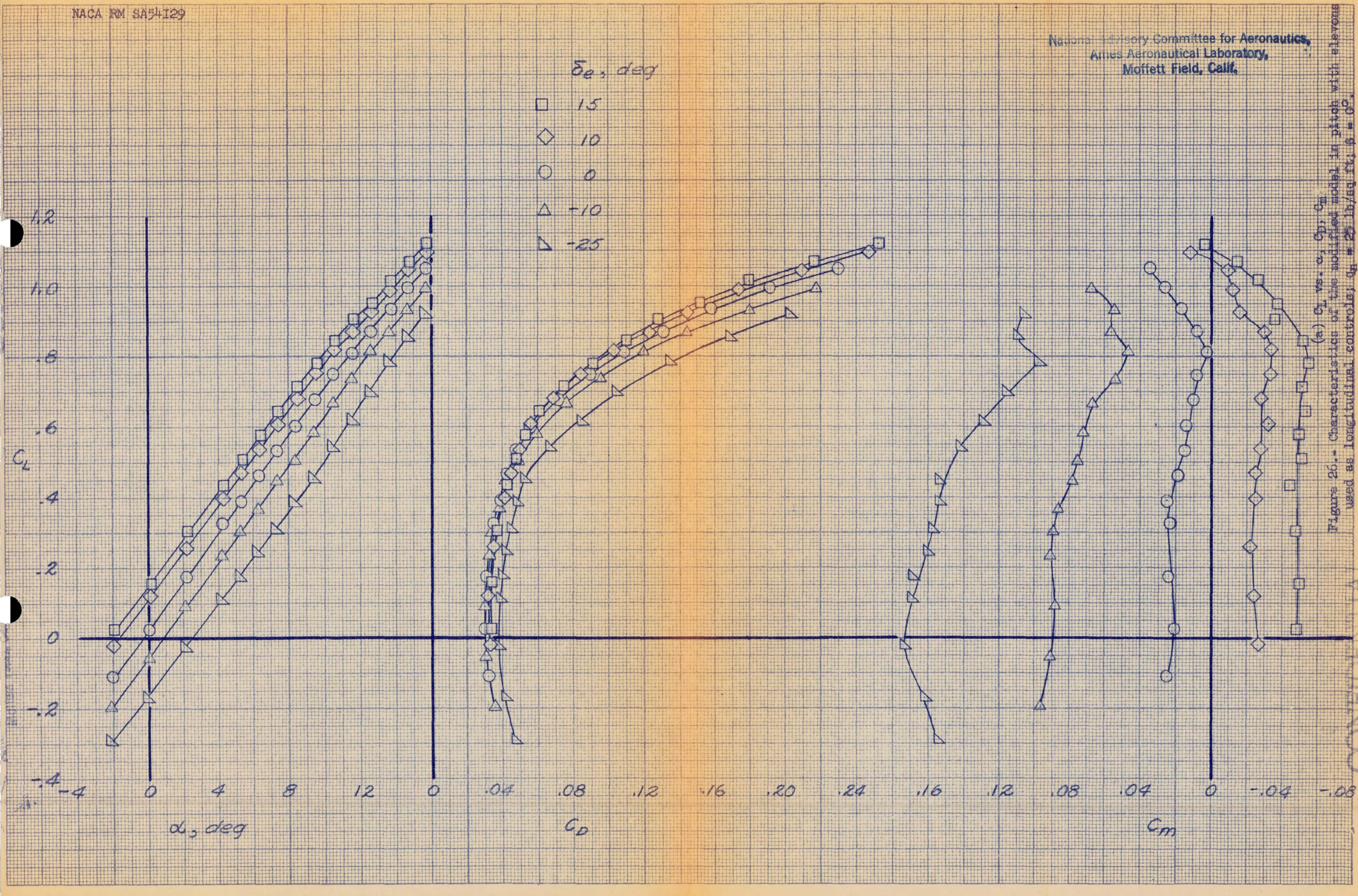

Figure 26.- Characteristics of the modified model in pitch with elevons used as longitudinal controls; q_a = 25 lb/sq ft, β = 0°.

(a) C_L vs. α; C_D, C_m

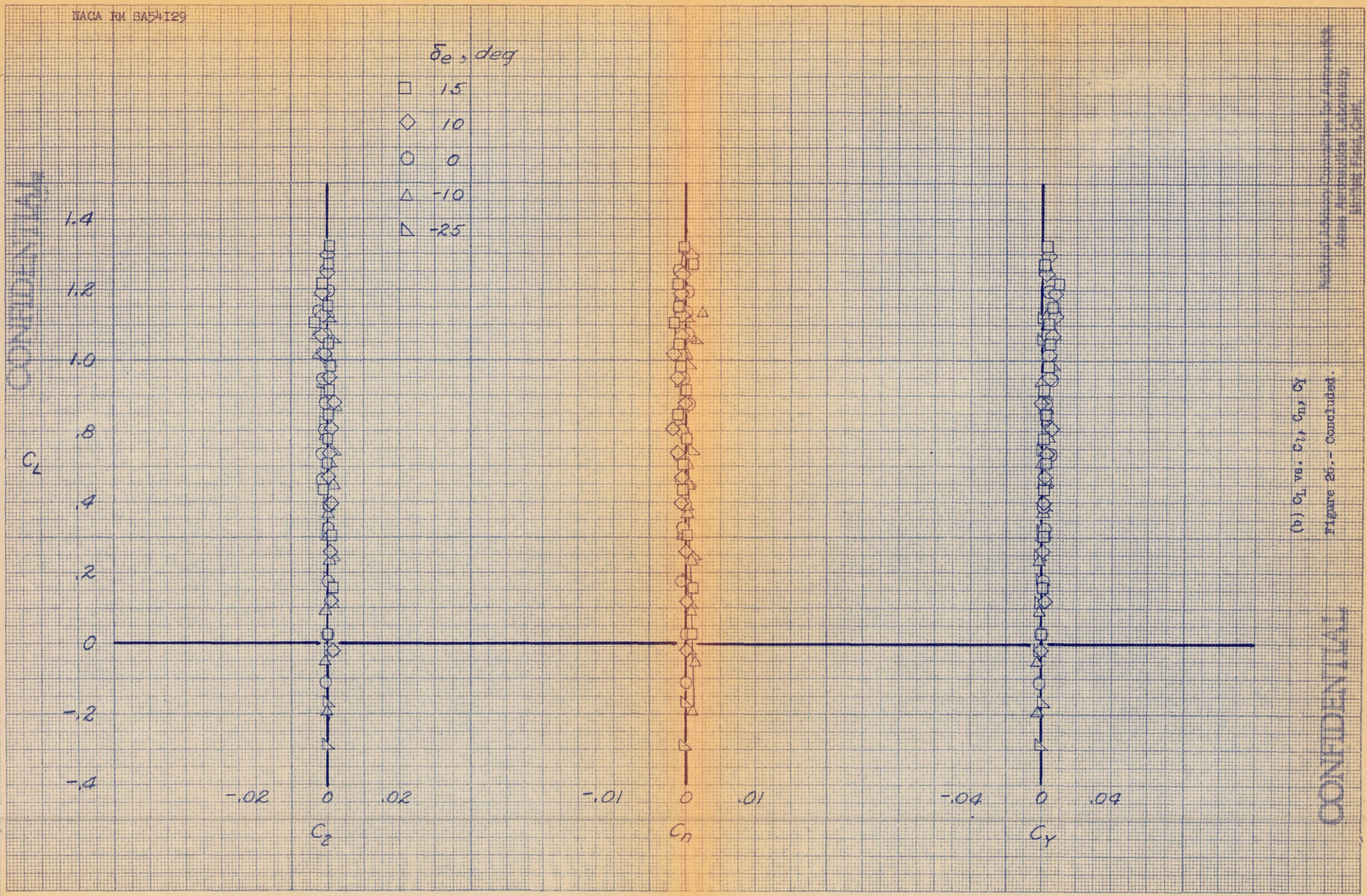

(b) C_L vs. C_z, C_n, C_Y

Figure 26.- Concluded.

δ_e, deg

- 15
- 10
- 0
- -10
- -25

C_L

.6
.4
.2
0

C_D

.08
.04
0

C_m

.20
.16
.12
.08
.04
0
-.04
-.08

-10 -8 -6 -4 -2 0 2 4 6 8 10

β, deg

(a) C_L, C_D, C_m vs. β

Figure 27.- Characteristics of the modified model in sideslip with elevons used as longitudinal controls; q_m = 25 lb/sq ft; α = 6.3°.

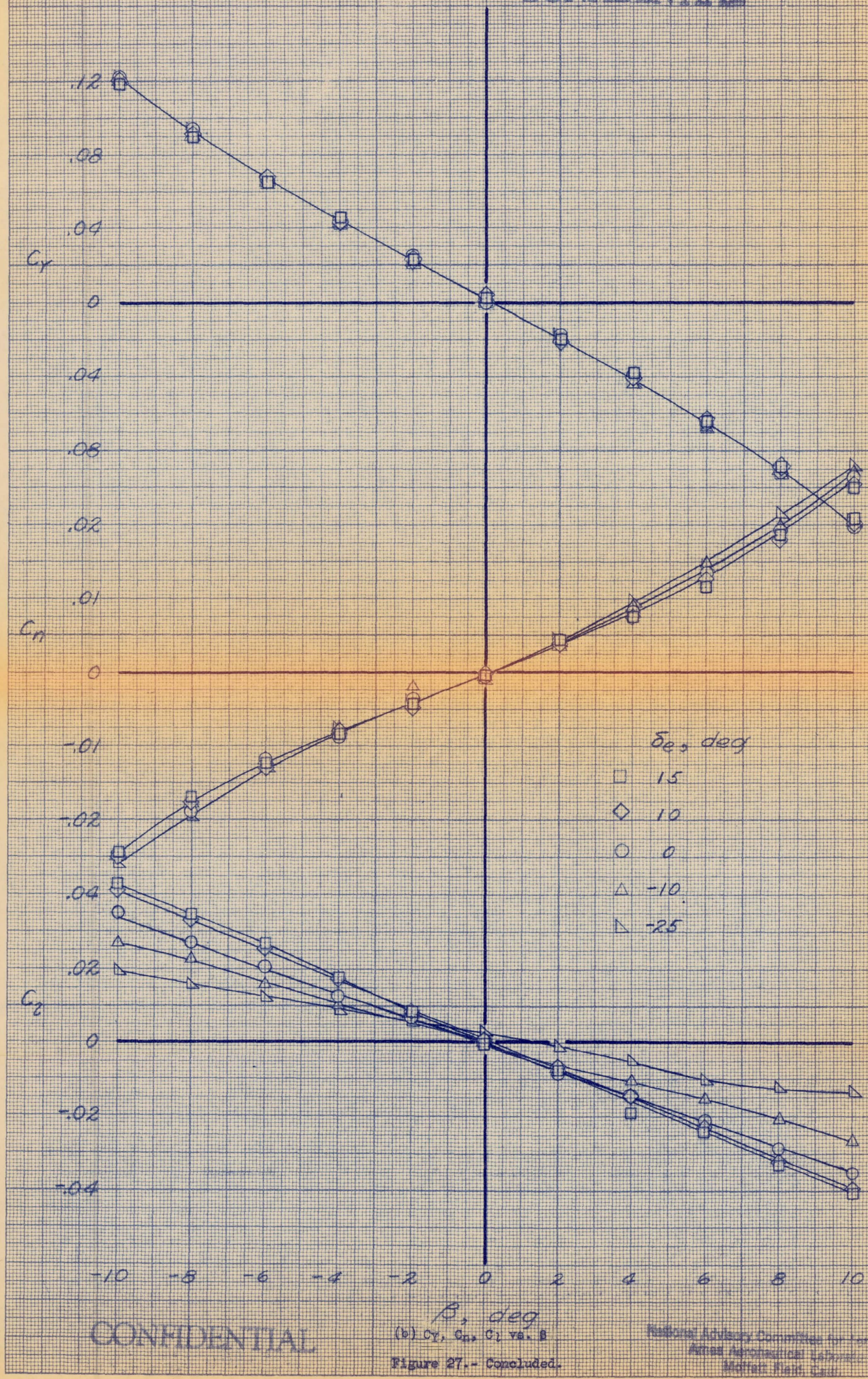

(b) C_Y, C_n, C_l vs. β

Figure 27.- Concluded.

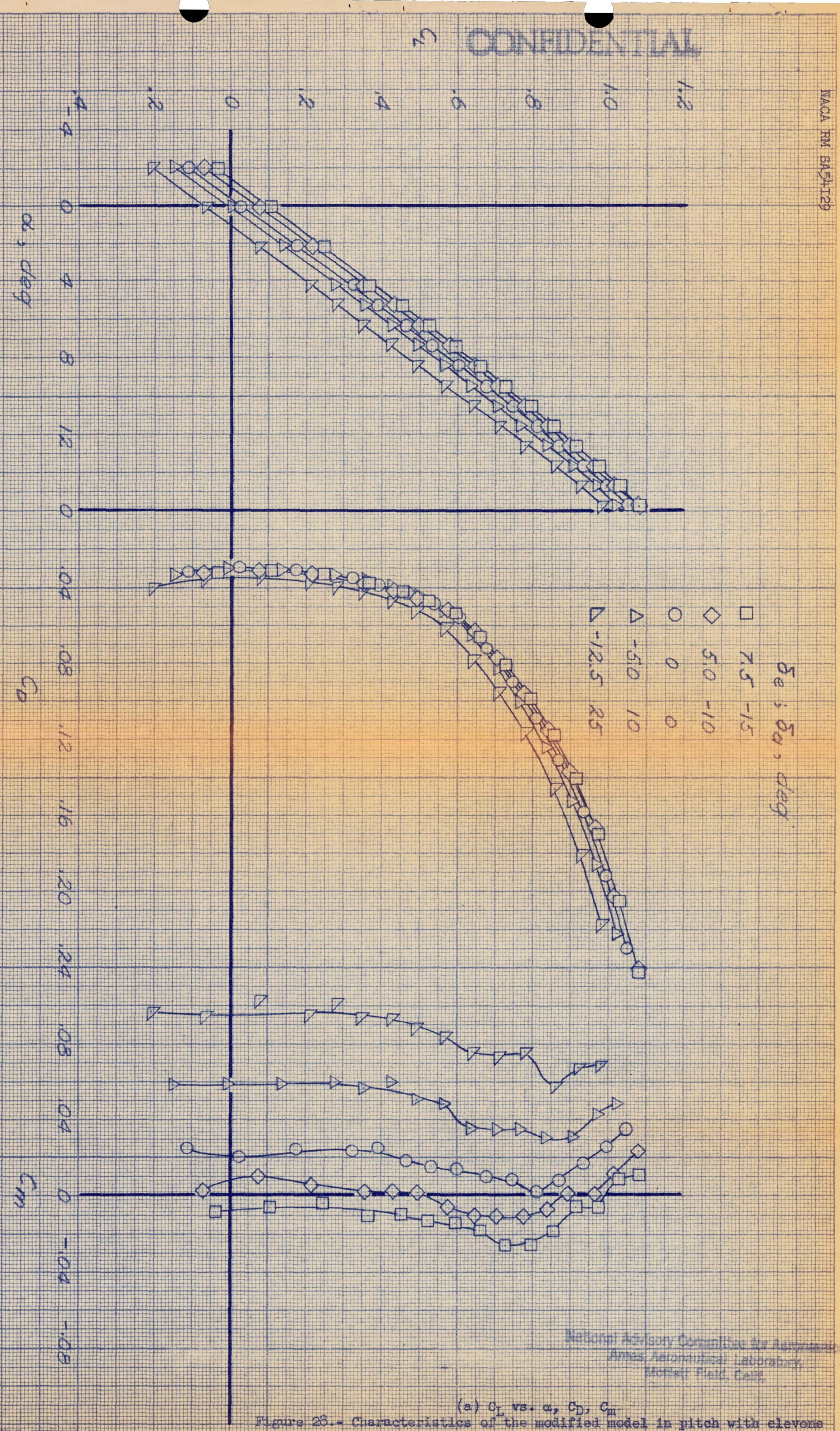

(a) C_L vs. α, C_D, C_m

Figure 28.- Characteristics of the modified model in pitch with elevons used as combined lateral and longitudinal controls; q_n = 25 lb/sq ft; $\beta = 0^\circ$.

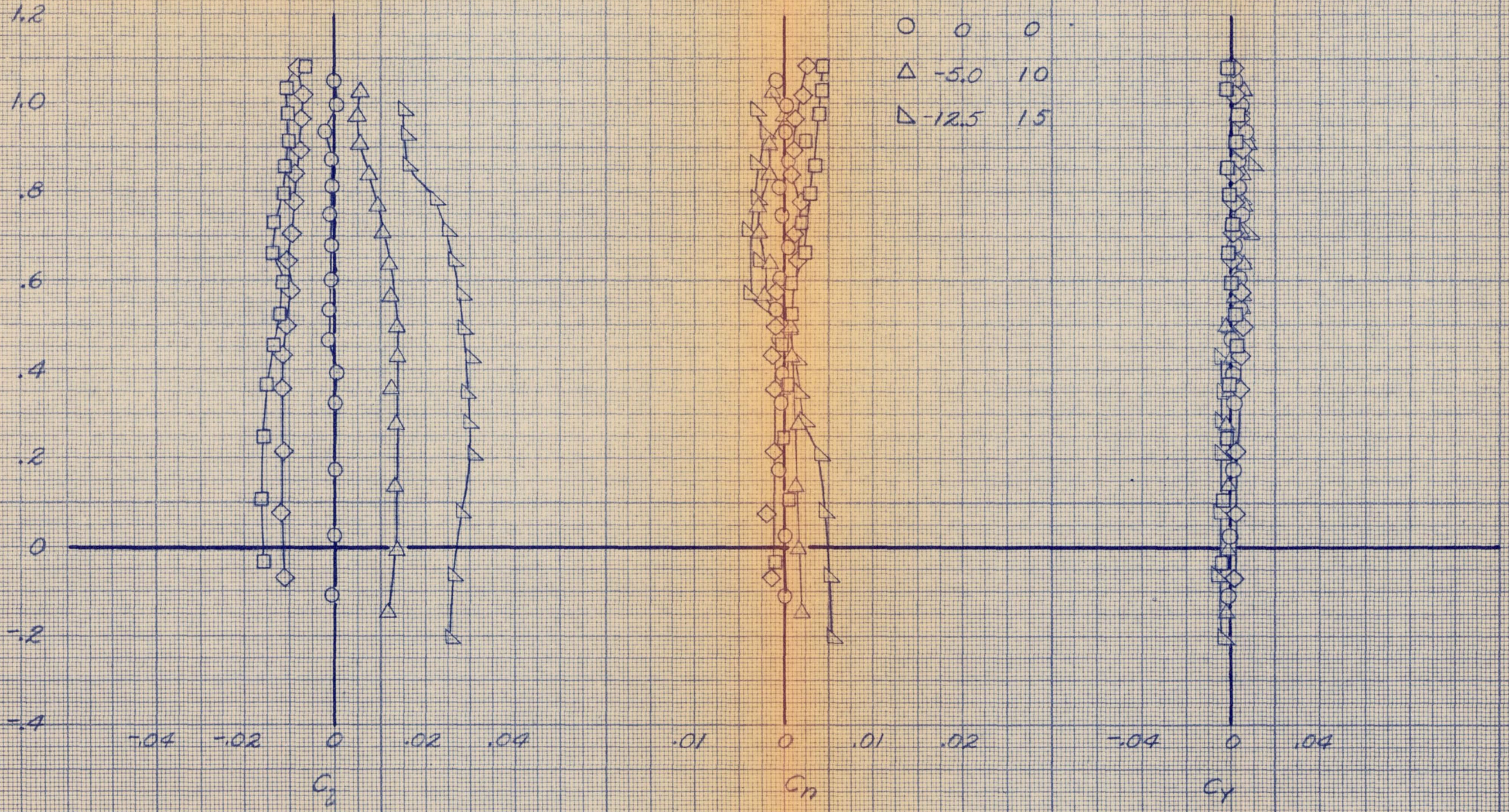

Figure 28.- Concluded.

(a) C_L vs. C_l, C_n, C_Y

Langley Aeronautical Laboratory, Langley Field, Va.
Ames Aeronautical Laboratory, Moffett Field, Calif.

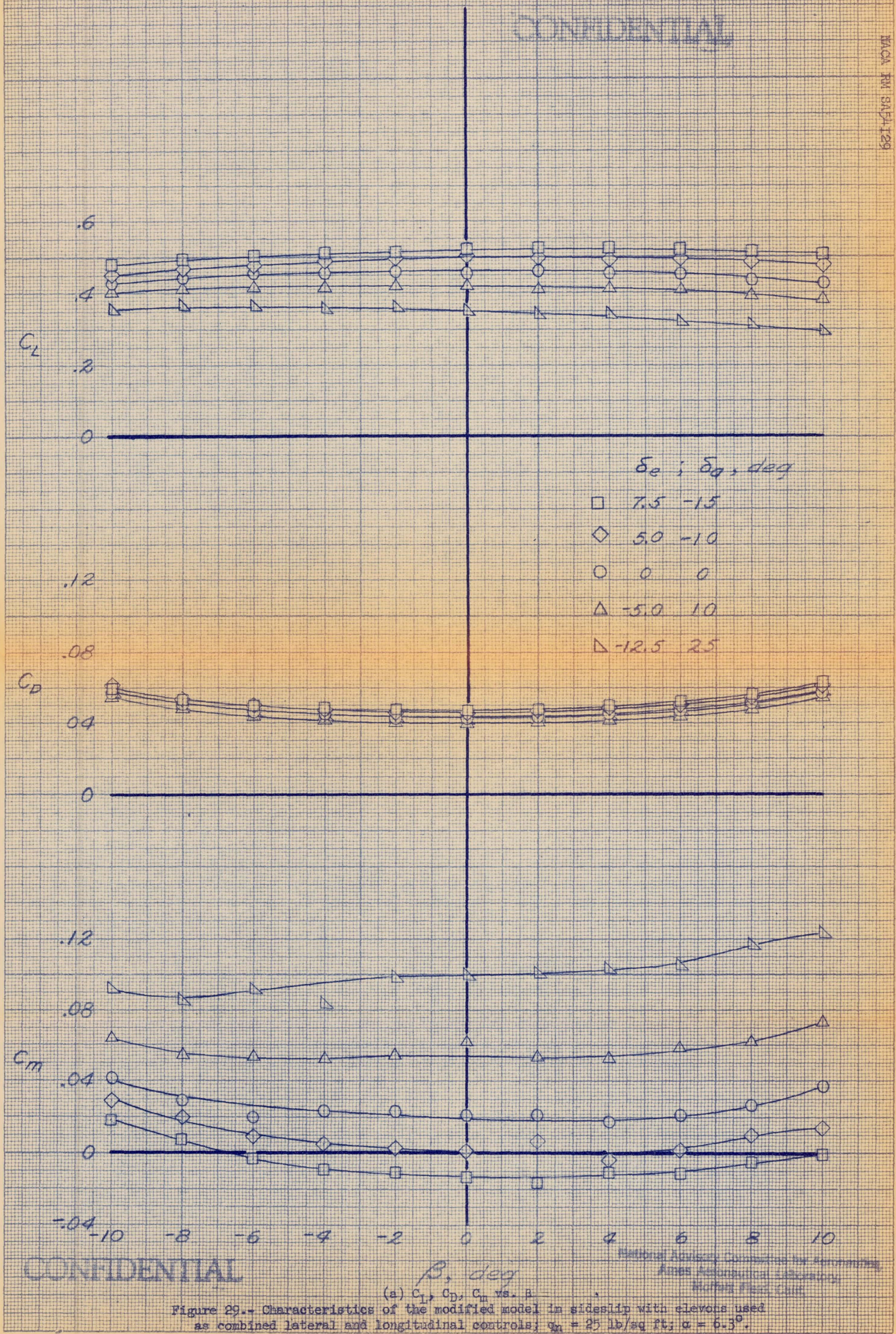

(a) C_L, C_D, C_m vs. β.

Figure 29.- Characteristics of the modified model in sideslip with elevons used as combined lateral and longitudinal controls; q_m = 25 lb/sq ft; α = 6.3°.

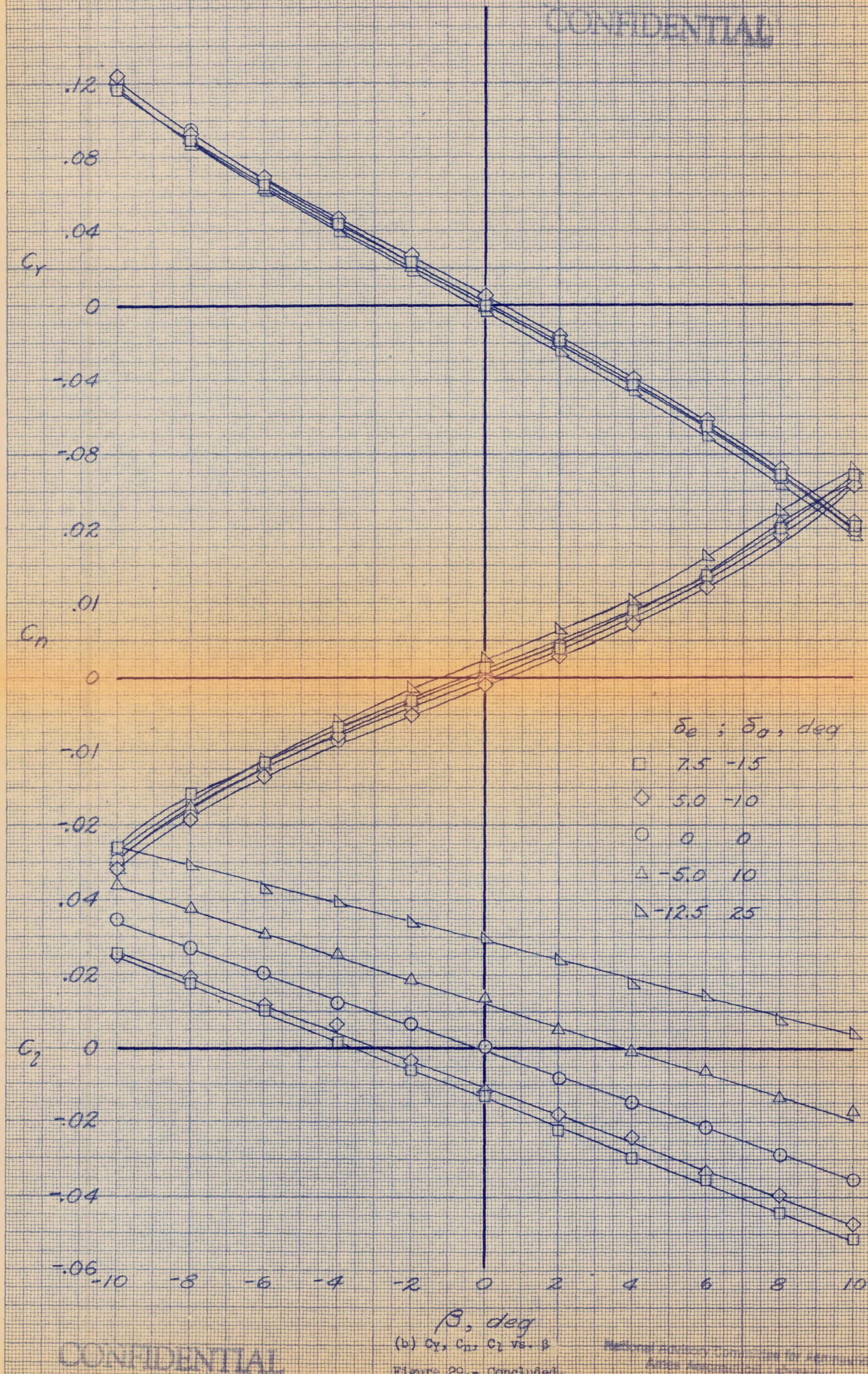

(b) C_Y, C_n, C_l vs. β

Figure 29.- Concluded.

Skids	q_n, psf
○ Extended	25
□ Extended	108
◇ Retracted	25

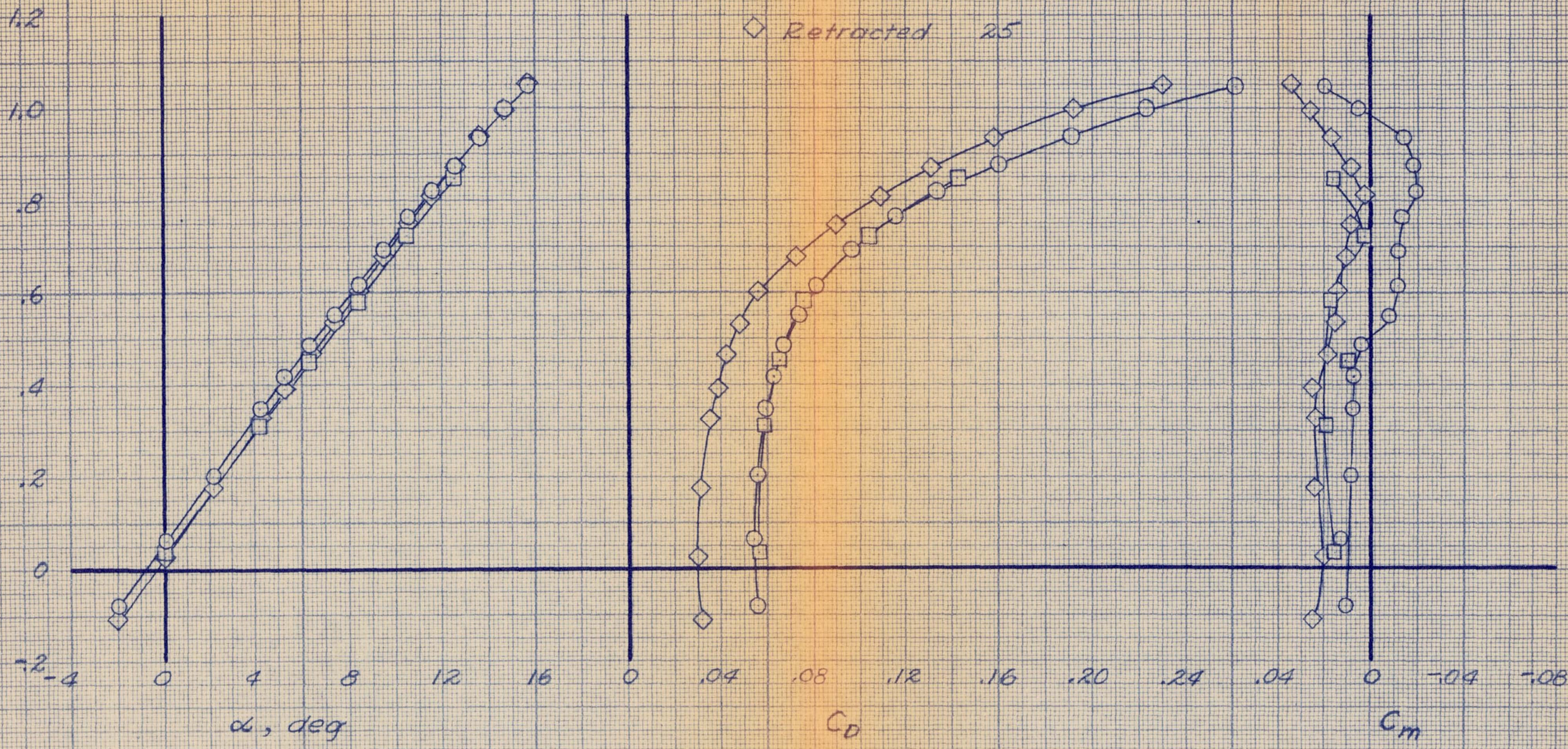

Figure 30.- Effect of extending the landing skids on the characteristics of the modified model in pitch, $\beta = 0°$.

(a) C_L vs. α, C_D, C_m

Skids	q_n, psf
○ Extended	25
□ Extended	108
◇ Retracted	25

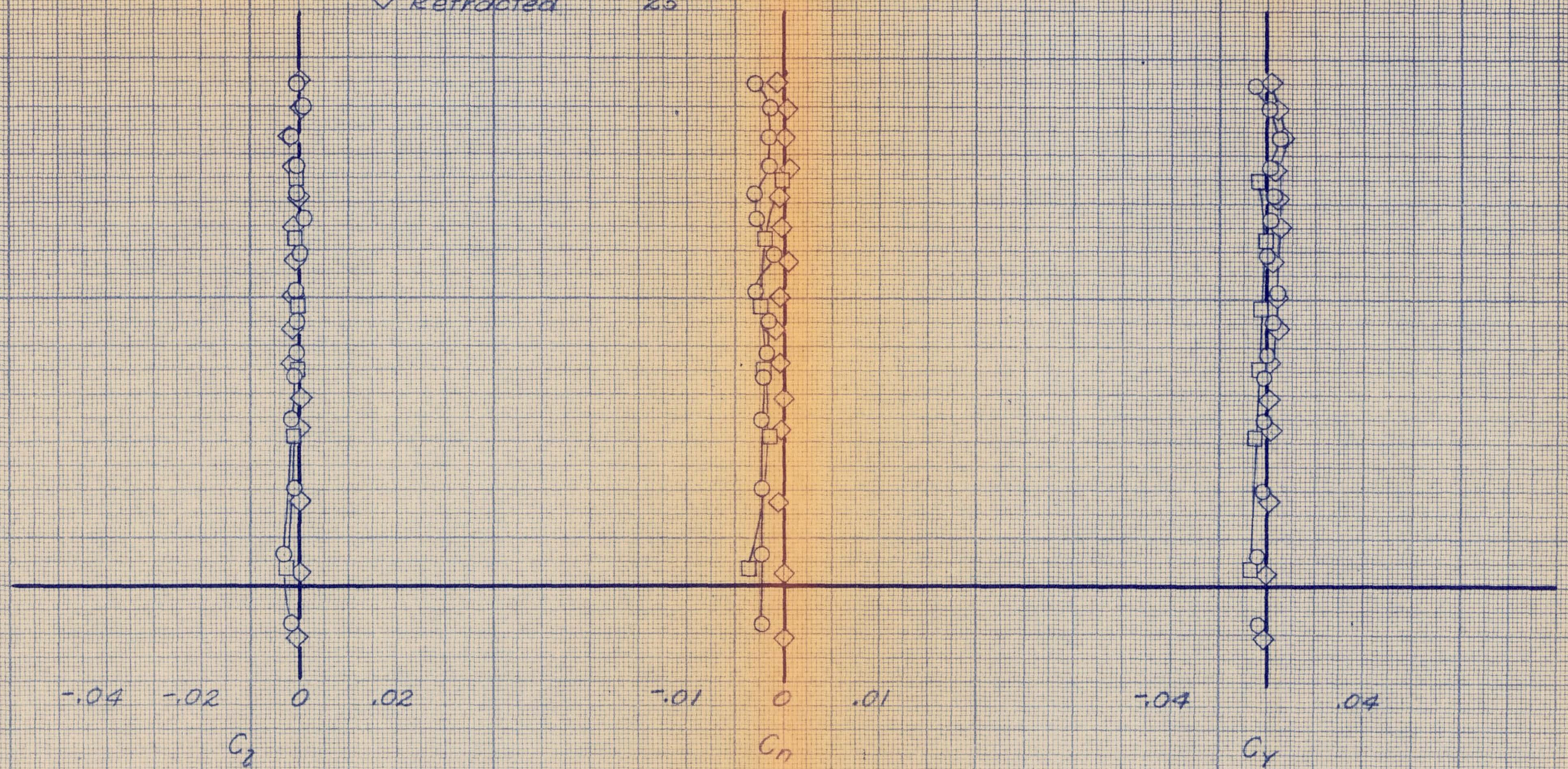

(b) C_L vs. C_l, C_n, C_Y

Figure 30.- Concluded.

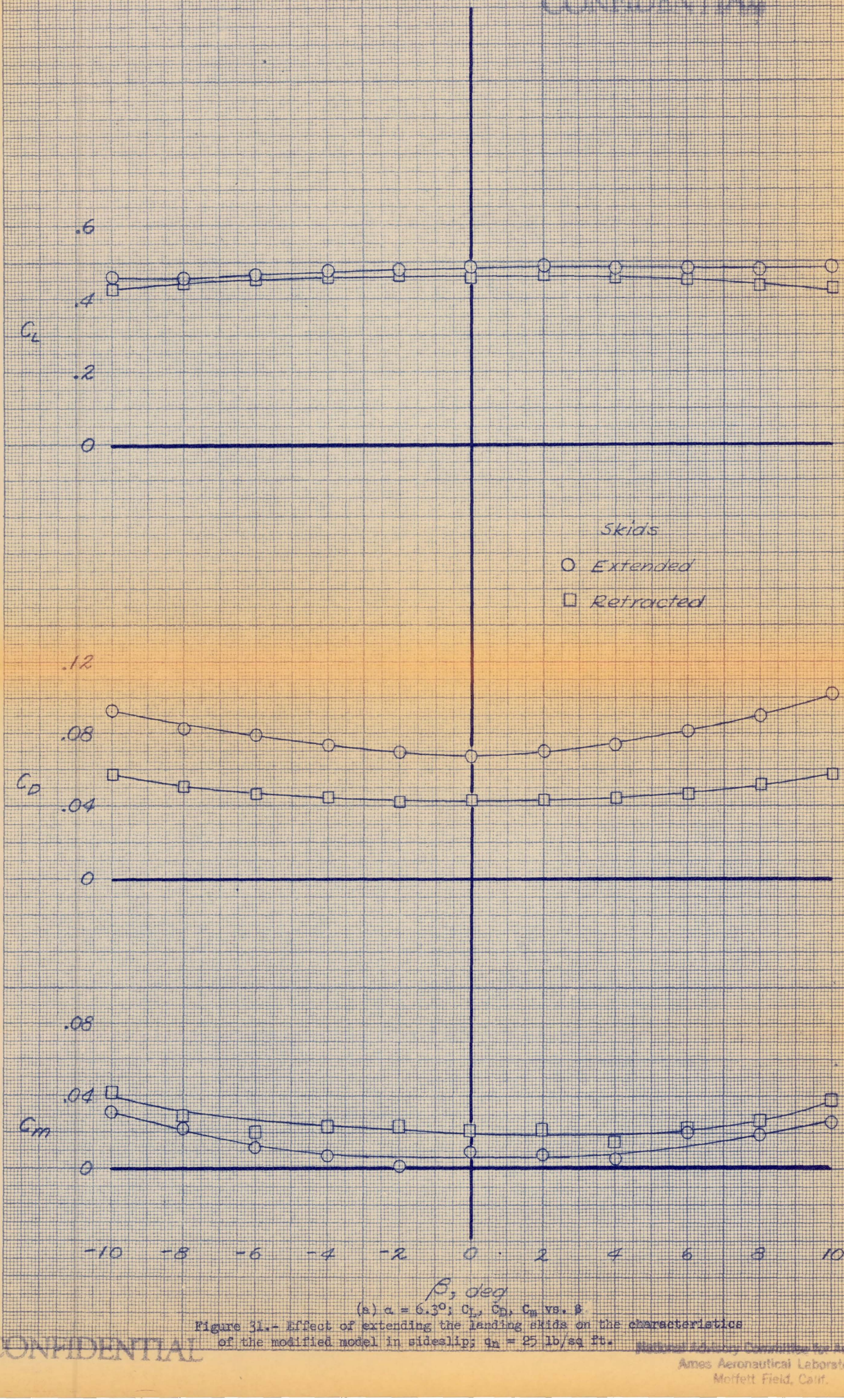

(a) $\alpha = 6.3°$; C_L, C_D, C_m vs. β

Figure 31.- Effect of extending the landing skids on the characteristics of the modified model in sideslip; q_m = 25 lb/sq ft.

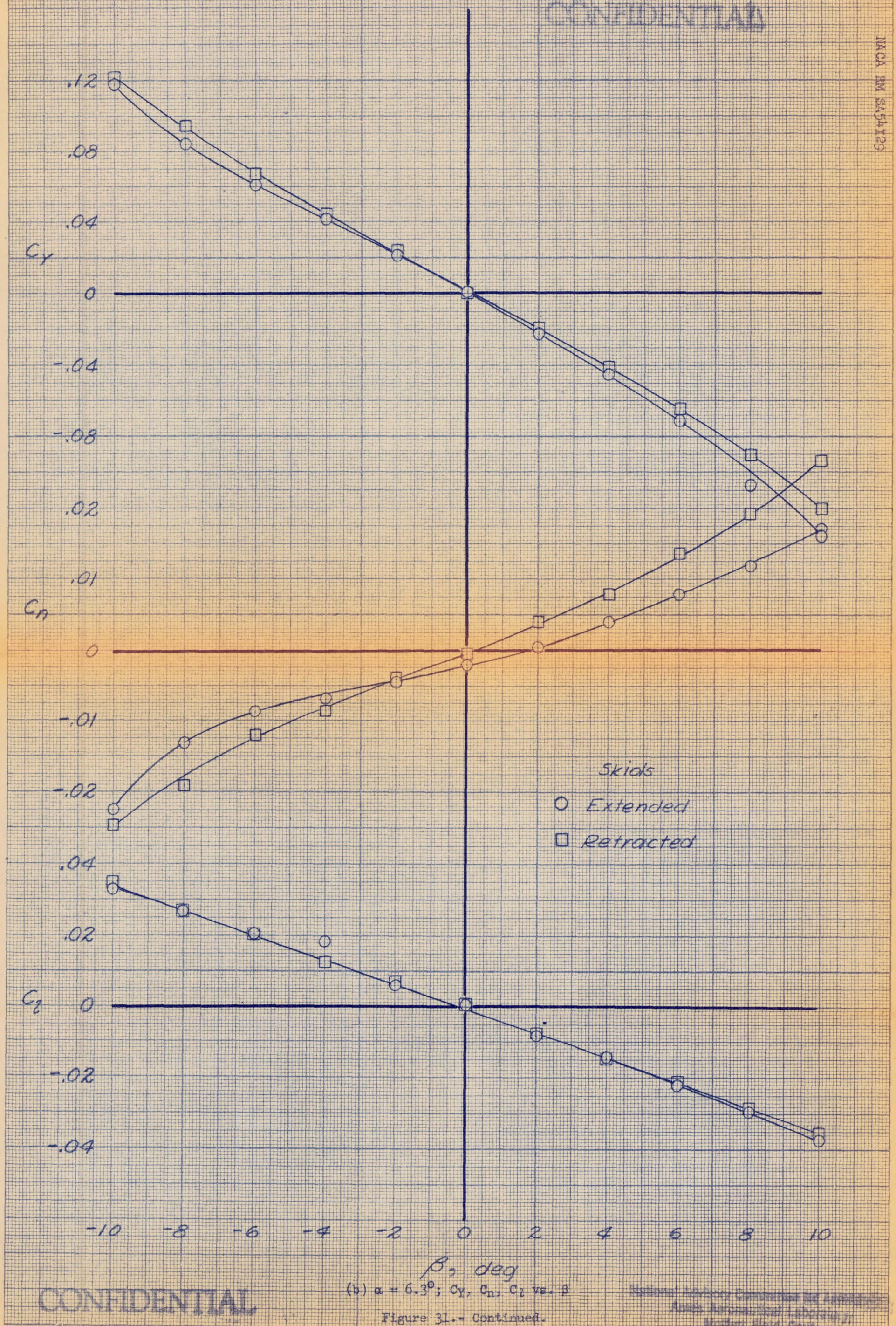

(b) $\alpha = 6.3^{\circ}$; C_Y, C_n, C_l vs. β

Figure 31.- Continued.

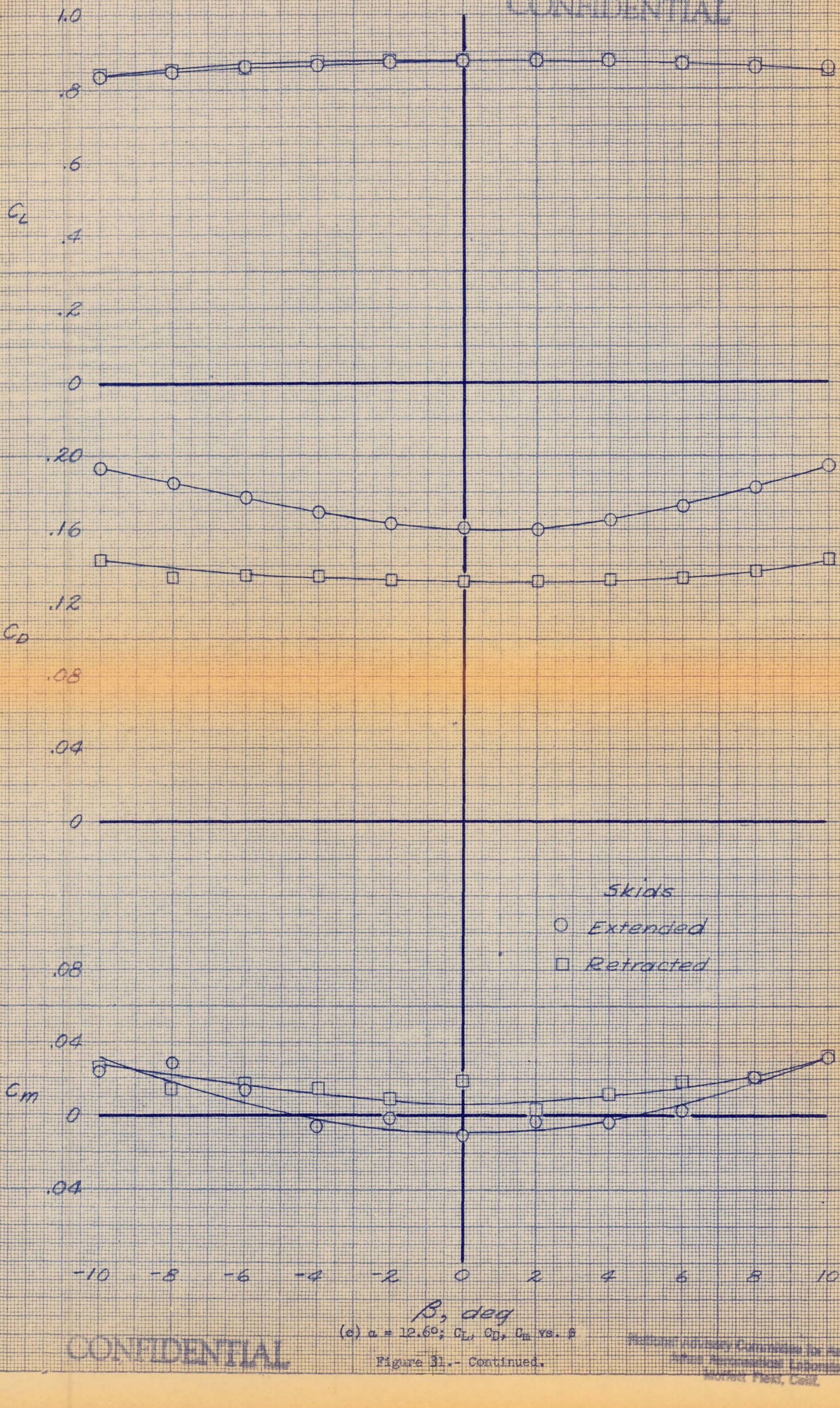

(e) $\alpha = 12.6^{\circ}$; C_L, C_D, C_m vs. β

Figure 31.- Continued.

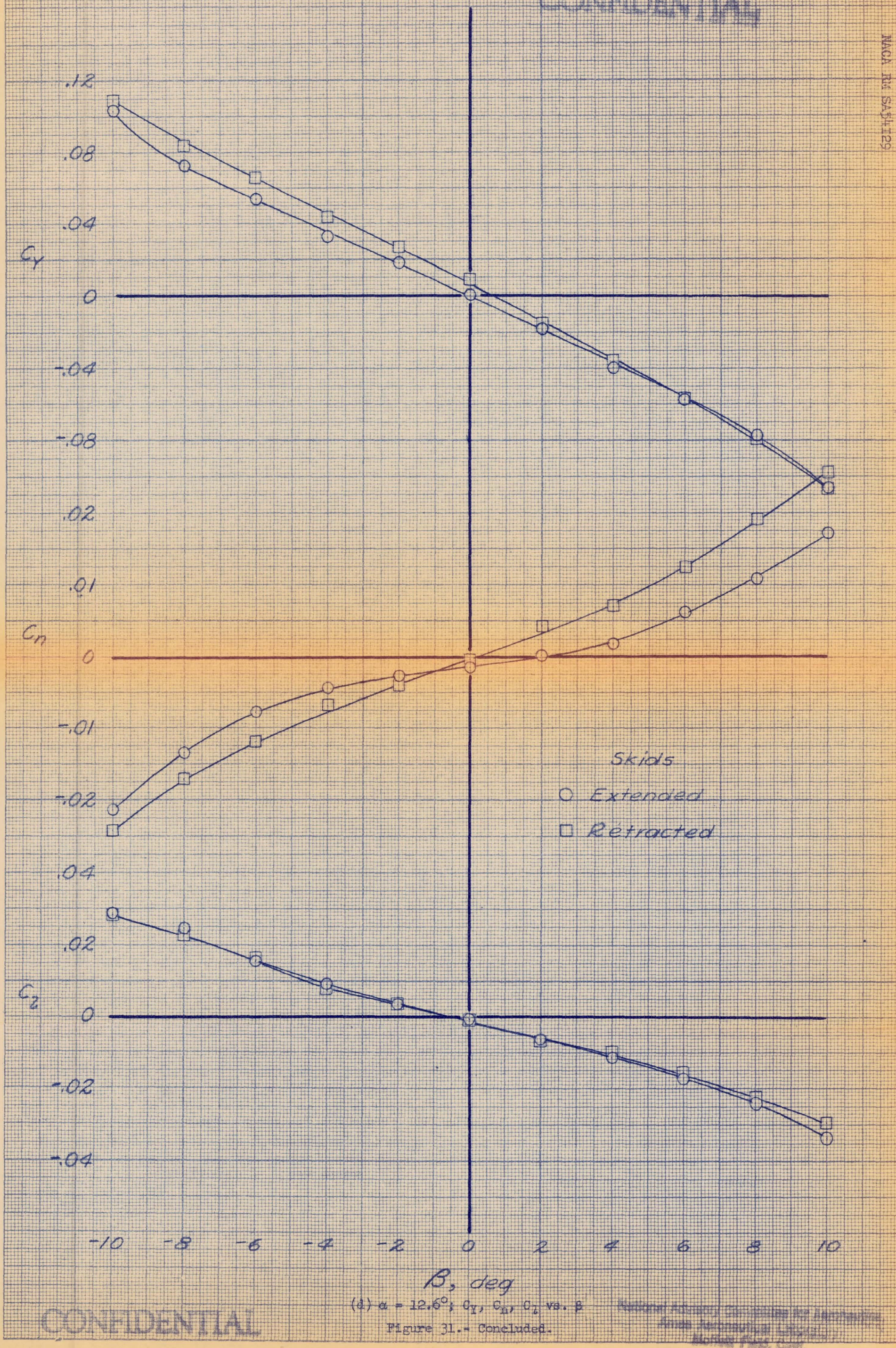

(d) $\alpha = 12.6°$; C_Y, C_n, C_l vs. β

Figure 31.- Concluded.

	Power	q_n, psf
○	Off	25
□	3800 # thrust	25
◇	Off	108
△	3000 # thrust	108

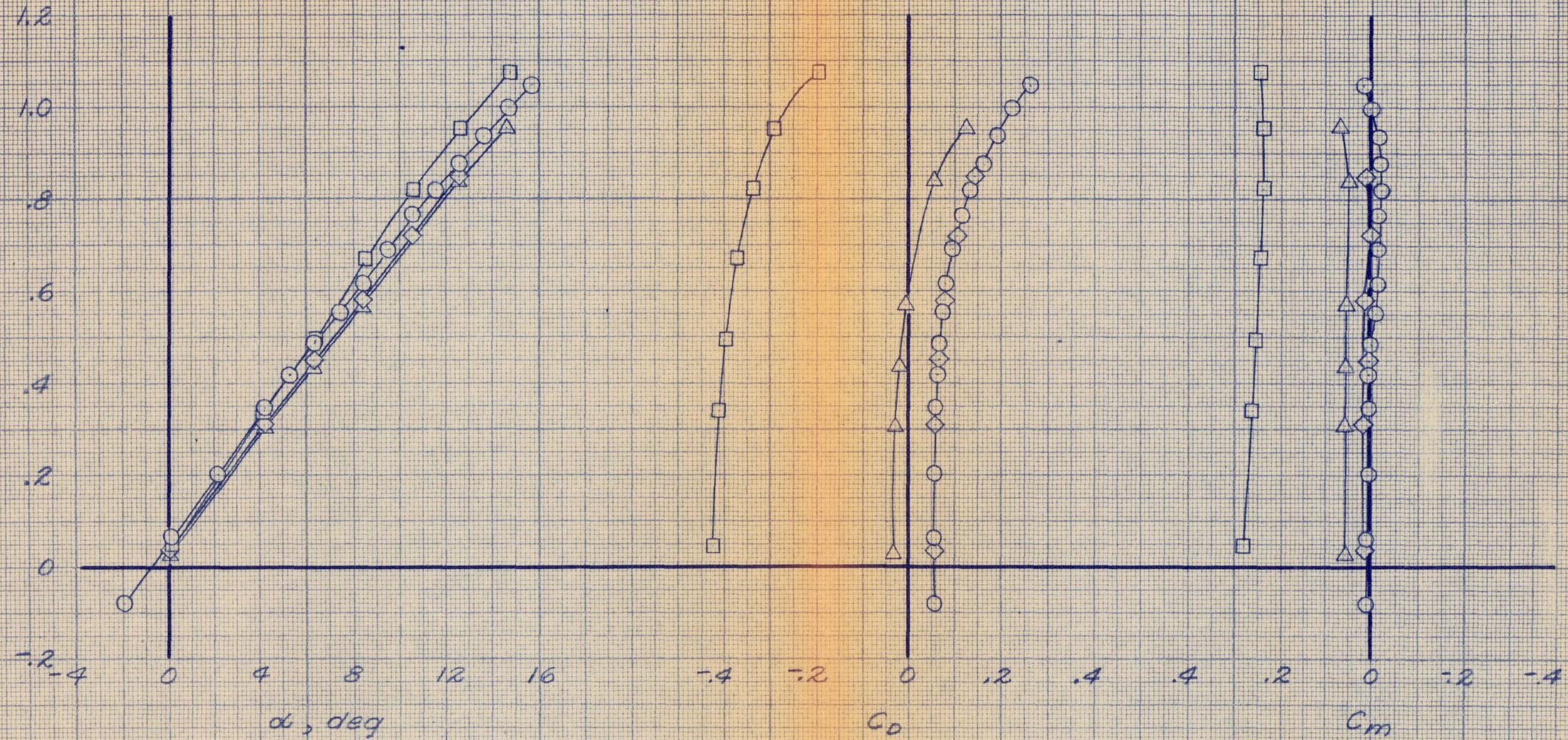

(a) C_L vs. α, C_D, C_m

Figure 32.- Effect of the addition of power on the characteristics of the modified model in pitch with landing skids extended; $\beta = 0°$.

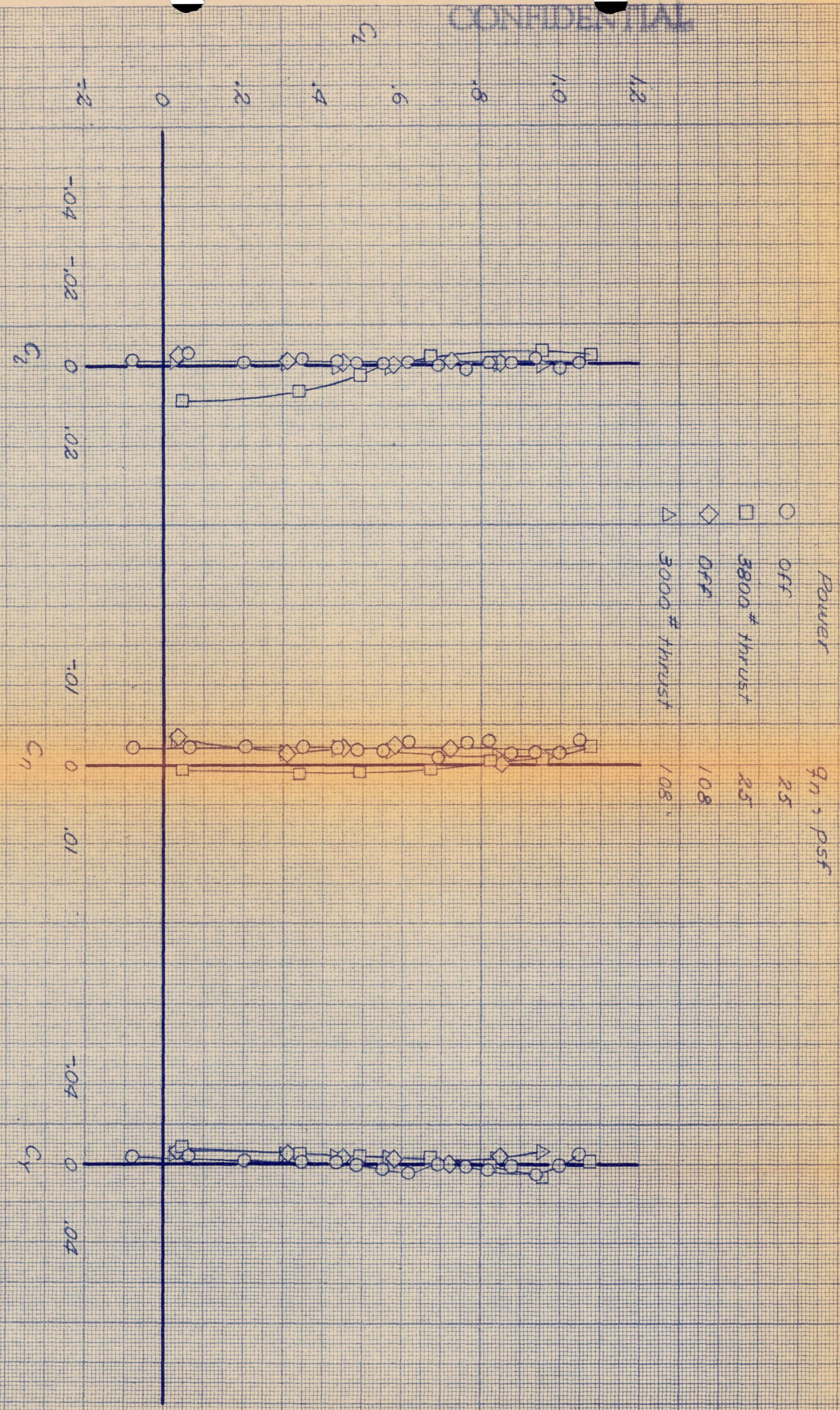

(b) C_L vs. C_l, C_n, C_Y

Figure 32.- Concluded.

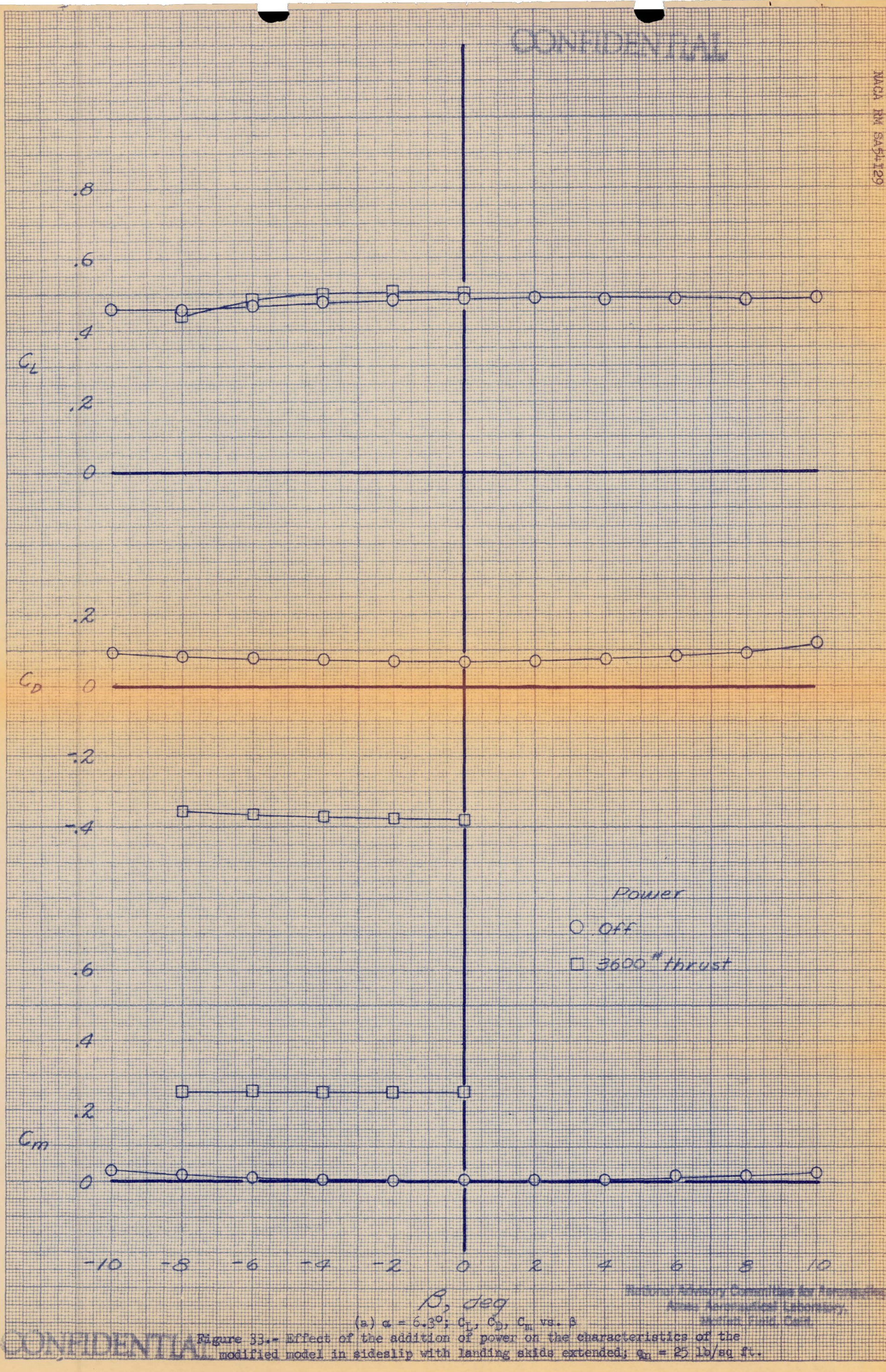

(a) $\alpha = 6.3°$; C_L, C_D, C_m vs. β

Figure 33.- Effect of the addition of power on the characteristics of the modified model in sideslip with landing skids extended; q_m = 25 lb/sq ft.

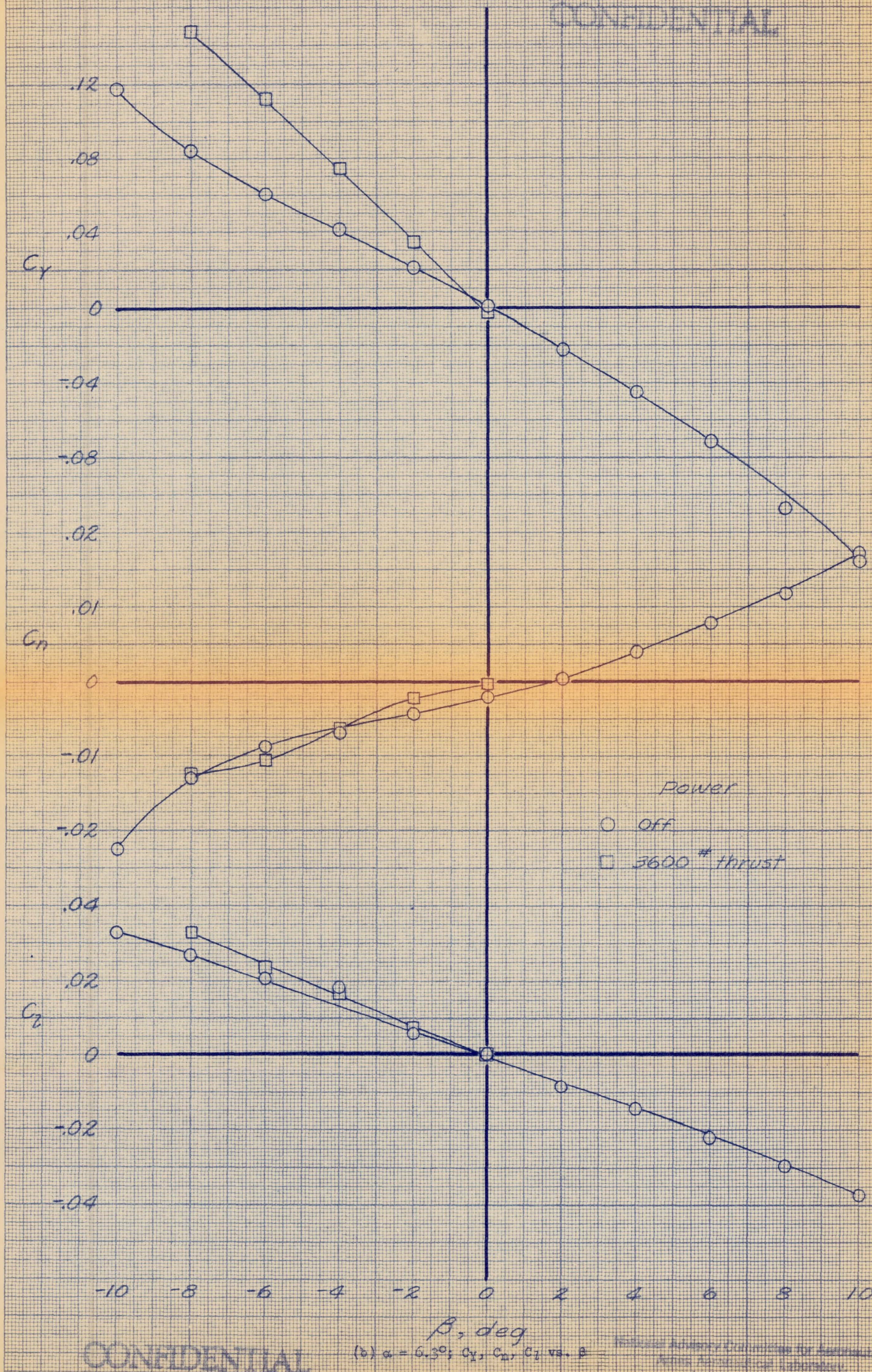

(b) $\alpha = 6.3°$; C_Y, C_n, C_l vs. β

Figure 33.- Continued.

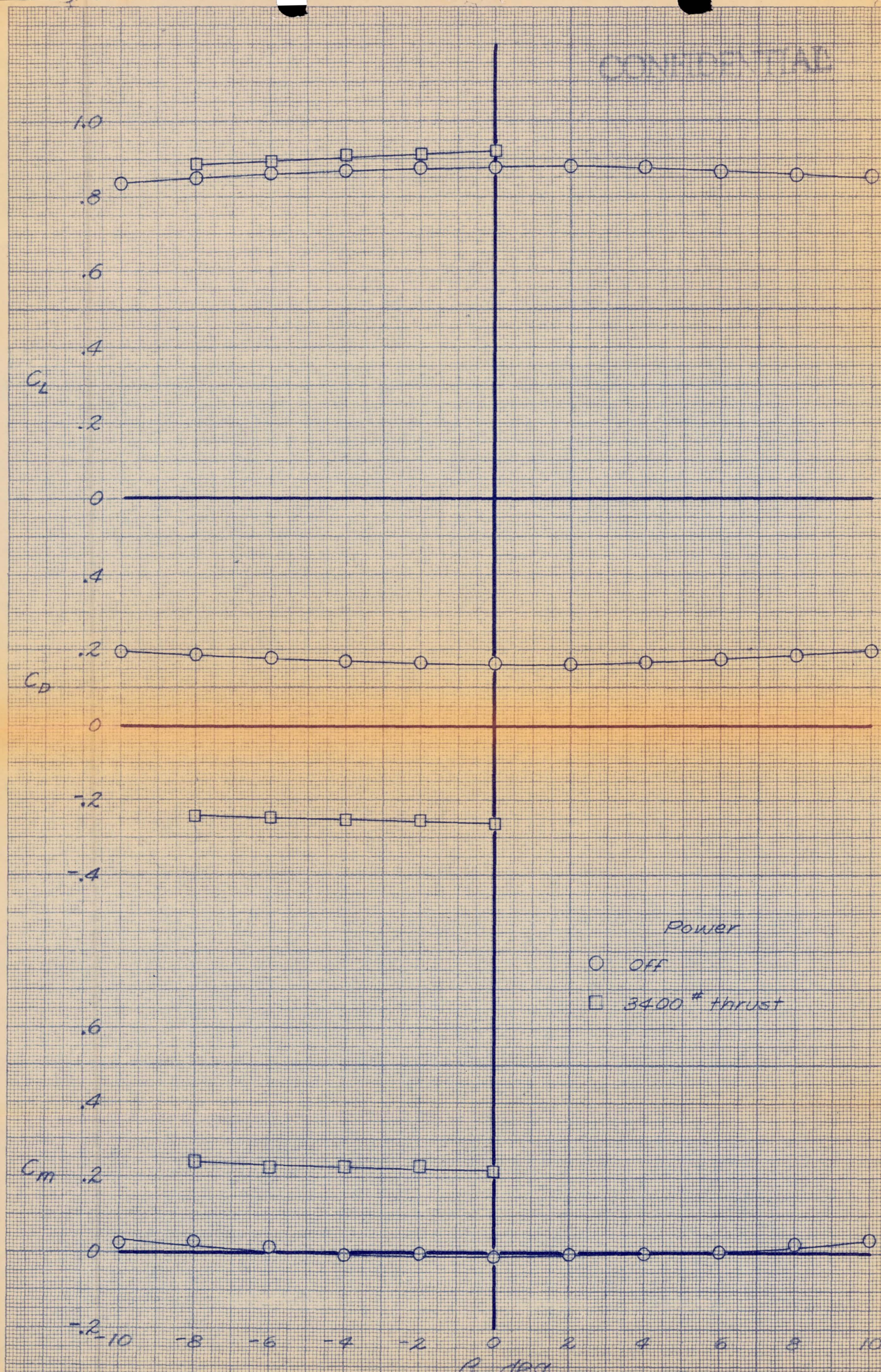

(c) $\alpha = 12.6°$; C_L, C_D, C_m vs. β

Figure 33.- Continued.

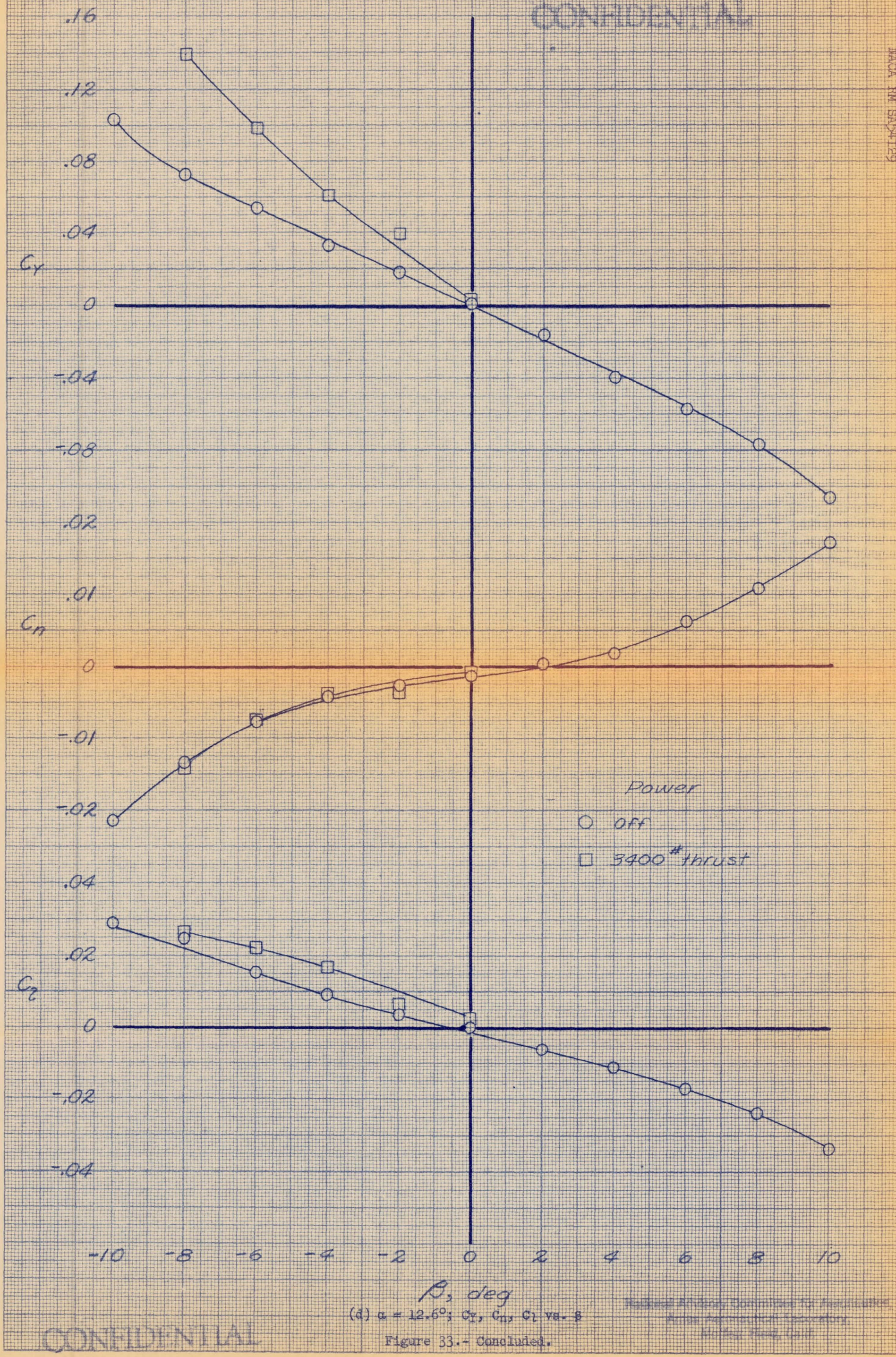

(d) $\alpha = 12.6°$; C_Y, C_n, C_l vs. β

Figure 33.- Concluded.

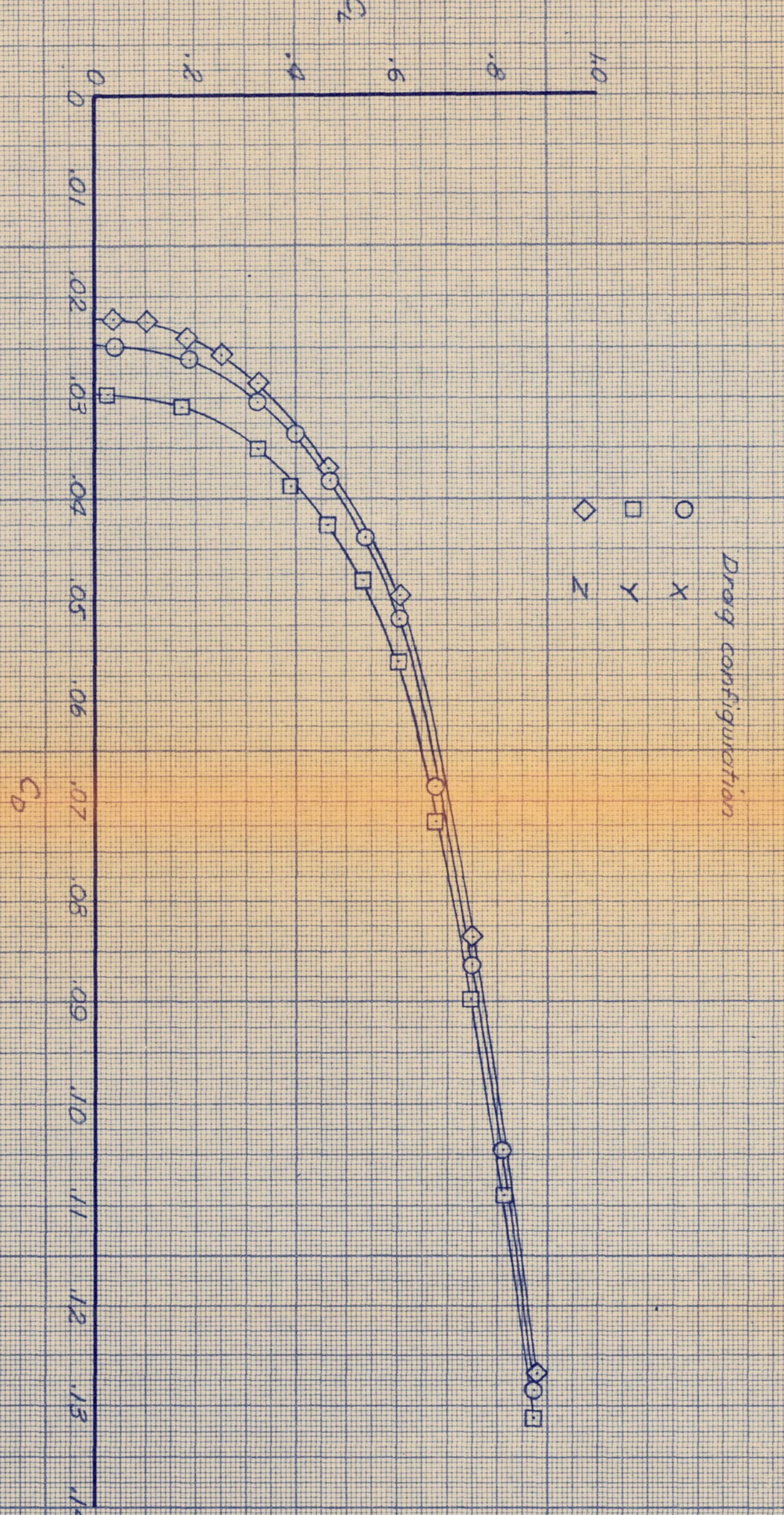

(a) C_L vs. C_D; q_m = 25 lb/sq ft

Figure 34.- Effect of the various drag configurations on the longitudinal characteristics of the model; $\beta = 0^\circ$.

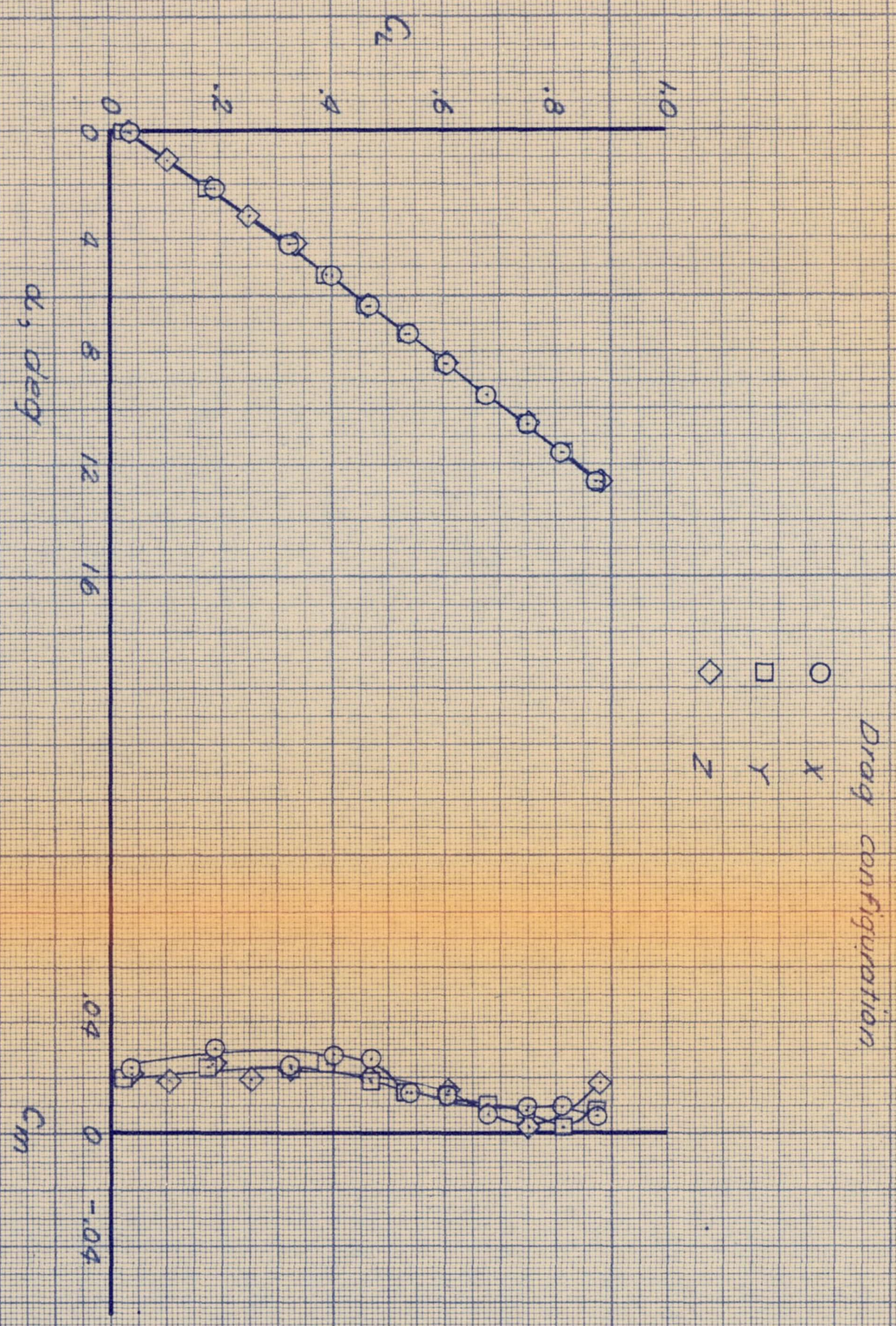

(b) C_L vs. α, C_m; q_n = 25 lb/sq ft

Figure 34.- Continued.

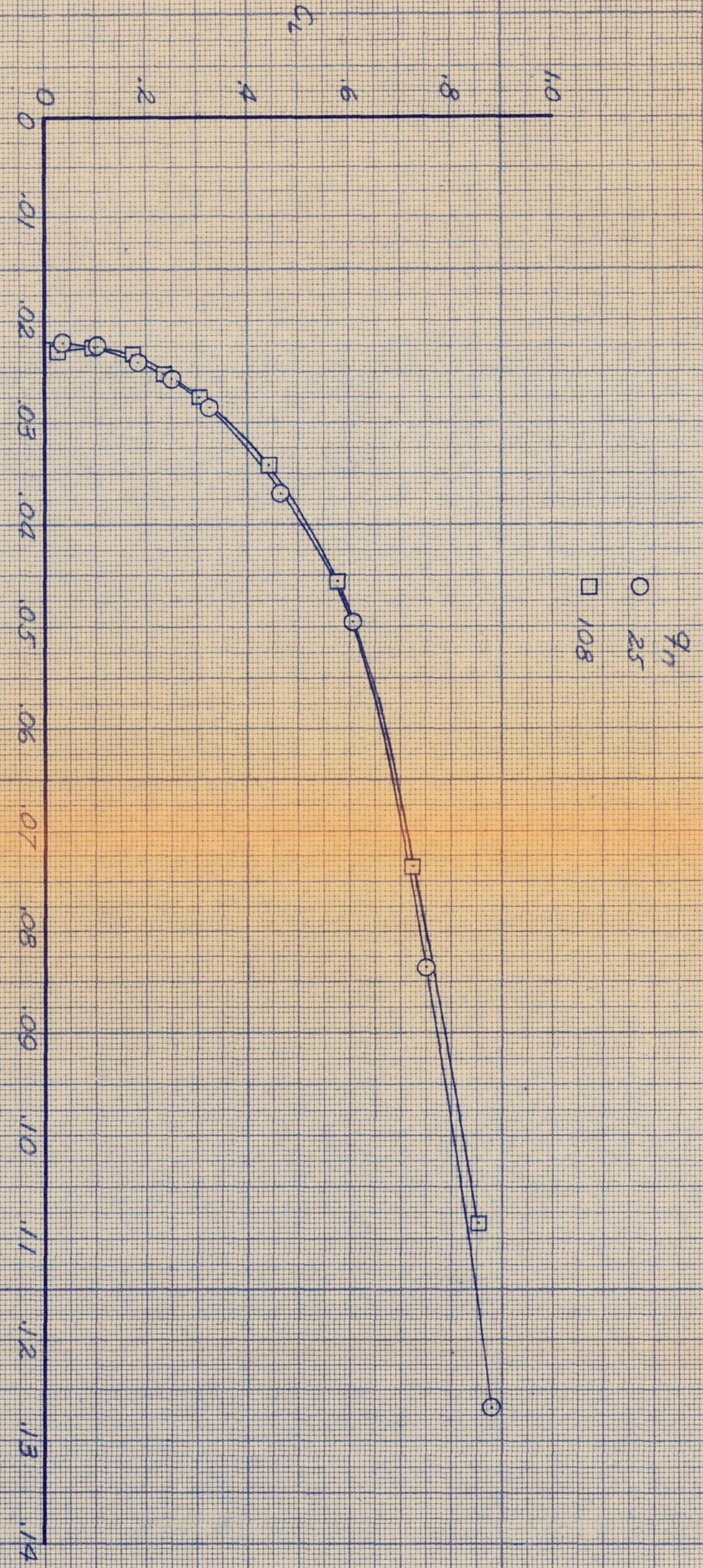

(c) C_L vs. C_D; configuration Z

Figure 34.- Continued.

(d) C_L vs. α, C_m; configuration Z

Figure 34.- Concluded.

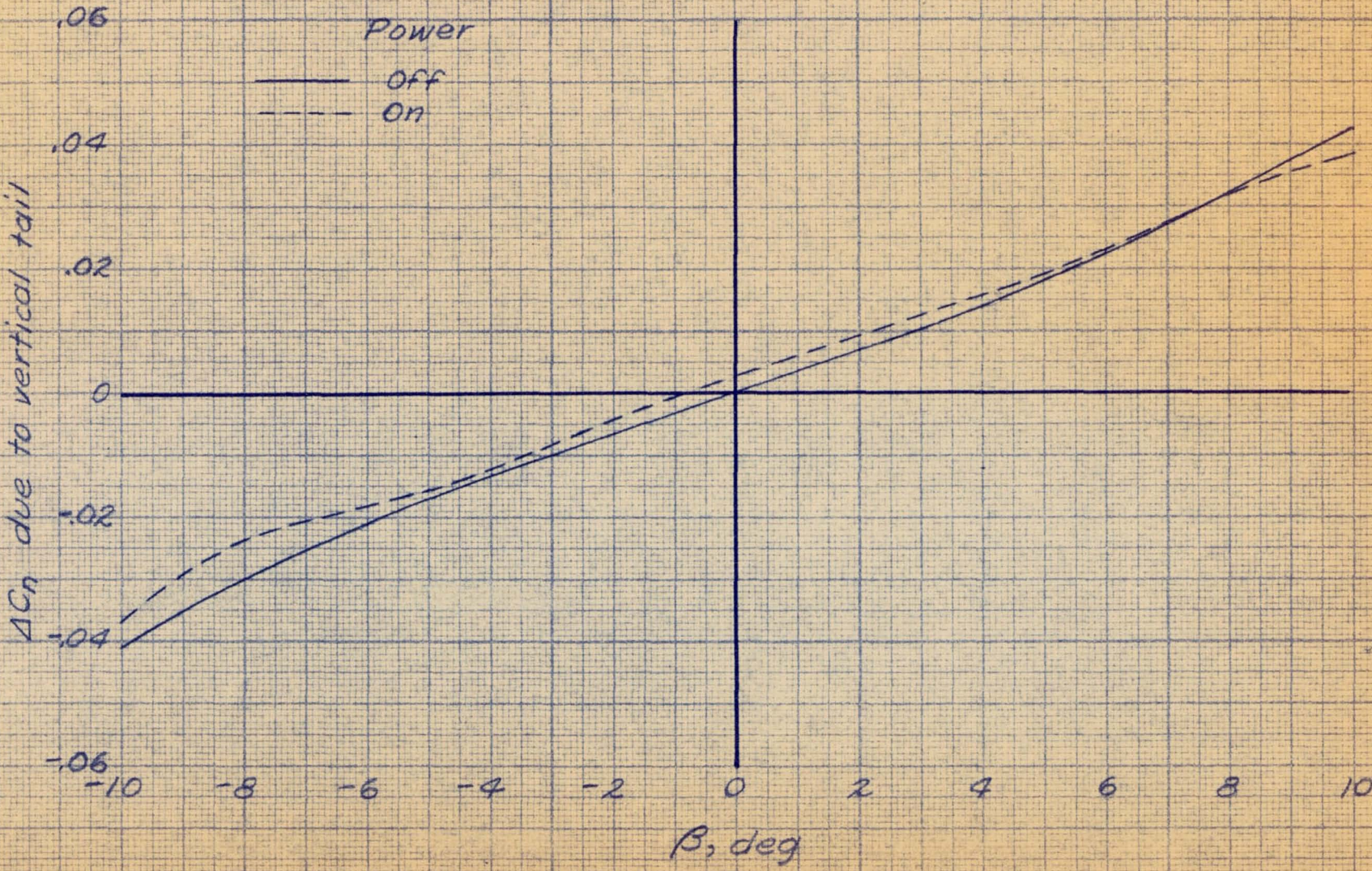

Figure 35.- Increment of yawing moment due to the vertical tail with power off and power on; q_n = 25 lb/sq ft.

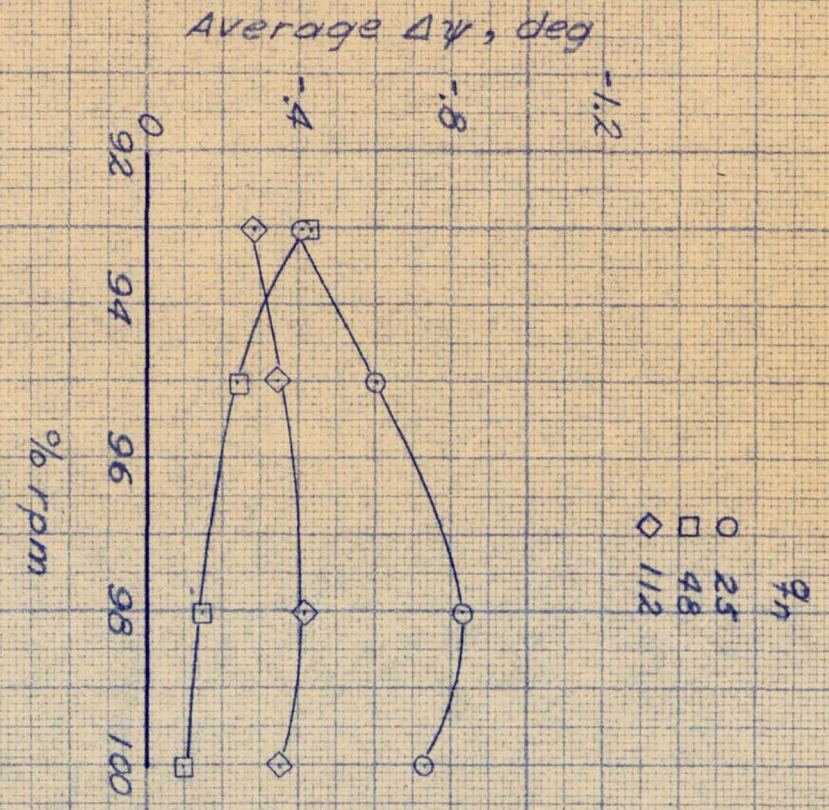

Figure 36.- Variation of change in average sidewash angle with change in engine rpm at given values of dynamic pressure; $\alpha = 6.3^{\circ}$; $\beta = 0^{\circ}$.

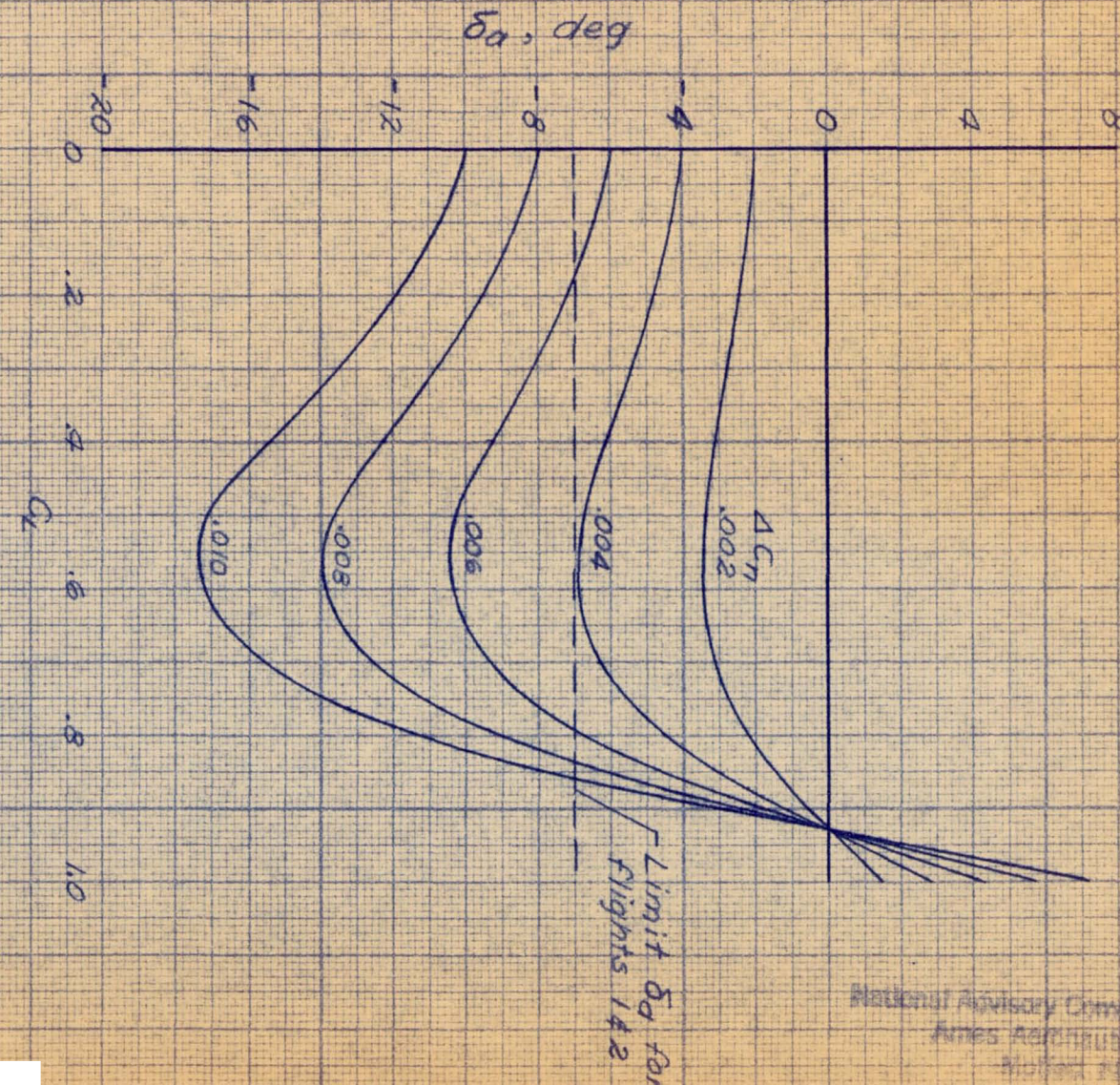

Figure 37.- Computed aileron deflections required to hold C_l and $C_n = 0$ at given values of C_L and ΔC_n.